Journal of Geophysical Research

VOLUME 64 MARCH 1959 NUMBER 3

THE SCIENTIFIC PUBLICATION
OF THE AMERICAN GEOPHYSICAL UNION

Journal of Geophysical Research

An International Scientific Publication

This Journal welcomes original scientific contributions on the physics of the earth and its environment.

Manuscripts should be transmitted to J. A. Peoples, Jr., Geology Department, University of Kansas, Lawrence, Kansas. Authors' institutions, if in the United States or Canada, are requested to pay a publication charge of $15 per page, which, if honored, entitles them to 100 free reprints.

Subscriptions to the *Journal of Geophysical Research* and *Transactions, AGU* are included in membership dues.

Non-member subscriptions, *Journal of Geophysical Research*.....$16 per calendar year, $2 per copy

Non-member subscriptions, *Transactions, AGU*.....$4 per calendar year, $1.25 per copy

Subscriptions, renewals, and orders for back numbers should be addressed to American Geophysical Union, 1515 Massachusetts Ave., Northwest, Washington 5, D. C. Suggestions to authors are available on request.

Advertising Representative: Howland and Howland, Inc., 114 East 32nd St., New York 16, N. Y.

Beginning with the January 1959 issue (Vol. 64, No. 1) the *Journal of Geophysical Research* is published monthly by the American Geophysical Union, 1515 Massachusetts Ave., Northwest, Washington 5, D. C., with the support of the Carnegie Institution of Washington and the National Science Foundation. The new monthly combines the type of scientific material formerly published in the bi-monthly *Transactions, American Geophysical Union*, and the quarterly *Journal of Geophysical Research*. The *Transactions, American Geophysical Union* will continue as a quarterly publication for Union business and items of interest to members of the Union.

Second-class postage paid at Richmond, Virginia

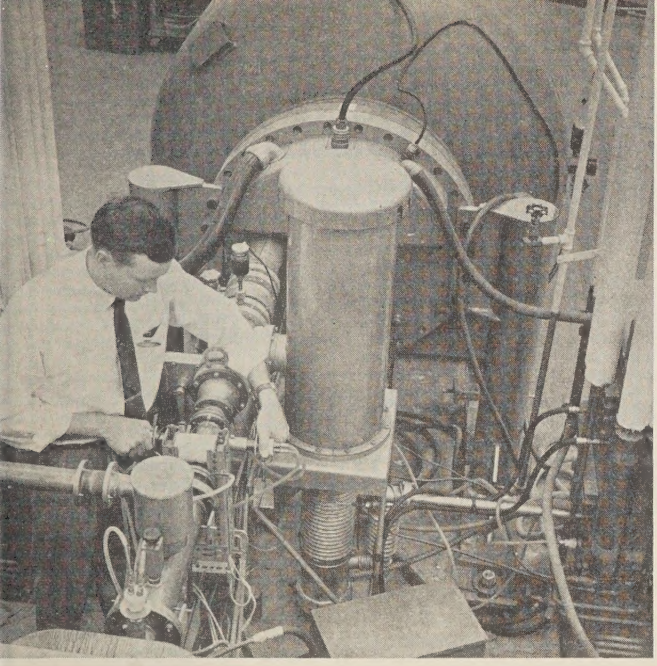

3 mev Van de Graaff accelerator—typical of advanced equipment used by Lockheed research scientists.

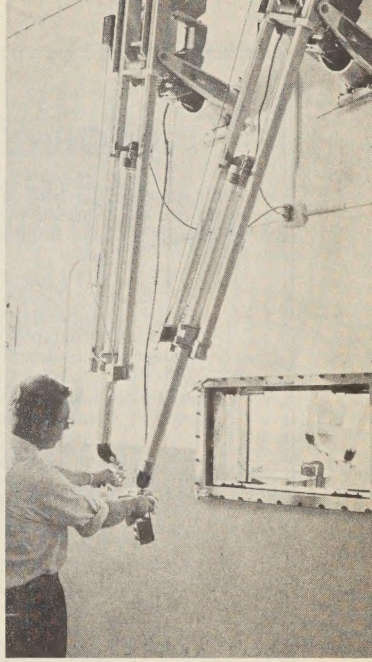

"Hot cell," for advanced radiation research in the nuclear physics laboratory.

PHYSICS

Expanding the Frontiers of Space Technology

Lockheed Missiles and Space Division is engaged in a broad, long-range program of basic scientific research at its Research and Development Laboratories in the Stanford Industrial Park at Palo Alto, California. Its modern facilities include a 3.5 mev Van de Graaff accelerator; a variety of shock tubes; extensive equipment for plasma and spectroscopic research; and one of the most modern computing centers in the nation. The Division was honored at the first National Missile Industry Conference as "the organization that contributed most during the past year to the development of the art of missiles and astronautics" and has several of the country's major programs under development.

A group of over fifty physicists is presently engaged in research and the fundamental investigation of problems in the following areas:

Nuclear Physics: Including the measurement and theory of nuclear cross sections; B-ray spectroscopy; theory of nuclear structure; reactor physics.

Weapon System Physics: The phenomenology and effects of atomic weapons, including laboratory simulation of radiation.

Space Physics: The study of the earth's upper atmosphere and beyond, including solar-terrestrial interactions.

Plasma Physics: The theoretical and experimental study of transport properties; micro-wave diagnostics; and magnetohydrodynamics.

Atomic Physics: Mass spectroscopy; theory and measurements of low energy interactions.

Members of the technical staff have every opportunity to participate in the initiation of advanced technological developments. The company encourages and sponsors individual communication with other scientists, the publication of papers and articles, and participation in symposiums and conventions.

If you have an advanced degree in physics, you are invited to join us in one of the most interesting basic scientific research programs in the nation. Write: Research and Development Staff, Dept. C-59, 962 W. El Camino Real, Sunnyvale, California.

"The organization that contributed most in the past year to the advancement of the art of missiles and astronautics." NATIONAL MISSILE INDUSTRY CONFERENCE AWARD.

Lockheed / **MISSILES AND SPACE DIVISION**

SUNNYVALE, PALO ALTO, VAN NUYS, SANTA CRUZ, SANTA MARIA, CALIFORNIA • CAPE CANAVERAL, FLORIDA • ALAMOGORDO, NEW MEXICO

PREPUBLICATION OFFER

BY

AMERICAN GEOPHYSICAL UNION

1515 Massachusetts Ave., N.W., Washington 5, D. C., U.S.A.

The Atmospheric Chemistry of Chlorine and Sulfur Compounds

Geophysical Monograph No. 3 of the American Geophysical Union (Publication No. 652 of the National Academy of Sciences—National Research Council), based on a conference held in Cincinnati, Ohio, in November, 1957, under the Chairmanship of Dr. James P. Lodge, Jr., will be ready for distribution in late spring or early summer of 1959. It will make an illustrated book of about 110-120 pages in the two-column format of Geophysical Monographs Numbers 1 and 2, in a size 7 × 10 inches. It will be cloth bound and contain some 20 papers (of some only summaries) and extended discussions relating to the subject. Included will be the following contributions by well-known authorities. To most of these, as noted, are added discussions by participants in the Conference.

S. TWOMEY: Hygroscopic Particles in the Atmosphere and Their Identification by a Phase-Transition Method
N. H. FARLOW: Applications of the Chloride Reagent Film
R. D. CADLE: Micrurgic Identification of Chloride and Sulfate
E. ERIKSSON: Techniques of Precipitation Analysis (summary)
M. B. JACOBS: Techniques for Measurement of Hydrogen Sulfide and Sulfur Oxides
P. W. WEST and H. COLL: Spectrophotometric Determination of Chloride in Air (summary)
P. W. WEST and G. C. GAEKE, JR.: Determination of Sulfur Dioxide in the Atmosphere (summary)
J. S. NADER and J. L. DOLPHIN: Improved Titrilog Sensitivity (summary)
H. C. McKEE and W. L. ROLLWITZ: Improved Titrilog Sensitivity—Part II. Field Performance and Evaluation (summary)
D. BIENSTOCK, J. H. FIELD, and H. E. BENSON: Sulfur Dioxide in Atmospheric Pollution, and Methods of Control
F. E. GARTRELL, F. W. THOMAS, and S. B. CARPENTER: Transport of SO_2 in the Atmosphere from a Single Source
L. SUMI, A. CORKERY, and J. L. MONKMAN: Calcium Sulphate Content of Urban Air
M. B. JACOBS: Concentration of Sulfur-Containing Pollutants in a Major Urban Area
P. J. LAWTHER: Some Analytical and Clinical Aspects of British Urban Air Pollution
W. D. CROZIER: Chloride Particle Measurements in the Southwestern United States
H. R. BYERS: Chloride and Sulfate Particles in the Atmosphere (summary)
E. M. FOURNIER D'ALBE: Artificial Cloud Nucleation with Sodium Chloride
C. E. JUNGE and T. G. RYAN: Study of the SO_2 Oxidation in Solution and its Role in Atmospheric Chemistry (summary)
R. D. CADLE and R. C. ROBBINS: Kinetics of the Reaction between Ammonia and Sulfuric Acid Droplets in an Aerosol
A. R. MEETHAM: The Behavior of Sulphur Dioxide in the Atmosphere
C. E. JUNGE: The Distribution of Sea Salt and Sulfate in Rain Water over the United States (summary)
A. H. WOODCOCK: Chloride Carried Inland by Maritime Winds Compared to Chloride Found in Rain and River Waters (summary)
E. ERIKSSON: On the Geochemistry of Chloride and Sulfate

The book (list price, $5.50) is offered at prepublication prices as follows:

	To Members	To Non-Members*
Payment with order, postage paid	$3.50	$4.00
Payment on delivery, plus postage	$4.25	$4.75

*Note that subscribers to publications of the American Geophysical Union are not members.

These prepublication prices are valid only until May 4, 1959 (U. S. and territories, Canada, and Mexico) and until May 20, 1959 (all others). Subjoined is an order form.

STANDING ORDERS: For those having standing orders for the Geophysical Monograph Series and those having standing orders for publications of the National Academy of Sciences—National Research Council, the order will be entered at the $4.75 rate, net, plus postage, unless advance payment is received. Those having standing orders who send payments should note that the payment is to cover a standing order.

PREVIOUS GEOPHYSICAL MONOGRAPHS: Geophysical Monograph No. 1 (Antarctica in the International Geophysical Year, price $6.00) and Geophysical Monograph No. 2 (Geophysics and the IGY, price $8.00) are still available.

Purchase Order

TO AMERICAN GEOPHYSICAL UNION

1515 Massachusetts Avenue, N.W., Washington 5, D. C., U.S.A.

Please enter {my / our} order for _____ copy/copies of Geophysical Monograph No. 3.

☐ Enclosed is $_____ for this order at $_____
($3.50 per copy—price to members only)
($4.00 per copy—price to non-members, including subscribers to AGU publications)

☐ Upon receipt of the invoice, {I / we} will remit $_____ (plus postage)
promptly at ($4.25 per copy—price to members, plus postage)
($4.75 per copy—price to non-members, plus postage)
(List price, $5.50)

Typed Name_____ Address_____

Signature_____

[Offer void after May 4, 1959 (U. S. and Territories, Canada, and Mexico) and after May 20, 1959 (all others).]

Journal of

GEOPHYSICAL RESEARCH

VOLUME 64 MARCH, 1959 No. 3

Radiation Observations with Satellite 1958 ε*

JAMES A. VAN ALLEN, CARL E. MCILWAIN, AND GEORGE H. LUDWIG**

Department of Physics
State University of Iowa
Iowa City, Iowa

Abstract—A preliminary account is given of the radiation observations made with Satellite 1958ε. The earlier discovery of the great radiation belt around the earth with Satellites 1958α and 1958γ has been confirmed and greatly extended with an apparatus of much greater dynamic range and discrimination. It appears likely that many important geophysical phenomena are intimately related to the reservoir of charged particles found to be trapped in the outer reaches of the earth's magnetic field.

INTRODUCTION

The existence of a high intensity of corpuscular radiation in the vicinity of the earth was discovered by apparatus carried by Satellite 1958α, launched at 0348 UT on February 1, 1958. The discovery was confirmed and knowledge of the distribution of radiation was greatly extended with more elaborate equipment in Satellite 1958γ, launched at 1738 UT on March 26, 1958. A preliminary account of this work has been given.*** [*Van Allen* and others, 1958a, 1958b]

A full report will be made as soon as comprehensive reduction of the observation has been completed.

The data from 1958α and 1958γ showed that:

(a) The intensity of radiation up to some 700 km altitude was in good accord with that to be expected for cosmic rays only, when proper account was taken of the increasing opening angles of geomagnetically allowed cones with increasing altitude and of the concurrent shrinking of the solid angle subtended at the observing point by the solid earth.

(b) Above some 1000 km (this transition altitude being longitude and latitude dependent) the intensity of radiation increased very rapidly with increasing altitude, in a way totally inconsistent with cosmic ray expectations.

(c) At the higher altitudes (~2000 km) the true counting rate of a Geiger tube with a geometric factor**** [*Vouk*, 1948] $G_0 = 17.4$ cm² and with total shielding of about 1.5 g/cm² of stainless steel (extrapolated range for electrons of energy 3 Mev or range for protons of 30 Mev) exceeded 25,000 counts per second. Hence the omnidirectional intensity exceeded 1700 cm^{-2} sec^{-1} if the radiation consisted wholly of pene-

* Assisted by US/IGY Project 32.1 of the National Academy of Sciences and the National Science Foundation; by the U. S. Army Ordnance Department; and by the Office of Naval Research and the Atomic Energy Commission.

** Now Research Fellow of U. S. Steel Foundation.

***Paper presented by J. A. Van Allen at joint meeting of National Academy of Sciences and American Physical Society on May 1, 1958.

****The omnidirectional geometric factor G_0 is defined so that the omnidirectional intensity of isotropic radiation is given by

$$J_0 = R/\epsilon G_0,$$

where J_0 is the flux of particles from all directions through a sphere of unit cross-section (J_0 measured in cm^{-2} sec^{-1}), R is the true counting rate of the detector and ϵ is its efficiency for the radiation in question.

For a cylindrical counter of effective length l and effective diameter a,

$$G_0 = 0.25\pi al(1 + a/2l).$$

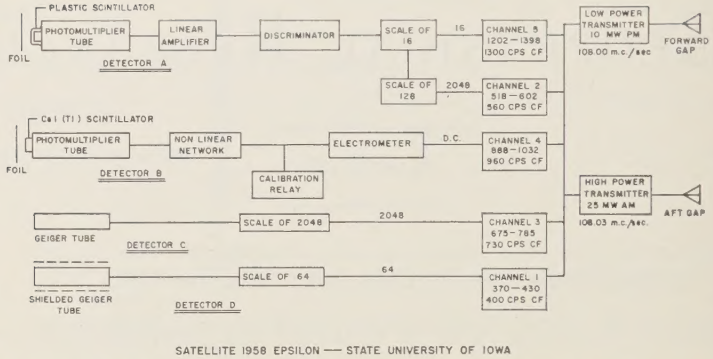

FIG. 1—Block diagram of detectors and associated circuitry of satellite 1958ϵ of the State University of Iowa

trating charged particles ($\epsilon = 0.85$); or it exceeded some 10^8 cm^{-2}sec^{-1} if the radiation consisted wholly of electrons whose range was less than 1.5 g/cm^2($E < 3$ Mev) but whose bremsstrahlung was sufficiently energetic to penetrate the absorber with little attenuation ($E \gtrsim 50$ kev).

(d) Since the atmospheric path length between altitudes of, for example, 1000 km and 700 km was negligible compared with the effective wall thickness of the counter, it was evident that the primary radiation was restrained from reaching lower altitudes by the earth's magnetic field and must therefore consist of *charged* particles.

It was proposed in our May 1, 1958, report [*Van Allen*, 1958a] that the radiation was corpuscular in nature, was presumably trapped in Stoermer-Treiman [*Treiman*, 1953] lunes about the earth, and was likely intimately related to that responsible for aurorae. On the basis of these tentative beliefs it was thought likely that the observed trapped radiation had originally come from the sun in the form of ionized gas which may or may not have been subjected to acceleration in the outer reaches of the earth's magnetic field, in some such manner as discussed by Chapman and Ferraro.

The existence of such radiation had been presaged by our earlier rocket observations in the northern and southern auroral zones [*Meredith* and others, 1955; *Van Allen*, 1957]. Indeed, further specific experiments on the arriving auroral radiations has been planned by us [*Van Allen*, 1956] and by *Bennett* [1956] for satellites in high inclination orbits; but it had not been anticipated that the "auroral soft radiation," as we originally called it, would be encountered at such low altitudes and low latitudes as was found with 1958α and 1958γ to be the case.

APPARATUS FOR 1958ϵ

The opportunity made available in late spring 1958 by several federal agencies for further satellite experiments was eagerly accepted. The apparatus devised for this purpose is shown in block diagram form in Figure 1. An outline sketch of the physical arrangement of components in the satellite payload is shown in Figure 2. Salient characteristics of the four radiation detectors were as follows:

Detector A—Circular disc of plastic scintillator (National Radiac Scintilon), thickness 0.178 cm, diameter 0.762 cm cemented on the face of an RCA photomultiplier tube, type 6199. The PM

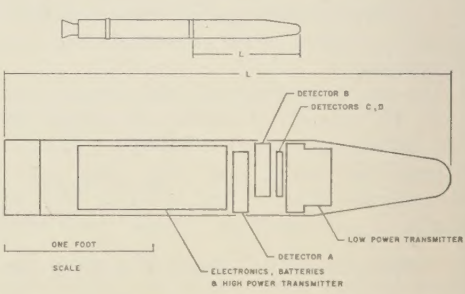

FIG. 2—Outline sketch of the arrangement of principal components of the payload of Satellite 1958ϵ; small diagram in upper part of the figure shows appearance of the orbiting body, of which the payload was a permanent part

tube was mounted with its axis orthogonal to the longitudinal axis of the payload and with the scintillator near an open hole in the wall of the payload shell. The unidirectional geometrical factor (defined by $G = R/\epsilon j$, where j is the unidirectional intensity in particles cm^{-2} sec^{-1} $steradian^{-1}$) of the scintillator was $G = 0.040$ cm^2 steradian through an aperture covered by 0.14 g/cm^2 of aluminum. The geometrical factor as a function of stopping power rose rapidly for stopping power greater than 1.6 g/cm^2 to an asymptotic value of $G = 4.2$ cm^2 steradian (or $G_0 = 0.334$ cm^2) for stopping powers greater than 5 g/cm^2. The collimating apertures were such that the area of the scintillator 'visible' through the foil had its full value for a cone of half angle 6° and fell linearly to zero at a half angle of 19°. The electronic bias was selected so that about five per cent of the β-rays from a Tl^{204} source on the outside of the stopping foil were recorded. The upper limit of the β-ray spectrum of Tl^{204} is 780 kev. A weak Tl^{204} source was permanently deposited on the foil of the flight instrument to provide an over-all check on performance of the system; it gave an average background rate of 0.50 counts/sec, with slight but known dependence on temperature of the amplifier. Over-all response of the system was well represented by the following equation:

$$R = \frac{r}{1 - r\tau}$$

in which r = apparent counting rate, $\tau = 91$ μsec, R = true counting rate. Two scaling factors were provided in order to extend the dynamic range of the system: Channel 2 with a scaling factor of 2048 and Channel 5 with a scaling factor of 16.

Detector B—Circular disc of Cs I (Tl) scintillating crystal, thickness 0.203 cm, diameter 0.762 cm, cemented to the face of an RCA 6199 PM tube. Mounting of the assembly was similar to that of Detector A, except that its aperture faced in the opposite direction. A thin layer of aluminum (about 0.2 mg/cm^2) was first evaporated onto the crystal. Then it was further shielded by a nickel foil of 0.8 mg/cm^2 thickness. This arrangement permitted exposure of the detector to direct sunlight without any detectable response. The nickel foil was cemented to and supported by a plastic disc having seven closely spaced No. 46 drill-size holes. The geometrical factor G was 0.0235 cm^2 steradian for a stopping power of 1 mg/cm^2 and rose rapidly to an asymptotic value of 4.4 cm^2 steradian (or $G_0 = 0.350$ cm^2) for a stopping power greater than 5 g/cm^2. The angular opening angles were very nearly the same as for Detector A. The anode current of the PM tube was passed through a non-linear Zener-diode network, whose output voltage was applied to the grid of a hard vacuum electrometer tube and thence to the subcarrier oscillator. The frequency deviation of the subcarrier was approximately proportional to the logarithm of the anode current of the PM tube over a range of six decades. The absolute calibration of the system was determined with the help of a polonium α-particle source of known strength. The constant of the system was 1 ampere = 0.47×10^8 ergs/sec of ionization energy dissipated in the crystal by a fast, singly-charged particle. The workable dynamic range extended from about 10^{-1} erg/sec to 10^5 erg/sec. The zero of the electrometer was checked periodically throughout flight at 20-second intervals by connecting the grid of the electrometer tube to a fixed reference potential for 1.7 seconds.

Detector C—The basic detector was an Anton Type 302 Geiger tube. It was not deliberately shielded but was more or less surrounded by a miscellany of electronic components and mechanical structure such that the omnidirectional geometric factor G_0 was 0.14 cm^2 for a stopping power of 1.2 g/cm^2 and rose to its full value of 0.705 cm^2 for stopping power of 5 g/cm^2. The material in the low stopping power case was mainly stainless steel. The performance of the over-all circuit was found in detailed calibrations to be well represented by the following equation:

$$r = R\, e^{-R\tau}$$

where r is the apparent rate, R the true rate and $\tau = 62.5 \pm 1.3$ μsecs. The useful dynamic range for filtered 50 kv X rays, for example, extended up to about 20 roentgens/hr. The maximum value of r was 5900 counts/sec, and the value of r was very nearly proportional to radiation intensity at rates below 1000 counts/sec. No difficulty was experienced in practice in resolving the ambiguity presented by the fact that r was a double valued function of radiation intensity. The maximum value of r was easily read on the telemetered record due to the large scaling factor, namely 2048.

Detector D—The basic detector was again an Anton type 302 Geiger tube. The tube was surrounded by a lead cylinder of 1.6 g/cm² thickness and was further shielded on the ends by lead plugs of somewhat greater thickness. $G_0 = 0.14$ cm² for a total stopping power (lead + stainless steel) of 2.8 g/cm², and G_0 had substantially its full value of 0.823 cm² for stopping powers greater than 6 g/cm². Detectors C and D were located side by side with center line separation of 3.6 cm in the position shown in Figure 2. The maximum observable counting rate of Detector D was determined by the information-band-width of the telemetering system. It was about 1500 counts/sec under favorable conditions. The low scaling factor, 64, was selected in order to get a determination of radiation intensities at low altitudes during the often-brief periods of satisfactory telemetering reception by a given station on a given pass. Periods as brief as one or two minutes were anticipated and did indeed occur not uncommonly, though many of the stations were successful in receiving workable signals for up to 15 minutes and in rare cases for longer.

Every reasonable effort was made to assure reliable operation of all elements of the apparatus over a large range of temperature. The entire detector assembly operated reliably from −15°C to +100°C, though the characteristics of Detectors A and B had small, known temperature coefficients. The practical low-temperature limit for the complete payload package was about 0°C (determined by mercury batteries) and the practical high-temperature limit was about +60°C (determined by rf transmitter using germanium transistors). Temperature of the interior of the payload of 1958ϵ was determined roughly from the frequency of the subcarrier oscillators. It lay always in the range +10°C to +50°C during its orbital flight.

All components and completely assembled payloads were subjected to a full program of acceleration, vibration, shock, vacuum, and temperature cycling tests. No attempt was made to pressure seal the payload shell. The integrity of all high voltage (up to 700 v) circuits was assured by foam-potting and thorough vacuum testing.

Mallory mercury batteries were used throughout for powering the electronic apparatus.

Many potential improvements in the apparatus will doubtless occur to the reader, as they did to us during its development. But there were severe restrictions on power drain, physical arrangements, weight and information-bandwidth, and on available time, which precluded extensive refinements.

Four flight payloads were built, fully calibrated and subjected to the full gamut of environmental tests. One payload was flown on Explorer IV, which entered orbit successfully at 1506 UT on July 26, thus earning the astronomical designation Satellite 1958ϵ. The apparatus performed in all respects fully up to expectations, though its lifetime was somewhat shorter than had been anticipated.

The lower powered transmitter and Channels 2 and 5 'died' about September 3. Channels 1, 3, and 4 continued to operate properly until September 19. The higher powered transmitter ceased sending signals on October 5. There is no reason to believe that the demise of the apparatus was due to any other cause than simple exhaustion of the batteries.

The lower powered transmitter and the subcarrier oscillators were supplied by the Jet Propulsion Laboratory (JPL), the higher powered transmitter by Project Vanguard.

Design, development, construction, and calibration of the detectors, associated electronics, etc. were accomplished in the Department of Physics at the State University of Iowa. Final environmental tests and over-all flight specifications were in the hands of the Army Ballistic Missile Agency (ABMA), as were the supply of payload shells, thermal design of the shells, and, of course, many other essential aspects of the flight operations.

The Army Jupiter C vehicle and the flight operations were handled jointly by the ABMA and the JPL in collaboration with the Patrick Air Force Base.

A second payload was flown on Explorer V, launched on August 24, 1958. This rocket failed to go into orbit. However, the on-board apparatus functioned satisfactorily during its brief, ten-minute flight.

Orbit of 1958ϵ

In order to obtain wide geographical coverage we requested an orbit as steeply inclined to the geographical equator as was feasible. The ABMA and the Patrick Air Force Base agreed to shoot

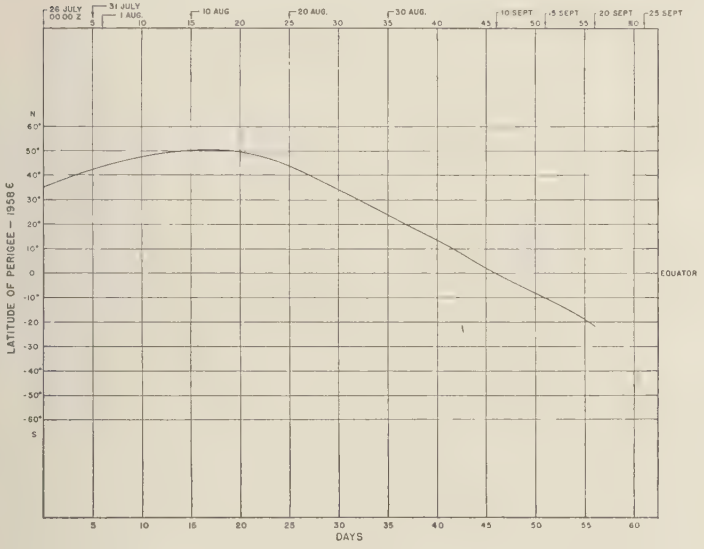

FIG. 3—The observed latitude of perigee of the orbit of 1958ε as a function of time (courtesy Vanguard Computing Center)

on a northeasterly bearing from Cape Canaveral, Florida, so as to produce an orbital inclination of about 51°. This was accomplished. An inclination of 90° would, of course, have been desirable, but this was judged unwise from a 'range safety' point of view. The inclination of 51° permitted a very great extension of knowledge over what would have been possible with the inclinations of 34° of previous U. S. satellites.

The satellite was tracked by radio interferometric methods by ten Minitrack stations, by optical methods by stations of the Smithsonian Institution Astrophysical Observatory's network (SIAO), and by various other methods by other stations .[*Berkner* and others, 1958]. A smoothed orbit was computed by the Vanguard Computing Center and jointly by the SIAO and ABMA groups. Altitude above the

TABLE 1—*Sample of ephemeris of 1958ε*
(Courtesy Army Ballistic Missile Agency and Smithsonian Institution Astrophysical Observatory)

Day	UT	Longitude East	Latitude	Height (km)
August	0015	292.25°	−28.10	2054.8
2, 1958	0016	294.19	−29.91	2080.9
	0017	296.19	−31.67	2104.7
	0018	298.28	−33.39	2126.1
	....	.....	.....	....
	0118	110.52	+38.15	287.9
	0119	114.78	+40.56	278.2
	0120	119.38	+42.78	272.5
	0121	124.31	+44.79	270.9
	0122	129.61	+46.55	273.3
	0123	135.23	+48.02	279.7
		etc.		

TABLE 2—*Principal orbital parameters of 1958ε*
(Courtesy Vanguard Computing Center)

Mean date	Altitude of apogee (km)	Altitude of perigee (km)	Period (min)
1958			
July 28	2210	262	110.2
Aug. 1	2203	257	110.1
Aug. 5	2194	257	110.0
Aug. 9	2184	256	109.9
Aug. 13	2172	256	109.7
Aug. 17	2161	258	109.6
Aug. 21	2150	257	109.5
Aug. 25	2140	258	109.4
Aug. 29	2127	258	109.3
Sept. 2	2115	258	109.1
Sept. 6	2100	262	109.0
Sept. 10	2084	267	108.9
Sept. 14	2079	262	108.8
Sept. 18	2070	261	108.7

international geoid and geographic latitude and longitude were tabulated at each minute of real time. Precision of the presently available ephemeris is typically such as to locate the satellite with high probability within a sphere of radius 10 km. Table 1 lists two typical sequences of entries. An over-all view of the history of the orbit is provided by Table 2 and by Figure 3.

In addition, ABMA has computed recently an ephemeris in terms of eccentric geomagnetic coordinates.

Data Transmission and Reception

The data from 1958ε were telemetered according to the scheme shown in Figure 1, identical intelligence being supplied continuously to the two independent transmitters. In flight, the recorded signals from the 108.03 Mc/sec transmitter were of much better quality than those from the other and formed the principal body of observations. A total of 22 receiving stations were in regular operation, recording on magnetic tape the mixed audio signal together with coded time signals whenever the satellite passed sufficiently close to provide a workable signal level. A number of other stations contributed during some portions of the flight. Table 3 lists the sites of the regular telemetry stations.

Table 3—*Regular telemetry stations for 1958ε*

Antigua, British West Indies
Antofagasta, Chile
Azores Islands, Portugal
Blossom Point, Maryland
Bonn, Germany
Fort Monmouth, New Jersey
Fort Stewart, Georgia
Goldstone Lake, California
Havana, Cuba
Heidelberg, Germany
Huntsville, Alabama
Ibadan, Nigeria
Johannesburg, South Africa
Lima, Peru
Patrick Air Force Base, Florida
Quito, Ecuador
Salisbury, Southern Rhodesia
San Diego, California
Santiago, Chile
Singapore, British Malaya
Van Buren, Maine
Woomera, Australia

Observations

Remarks concerning data—For the entire operating lifetime of 1958ε we have now received at the State University of Iowa data center some 3600 recorded 'passes.' The original records are made on magnetic tape with coded absolute time signals. The mixed-audio signal from the five subcarriers is played back through a set of five band-pass filters and frequency discriminators to a multichannel, pen-and-ink Offner oscillograph. Several hundreds of the records have been surveyed thus far, and detailed reading and tabulation of the data from a substantial number of selected records have been accomplished. A typical pass yields workable data over a several-minute period. The rf radiation pattern of the satellite is that of a linear antenna fed asymmetrically. Hence nulls in the signal strength occur periodically as the satellite tumbles. The angular motion was originally a rapid rotation about the longitudinal axis of the cylindrical satellite. But by early August the motion had become a propellor-like tumbling motion with a period of about seven seconds, and a slow rotation about the longitudinal axis (period of the order of one second).

Sample sets of data—In Table 4 are tabulated a number of sets of data for illustrative purposes. It is seen that in a broad way the earlier results of 1958α and 1958γ have been amply confirmed with a diversity of detectors of quite different properties. The detectors of 1958ε, designed with the knowledge of the earlier results, have provided a vastly more full and detailed knowledge of the distribution and nature of the radiation.

Altitude, latitude, and longitude dependence of intensity—In geographical longitude 80° ± 20°W and low latitudes the intensity as measured by all detectors increases slowly up to some 800 to 1000 km, then increases very rapidly to the highest altitude reached, 2200 km. The increase in the region 1000 to 2200 km is by approximately a factor of two per hundred kilometers.

In order to gain a more comprehensive idea of the geographical distribution of intensity, the counting rate of each detector has been written on a large chart representing a meridian section through the earth and its atmosphere. A different chart is used for each of several longitudinal sectors of the earth. The numbers on each chart progressively produce a two-dimensional array, as the position of perigee moves in

TABLE 4—*Some sample observations with 1958ε*

Telemetry station	Date and UT	Detector D Channel 1 counts/sec (True rate)	Detector A Channel 2 or 5 counts/sec (True rate)	Detector C Channel 3 counts/sec (True rate)	Detector B Channel 4 ergs/cm² sec sterad	Long. E	Lat.	Alt. (km)
Woomera	Aug. 5 1047	10.4	310	470	0.2 av	130.2°	−36.4°	2080
	Aug. 6 0839	39.4	290 av 60 min	74	0.45 min 0.9 max	143.0	−24.9	1841
	Aug. 12 1321	6.2	580	62	—	143.0	−46.0	2142
Antofagasta	Aug. 14 0550	—	14,500	10,500	5 min 20 max	290.9	−18.4	1685
	Aug. 3 2353	—	30,000 min 110,000 max	11,400	21 min 76 max	287.0	−26.4	1959
Patrick Air Force Base	Aug. 6 1131	1.9	2.2	—	—	281.4	+26.6	474
	Aug. 15 1517	1.1	1.5	—	—	259.5	+50.0	277
	July 30 2220	1.2	40.	—	—	280.8	+25.9	1035
Singapore	Aug. 1 2316	0.8	1.3	—	—	104.0	+ 3.5	676
Blossom Point	Aug. 15 0940	2.8	40 av 130 max 20 min	38	—	295.6	+43.5	458
Santiago	Aug. 14 0346	670	2,900 min 30,000 max	1,430	1.7 min 13 max	286.9	−43.3	2133
	Aug. 2 0213	910	8,000 av	1,660	4 min 20 max	282.1	−41.3	2210
Antigua	Aug. 1 2208	1,280	4,800	1,420	2.2 min 6.5 max	291.2	+ 8.9	1328
Huntsville	Aug. 19				Min Max			
	0631	—	12,100	4,100	0.9 5	275.0	+ 1.6	1492
	0632	1,220	11,700	2,020	0.7 3.5	276.6	+ 3.9	1442
	0633	950	2,700	980	0.55 2.4	278.4	+ 6.3	1390
	0634	470	1,230	466	0.37 0.8	280.2	+ 8.7	1337
	0635	180	630	180	0.23 0.35	282.0	+11.1	1284
	0636	51	220	48	0.14 —	283.9	+13.6	1230
	0637	17	74	—	~0.1 —	285.9	+16.0	1176
	0638	3.3	76	—	—	288.0	+18.5	1122
	0639	2.2	115	—	—	290.1	+21.0	1067
	0640	3.8	68	—	—	292.4	+23.5	1013
	0641	2.5	44	—	—	294.8	+26.0	959
Quito	July 0046/28	—	14,500	5,600	20 av	278.9	+ 2.5	1694
	July 0048/28	—	45,000	9,900	60 av	282.0	− 1.9	1783

Notes on Table 4: (1) Where not otherwise indicated the rates of Detector A are 'apparent' average values over a tumbling cycle. Due to saturating characteristics of the detector these apparent averages are much too low when the maximum true rate exceeds 5000/sec. True rates are available from more detailed data reduction.

(2) The directional energy fluxes of Detector B are as attributed to a geometrical factor of 0.0235 cm² steradian.

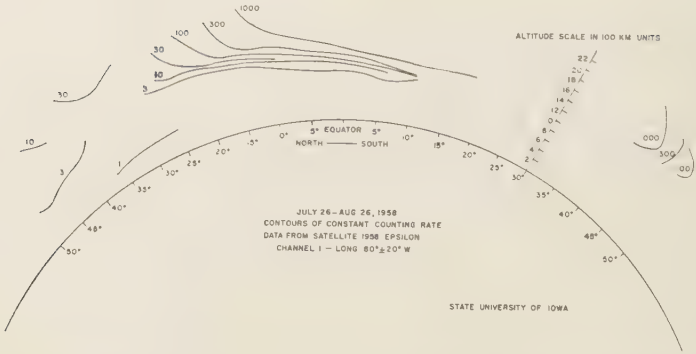

FIG. 4—A meridian section through the earth showing observed contours of specified counting rate of Detector D (Channel 1 of Fig. 1); partial summary of observations from 1958ε during the period July 26 to August 26, 1958 within longitude range 80 ± 20°W

latitude and as the corresponding data are reduced and plotted. We then sketch in contours of approximately constant counting rate. Four such charts are shown in Figures 4, 5, 6, and 7. It is seen that all contours at 80° ± 20°W have approximate symmetry about a plane through latitude 14°S. It is of special interest that a given contour lies at some 800 to 1000 km higher altitude in the southern hemisphere at 140° ± 20°E than it does in the northern hemisphere at 80 ± 20°W. Indeed the corresponding contours on the two charts become acceptably complementary if such an altitude displacement is made. This fact provides additional support for the belief in magnetic trapping, since the altitude displacement is quite suggestive of the eccentricity of the magnetic axis of the earth. Also, 14°S is near the location of the magnetic dip equator at 80°W.

It is especially noteworthy that the contours of constant intensity bend outwards from the earth at high latitude, both north and south. Indeed the outer latitude limits of the great radiation belt have a striking similarity to the latitudes of the auroral zones. The possible significance of this feature is discussed later.

In Figure 8 is given a speculative extension of the observed contours under the surmise that contours of constant intensity have a shape at very great altitudes resembling that of magnetic lines of force. A partial and tentative confirmation of this pattern has been obtained recently by our radiation measurements in the Pioneer I flight of October 11, 1958.

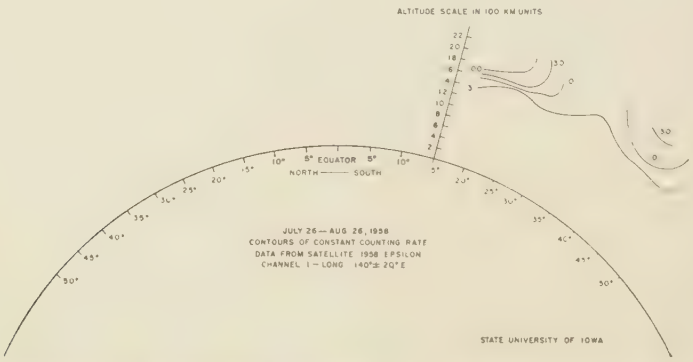

FIG. 5—A meridian section through the earth showing observed contours of specified counting rate of Detector D (Channel 1 of Fig. 1); partial summary of observations from 1958ε during the period July 26 to August 26, 1958 within longitude range 140 ± 20°E

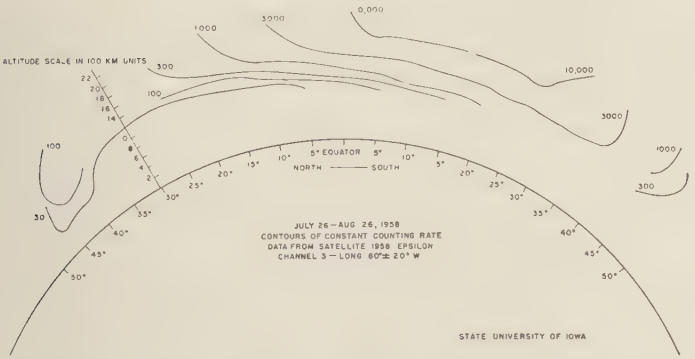

FIG. 6—A meridian section through the earth showing observed contours of specified counting rate of Detector C (Channel 3 of Fig. 1); partial summary of observations from 1958ε during the period July 26 to August 26, 1958 within longitude range 80 ± 20°W

Anisotropy of radiation—The axes of Detectors A and B, as noted above, are at right angles to the longitudinal axis of the satellite. Hence, as the satellite rolls and tumbles, these two detectors sweep out a complex motion on a unit sphere centered on the satellite. A strong 'modulation' of the counting rate of Detectors A and B is observed at all points in space, where their rates are sufficiently high to permit such an analysis. The situation has been particularly clear after the angular motion of the satellite approached pure tumbling. The observed ratio of maximum to minimum intensities on Detectors A and B ranges from two to 50, in a preliminary survey. And of course it must be noted that some particles may be sufficiently penetrating to enter the detectors from directions outside of their nominal acceptance cones. The maxima from A and from B are in phase, as are their minima. Since A and B look in diametrically opposite directions, it appears that the angular distribution of the radiation is disc-like in nature. There were no on-board devices for measuring absolute orientation, but we have hope that study of the pattern of nulls in the rf signal may provide some knowledge of the absolute orientation of the disc. For example, a pass nearly directly over the excellent receiving station at Huntsville, Alabama showed that maxima of intensity were nearly coincident with rf nulls. Hence the disc was horizontal to within ±30°. This is consistent with its perpendicularity to the local magnetic field vector.

Figure 9 gives a very illuminating example

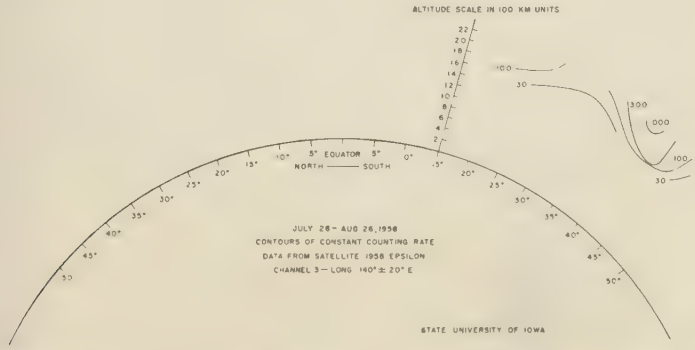

FIG. 7—A meridian section through the earth showing observed contours of specified counting rate of Detector C (Channel 3 of Fig. 1); partial summary of observations from 1958ε during the period July 26 to August 26, 1958 within longitude range 140 ± 20°E

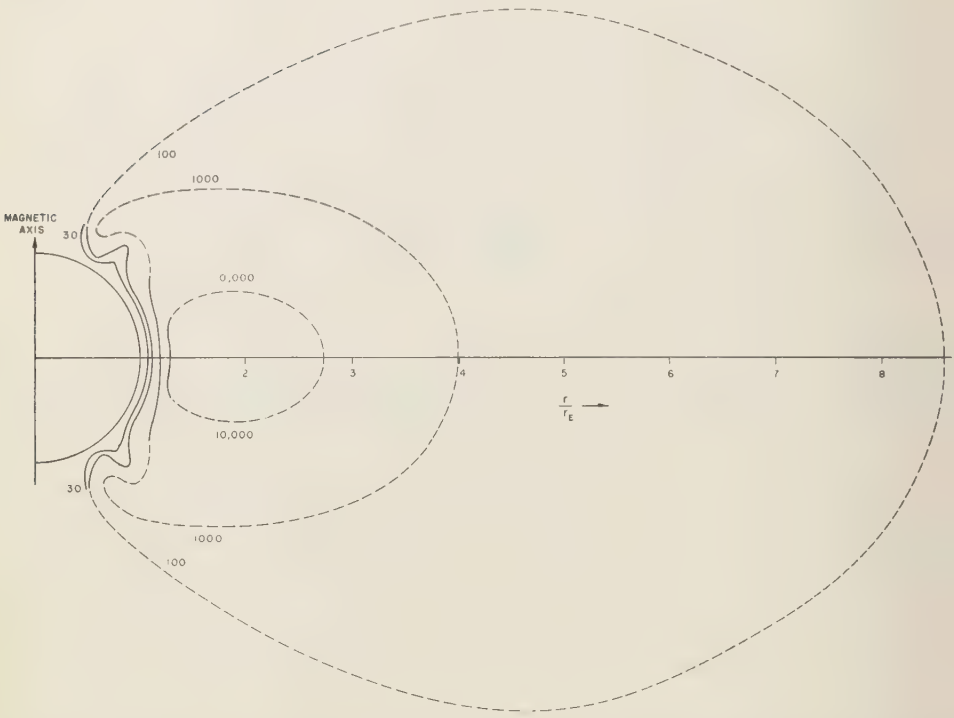

FIG. 8—A diagram of contours of specified counting rate of Detector C in the vicinity of the earth as observed with Satellite 1958ϵ (solid lines) and as extended in a speculative way (dashed lines); numbers associated with the contours are counting rates of Detector C; the linear scale of the diagram is in units of the earth's radius–6371 km

of the nature of the anisotropy. The interpretation of Figure 9 on the assumption of disc-like character of the angular distribution of the radiation is as follows. When the longitudinal axis of the satellite was perpendicular to the plane of the disc, the axis of Detector B lay in the plane of the disc; hence there was little or no modulation due to roll of the satellite about its longitudinal axis. When the longitudinal axis of the satellite lay in or nearly in the plane of the disc, there was the greatest 'amplitude modulation' of the intensity due to roll, with the maximum values being equal to the constant, unmodulated value of the preceding situation. In the latter situation the axis of Detector B cuts through the disc of radiation twice per roll cycle.

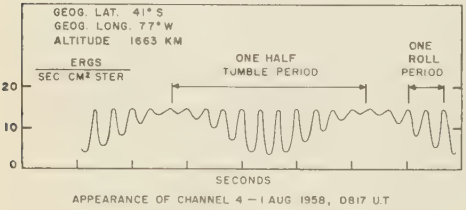

FIG. 9—A sample of the detailed output of Detector B (Channel 4 of Fig. 1) as observed at 0817 UT on August 1, 1958 at geographical latitude 41°S, geographical longitude 77°W, altitude 1663 km, illustrating the anisotropy of the radiation

When coupled with the further fact that the maxima of response of Detectors A and B are in phase in time, examples such as that shown in Figure 9 appear to establish conclusively the disc-like character of the angular distribution. We have been unable to visualize any other time-stationary situation which will account for the

observations. The 'flatness' of the disc is a function of latitude and altitude. A fuller study of this matter is in progress.

It already appears safe to conclude that the angular distribution of the radiation provides an important substantiation of our belief in magnetic trapping. See Figure 10 (not to scale) for

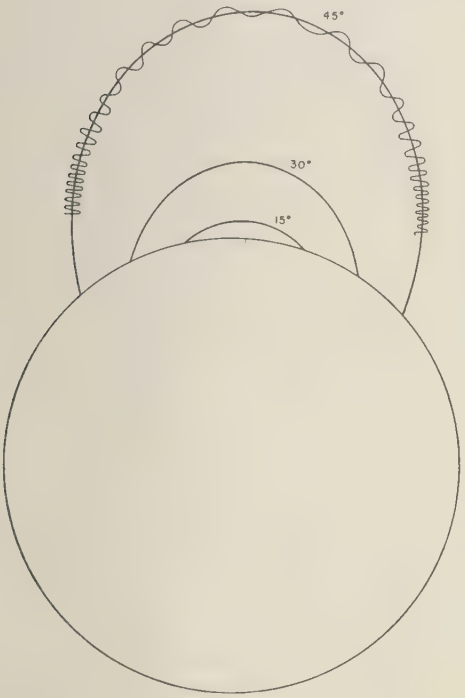

FIG. 10—An illustrative sketch, not to scale, of the spiral path of a trapped charged particle, the guiding center of whose motion lies along the line of magnetic force which intersects the earth's surface at a geomagnetic latitude of 45°; also shown are lines of force which intersect the earth's surface at geomagnetic latitudes 30° and 15°, respectively

a schematic view of the way in which magnetic trapping in the earth's field gives rise to a disc-like angular distribution at altitudes near the mirror altitudes.

Temporal fluctuations—A number of important geophysical fluctuations occurred during the observing periods of 1958α, 1958γ, and 1958ε. Of special interest is the great auroral event of February 10–11, 1958. The 1958α data during February are now being studied in detail. Inasmuch as the intensity is a rapidly changing function of altitude and is also a function of latitude and longitude, any apparent temporal fluctuations must be critically examined to assure that proper account has been taken of spatial dependencies. We now wish to withdraw for further examination a previous report (a section of the paper kindly communicated for us by Professor Sydney Chapman to the Conference of the Royal Society of London on November 13, 1958) on the subject of temporal fluctuations in early February 1958.

Aono and *Kawakami* [1958] have examined some 1958α observations which were made in Japan in early February and have suggested that temporal variations in the intensity at the lower fringe of the radiation belt were associated with the value of planetary magnetic index K_p, and with the ionospheric state as measured by the $foF2$ value. If these conclusions are substantiated by more comprehensive studies, it may be possible to reach conclusions of importance on the origin of the trapped radiation. If its intensity does indeed fluctuate with solar activity, then it would appear that the reservoir of trapped radiation is replenished from time to time by fresh batches of solar gas. It is conceivable that the total quantity of trapped radiation may fluctuate little from day to day, the most readily observable effect of the arrival of new gas being perturbations of the reservoir. Such perturbations would likely be evidenced by an enhanced leakage rate at the lower and lateral boundaries.

No detailed study of temporal fluctuations in 1958ε data has yet been made. As an over-all impression, the pattern of selected intensity contours has been stable during the month July 26 to August 26. But this statement has precision to only a factor of two at present. The intensities have a latitude and longitude dependence in addition to the sharp altitude dependence. Hence we must reserve judgment on the matter of temporal fluctuations during this period pending a closer study of the observed data.

At one time we were tempted to believe that there was a marked diurnal variation. But more thoughtful inspection showed that this effect was largely, if not wholly, a composite of altitude, latitude, and longitude dependence. The possi-

bility for such confusion results from the fact that the satellite's orbit is only slowly varying in an inertial frame of reference and therefore has a more-or-less fixed relationship to the solar 'vector' for a period of a few days. Hence, there is, in general, an *apparent* local time variation of the intensity observed at any chosen station.

Nature of the radiation—In the design of the detectors for 1958ε our working point of view was strongly conditioned by our earlier observations at rocket altitudes in the auroral zones [*Meredith* and others, 1955; *Van Allen*, 1957]. The most definitive were those of McIlwain (private communication, unpublished) in early 1958 at Fort Churchill and those of Meredith, Davis, Heppner, and Berg (private communication, unpublished) U. S. Naval Research Laboratory, also at Fort Churchill. These sets of observations showed that the energetic radiation within and beneath visible aurorae had a quite variable character. It appeared that electrons having an energy spectrum rising very steeply toward low energies were usually the dominant component. In addition, protons (or at least nucleonic-type particles) were present with a somewhat similar spectrum but with a particle intensity at a given kinetic energy several orders of magnitude less than that of electrons.

A dominant feature of the 1958ε observations is the apparent spatial variability of the composition of the radiation. Such variability is most simply illustrated by noting the variability of the ratios of counting rates (or outputs) of the several detectors. (See Table 4 for examples.) We regard it as unwise at this time to attempt a definitive statement concerning the composition of the radiation and the spectra of the several components. On any reasonable view of the origin of the trapped radiation, it would be supposed that electrons and protons are the principal components. (We are indebted to Professor P. Morrison for calling our attention to the significance of the presence or absence of α-particles in discussing matters of origin.) If this be assumed, then the problem is to determine their respective absolute energy spectra and angular distributions as a function of position in space and as a function of time.

The 1958ε observations with the diversity of detectors are consistent with the presence of auroral-type soft radiation in the radiation belt. But, in addition, there appears to be a component which is considerably more penetrating than usually observed there [*Meredith* and others, 1955; *Van Allen*, 1957; McIlwain, private communication, 1958; Meredith and others, private communication, 1958. See, however, *Anderson*, 1958a and 1958b].

Detector A (the plastic scintillator) counts electrons having energies exceeding 650 kev; protons having energies exceeding 10 Mev; X rays having energies exceeding about 400 kev, with considerably lower efficiency; and particles or X rays of progressively lower energies than those specified, with rapidly diminishing efficiency (electronic 'pile up' of pulses!)*

Detector B has distinctively different properties. Its foil will stop electrons having energies of about 20 kev, or protons having energies of 400 kev. And it is an efficient detector of X rays.

Detector C responds to electrons of energy exceeding 3 Mev, to protons of energy exceeding 30 Mev, and, with much lower efficiency, X rays of energy exceeding some tens of kev.

Detector D responds to electrons of energies exceeding 5 Mev, protons of energy exceeding 40 Mev, and, with much lower efficiency, X rays of energy exceeding about 80 kev. The marked aspect 'modulation' of the output of Detectors A and B shows that the radiation which is mainly responsible for their response has a range between 140 mg/cm² and 5 g/cm² for A and between 1.0 mg/cm² and 5 g/cm² for B. Unfortunately, these ranges are quite large. Detectors C and D also exhibit a mild aspect sensitivity but their surroundings are more nearly isotropic.

Each set of simultaneous observations with Detectors A, B, C and D provides, in effect, a set of four independent, and complicated, equations in terms of the various unknown properties of the radiation.

We are not at this date prepared to report a range spectrum of the radiation, nor are we able to offer a definitive appraisal of the important matter of whether the more penetrating component consists of protons, of electrons, or of X rays resulting from the stopping of electrons in the

*In a sample pre-flight test with a dc X-ray machine irradiating Detector A at a 1400 roentgen per hour level, it was necessary to raise the accelerating voltage to 200 kv before an observable counting rate occurred. Detectors C and D were simultaneously driven far beyond their dynamic range, a situation never encountered in flight.

various portions of the apparatus. It appears probable that a tentative appraisal will result from more thorough study of the observations and from the further experimental tests on one of the spare payloads which are presently being undertaken.

One of the central questions has to do with the importance of the bremsstrahlung from electron impact on the material of the immediate environment of the detectors. The bremsstrahlung is much more penetrating than its parent electrons, and, for an electron spectrum which falls off very steeply toward higher energies, one can readily estimate that despite the lower detection efficiency it is possible for the bremsstrahlung to extend falsely the apparent particle spectrum.

A complete knowledge of the physical nature of the radiation is, of course, of the utmost importance in clarifying its origin. Further flights of more elaborate detection systems (for example, magnetic spectrometers; McIlwain, private communication, 1958) will be necessary to accomplish this.

Remarks on Interpretation

On the basis of the evidence presented above, we regard it as established that the great radiation belt around the earth consists of charged particles, temporarily trapped in the earth's magnetic field. The rapid diminution of intensity at the lower altitudes is almost certainly due to atmospheric scattering and absorption. The dominant loss mechanism for electrons is scattering. Thus, if an electron is trapped along a specified magnetic line-of-force (see Fig. 10), the 'guiding center' of its corkscrew paths spends most of its time near the points at which the velocity of the particle is nearly orthogonal to the magnetic line (the 'mirror' points). The cumulative effect of multiple coulomb scattering is to drive the mirror point to lower altitudes where the lifetime is rapidly reduced. If one adopts as a crude criterion for loss from the trapping region an rms scattering of one radian, then the 'lifetime' in the reservoir can be estimated as a function of mirror altitude.

Due to the eccentricity of the earth's magnetic field, a given magnetic shell (locus of lines of force having $\cos^3\lambda/\rho$ = constant) has its lowest altitude above the earth, for any given λ, at the longitude of the mid-Atlantic Ocean. Because of the radial component of grad H, there is a systematic drift in longitude of trapped particles (electrons toward the east and protons toward the west) as they 'corkscrew' their way back and forth from northern to southern hemisphere. The period of drift around the earth of one Mev electrons, for example, on the line of force meeting the earth at $\lambda = 45°$ is about 30 minutes.

Hence, the loss of particles from the reservoir is mainly caused by collisions at the longitude of minimum altitude.

Based on these simple ideas and on an extrapolation of the Sterne-Jastrow satellite atmosphere, the mean trapped lifetime of one Mev electrons is estimated to be of the order of 10^4 seconds for a mirror altitude of 400 km at the longitude at which the magnetic shell has its lowest altitude and 10^6 seconds (or about 10 days) for a mirror altitude of 1000 km. The lifetime T is proportional to the square of the electron's energy. The sample values given above possess considerable uncertainty but do serve to give some feeling for the physical situation.

The effective loss of protons from the reservoir is dominated by collisional energy loss, not by scattering. For example, a one Mev proton has an estimated lifetime of 3×10^5 sec for a mirror altitude as specified above of 1000 km; and a 10 Mev proton, 6×10^6 sec. From the above considerations, it is reasonable to expect that, irrespective of the origin of the radiation, its composition and the spectra of its various components will be functions of position.

A quasi-stationary state in the radiation belt will result when the time-averaged injection rate I of new particles is equal to the leakage or output rate O. Neglecting many important details and assuming that O is proportional to Q, the quantity of radiation present in the reservoir and to the reciprocal of T, the mean storage time in the reservoir, we have the simple equation for the well known 'leaky bucket' problem, namely

$$I = O = Q/T = nV/T \qquad (1)$$

where n is the average number density and V is the volume of the reservoir.

If, for example, we assume a trapping region having a volume equal to that of a sphere of radius four earth radii (10^{29} cm^3) and adopt an average number density of energetic particles of one per cubic centimeter, then

$$Q = 10^{29} \text{ particles}$$

or some 10^5 moles. A sample pair of values for T and I might be 10^7 sec and 10^{22} particles/sec respectively.

The equilibrium spectrum of stored particles will presumably be a much less steep function of energy than the spectrum of injected particles, since T diminishes rapidly toward lower energies for loss by either scattering or absorption.

It is difficult to avoid the belief that aurorae are related to the trapped radiation. Specific reasons for this belief are the following: (i) The contours of constant intensity (Figs. 4, 5, 6, 7) are more or less bounded, as they turn away from the earth at high latitudes, by a cone which lies at the lower latitude edge of the auroral zone. (ii) The nature and intensity of the radiation in the reservoir appears to resemble that encountered at low altitudes (~100 to 150 km) in the auroral zone. (iii) There is preliminary evidence that fluctuations in the intensity of radiation on the lower fringes of the radiation belt are correlated with magnetic and ionospheric activity, as are aurorae. (iv) There is sufficient stored energy in the radiation belt to supply the time-averaged auroral intensity if the mean storage life is of the order of 10^7 sec. (v) There is observed to be a more-or-less steady leakage of 'soft radiation' into the auroral zone even in the absence of visible aurorae [*Meredith* and others, 1955; *Van Allen*, 1957].

For the various reasons listed above we propose that the radiation belt is the reservoir whose leakage of particles is the direct cause of visible aurorae. It is further suggested that solar plasma replenishes the reservoir from time to time, working its way into the outer reaches of the earth's magnetic field when its density is sufficiently great, then being trapped in the field. On the occasion of the arrival of new batches of gas, the pattern of magnetic field lines at great altitudes, and hence at high latitudes, is distorted, thus permitting the leakage of particles from the reservoir into lower altitudes at a rate greatly exceeding that which is usual for the quiescent situation. The total quantity Q of plasma in the reservoir may fluctuate only slightly on such occasions, though it may be presumed that Q will vary with the general level of solar activity, averaged over a period of time of the order of T. Insofar as grad H has a longitudinal component, there will be a radial drifting tendency of the same nature as the longitudinal drifting tendency previously mentioned. The importance of this effect has not been assessed, but it may well provide the dominant mechanism for feeding plasma to low altitudes in the equatorial region. (We are grateful to Professor T. Gold for an opportunity to discuss a number of matters of general physical interpretation, including especially the contents of this section.)

It has been suggested by N. C. Christofilos (private communication, April 1958, unpublished), *Vernow* [1958], *Kellogg*, and *Singer* [1958a,b] that the radioactive decay of outward moving neutrons resulting from cosmic ray interactions in the atmosphere (neutron albedo) may provide an injection mechanism of significant intensity. The charged particle, cosmic ray albedo, has been the subject of considerable study during the past ten years particularly in this laboratory and by Winckler and associates at the University of Minnesota. The confinement to Stoermer-Treiman lunes has been intrinsic to discussions of the phenomenon. But since 'injection' occurs at altitudes such as 30 km, it has usually been supposed that charged albedo makes only a one-way transit to the conjugate latitude in the opposite hemisphere. The essential attractiveness of albedo neutrons is their ability to escape from the denser regions of the atmosphere, then to inject their decay products at an altitude where the storage life is long. The mean decay lifetime of the neutron at rest is about 12 minutes. Almost all upward moving slow neutrons therefore decay within the trapping region of the earth's magnetic field (tentatively assumed to extend to about seven earth radii). Their charged decay products are electrons with energies up to 782 kev and quite low energy recoil protons. Of the order of a few tenths of one per cent of fast neutrons (having a typical energy of, say, 40 Mev) decay during their traversal of the trapping region. Their charged decay products are protons of energies comparable to their own energy and electrons having a spectrum similar to that of slow-neutron-decay electrons.

We find a number density of the order of or greater than $10^{-6}/\text{cm}^3$ of particles sufficiently penetrating to correspond to 40 Mev protons, if indeed these are the particles which actuate Detector D. Hence by equation (1),

$$I \cdot T = 10^{23} \qquad (2)$$

or

$$\left(\frac{I}{A}\right) \cdot T = 2 \times 10^4 \text{ cm}^{-2} \qquad (3)$$

where A is the area of the surface of the dense atmosphere $= 4.2 \times 10^{18}$ cm^2. If 0.1 fast neutrons per square centimeter per second emerge from the atmosphere and if 0.3×10^{-2} of their decay products are captured in the earth's field then T must be of the order of 10^8 sec, a high but perhaps not inconceivable value.

Slow neutrons inject their decay electrons at lower altitudes and with an efficiency several hundred times as great as that for fast neutrons. Hence they appear to be a much more promising source of trapped electrons having energies of the order of several hundred kilo-electron volts.

Although it seems plausible from the above that outward moving cosmic ray neutrons may make a significant contribution to the intensity of the more penetrating component of the trapped radiation, we do not believe it is likely that their over-all contribution is the dominant one. This view arises from several lines of thought. First, as noted above, we feel that the trapped radiation is probably the direct source of aurorae. If this be so, then it is appropriate to note that the rate of supply of energy from cosmic ray neutron injection is inadequate by perhaps a factor of 10^4 to produce the time-averaged auroral intensity. Second, the energy spectra of electrons and protons from neutron decay are quite different from that observed in auroral displays and that apparently also present in the radiation belt, though the latter point is not yet well established. Moreover, by either scattering or absorption, there is a strong tendency to deplete the low energy end of the spectrum relative to that of the injected particles. Hence, the equilibrium spectrum of neutron-decay products in the reservoir will be even poorer at low energies than at injection, which is already much too depleted to agree with the observations. Third, the entire body of knowledge concerning solar terrestrial relationships (specifically the time association between solar flares and aurorae and magnetic storms) seems to demand the arrival of solar plasma in the outer reaches of the earth's atmosphere. Of course, some of the solar plasma may enter the auroral zones directly and not via the belt of trapped radiation.

The outward projecting 'horns' at high latitudes on the contours of constant radiation intensity (Figs. 4, 5, 6, 7) are of considerable interest. They suggest that the atmosphere is sufficiently heated there so that levels of given atmospheric pressure are several hundreds of kilometers above the corresponding levels at low latitudes [*Mitra*, 1947]. This can presumably happen if radiation leakage from the reservoir is favored there, as indeed it appears to be. The portion of the atmosphere which is ionized is constrained laterally by the magnetic field, and it is possible that there are 'plumes' of ionized terrestrial gas extending out from the earth's atmosphere (T. Gold) like those observed in the sun's corona. Even in neutral gas, some elevation of the levels of constant pressure can be maintained in dynamic equilibrium.

The radiation belt may well be the seat of a distributed 'ring' current encircling the earth, and the perturbations of the belt due to arrival of solar plasma may be directly responsible for magnetic storms. No detailed study of this possibility has yet been made.

Also it may well be that steady leakage of energetic particles contributes significantly to the general heating of the atmosphere at all latitudes.

References

Anderson, K. A., Ionizing radiation associated with solar radio noise storm, *Phys. Rev. Ltrs.*, **1**, 335–337, 1958a.

Anderson, K. A., Soft radiation events at high altitude during the magnetic storm of August 29-30, 1957, *Phys. Rev.* **111**, 1397–1405, 1958b.

Aono, Y., and K. Kawakami, Cosmic rays observed by satellite 1958 alpha, *Rep. Ionosphere Research Japan*, 12, 28–36, 1958.

Bennett, Willard H., Proposed measurement of solar stream protons, chap. 22, pp. 194–197 of *Scientific uses of earth satellites*, University of Michigan Press, Ann Arbor, 316 pp., 1956.

Berkner, L. V., J. G. Reid, J. Hanessian, Jr., and L. Cormier, editors, *Annals of the International Geophysical Year*, vol. VI, pts. I-V, Pergamon Press, London, 508 pp., 1958, a general reference on matters of satellite technology.

Kellogg, P. B., Possible explanation of the radiation observed by Van Allen at high altitudes in satellites, *Nuovo cimento*, in press.

Meredith, L. H., M. B. Gottlieb, and J. A. Van Allen, Direct detection of soft radiation above 50 kilometers in the auroral zone, *Phys. Rev.*, **97**, 201–205, 1955.

Mitra, S. K., The upper atmosphere, p. 407, Royal Asiatic Society of Bengal, Calcutta, 616 pp., 1947.

Singer, S. F., 'Radiation belt' and trapped cosmic-ray albedo, *Phys. Rev. Ltrs.*, 1, 171–173, 1958a.

Singer, S. F., Trapped albedo theory of the radiation belt, *Phys. Rev. Ltrs.*, 1, 181–183, 1958b.

Treiman, S. B., The cosmic-ray albedo, *Phys. Rev.*, 91, 957–959, 1953.

Van Allen, J. A., Study of the arrival of auroral radiations, chap. 21, pp. 188–193 of *Scientific uses of earth satellites,* University of Michigan Press, Ann Arbor, 316 pp., 1956.

Van Allen, J. A., Direct detection of auroral radiation with rocket equipment, *Proc. Natl. Acad. Sci. U. S.*, 43, 57–62, 1957.

Van Allen, J. A., G. H. Ludwig, E. C. Ray, and C. E. McIlwain, Observation of high intensity radiation by Satellites 1958 Alpha and Gamma, *IGY Satellite Rep. Ser. no. 3: Some preliminary reports of experiments in Satellites 1958 Alpha and Gamma,* pp. 73–92, Natl. Acad. Sci., Washington, D. C., 1958. Also *IGY Bull., Trans Am. Geophys. Union,* 39, 767–769, 1958a.

Van Allen, J. A., G. H. Ludwig, E. C. Ray, and C. E. McIlwain, Observation of high intensity radiation by Satellites 1958 Alpha and Gamma, *Jet Propulsion,* 28, 588–592, 1958b.

Vernov, S. N., Special lecture, Fifth General Assembly of CSAGI in Moscow, July 30-August 9, 1958.

Vouk, V., Projected area of convex bodies, *Nature,* 162, 330–331, 1948.

(Manuscript received December 3, 1958.)

Radio Interferometry at Three Kilometers Altitude above the Pacific Ocean

Grote Reber*

Research Corporation
405 Lexington Avenue, New York City

Part I: Installation and Ionosphere

Abstract—The apparent advantages of a Lloyd's mirror interferometer are enumerated. A detailed description is given of the installation which is a variable spacing interferometer whose spacing changes in a smooth and continuous manner from zero to six kilometers during about one half hour. The ionospheric effects which appear as fluctuations are discussed. The ionospheric horizon was observed to be peculiarly high in the east. This may be due to a bulge in the earth's atmosphere near the equator or to the proposed ring current circulating around the equator 5.5 earth radii distant. The radio astronomy of celestial sources will appear in Part II.

Introduction—These experiments were inspired by and undertaken during the spring of 1951 as an extension to those performed by Bolton at Dover Cliff near Sydney, Australia. [*Bolton* and *Stanley*, 1948]. The Lloyd's mirror-sea surface type of instrument appeared to have several advantages over the Michelson-vertical incidence type. These are:

1. A fixed frame of reference in form of the horizon H_1 .

2. Independent rising and setting observations which provide two sets of data and may be interpreted unambiguously into right ascension and declination of the source (see Fig. 2).

3. Possibility of separately observing a weak source very close to a strong source when latter is just over the horizon.

4. Short duration of pattern obtained by choosing a suitable geographic arrangement with only a narrow band of water around the horizon. The situation is rather similar to viewing a pattern through a slit. This will assist point three above.

5. Ability to investigate the fine structure in compound sources. The effective base line of interferometer varies in a few minutes of time from zero, when the source is on the horizon, to twice the height of the observer above the sea when the source is at a few degrees elevation. This amounts to a variable spacing interferometer.

6. Examination of the fine structure of a source in two different planes. The angle of rising from and setting into the sea is different. Thus the fine structure of a source may be

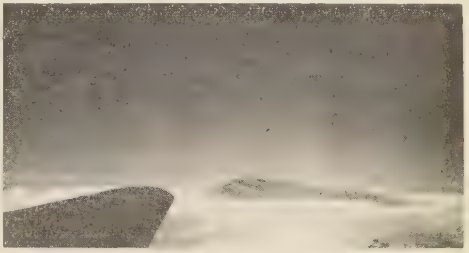

Fig. 1—Haleakala volcano from south at 20 miles; peak approximately one mile above clouds; sea surface an equal distance below clouds

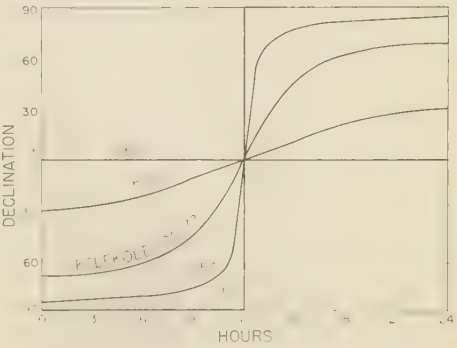

Fig. 2—Elapsed time from rising to setting versus declination for several selected latitudes

* Now at Associated Universities, Incorporated, Green Bank, West Virginia

examined in two different planes, which are, in some cases, nearly perpendicular.

The maps of the oceans of the world were searched for suitable locations. Mauna Kea and Mauna Loa on the island of Hawaii, each with 4.24 km altitude, are most desirable scientifically. However, Haleakala on the island of Maui is the most practical due to the relatively easy access. A view of this volcano is shown in Figure 1. Kole Kole cinder cone upon the summit provides ample area to install a rotating antenna. This cone has been a primary point on the Hawaiian surveying chain since 1866. Its position was redone very accurately in 1950. The marker is at 10,012 ± 4 feet altitude (3,288 m) 20° 42′ 37.79″ N, 156° 15′ 32.36″ W.

Troposphere—Before coming to Hawaii an investigation was made of the refraction of the atmosphere using radiosonde observations. These were extended from time to time and the results published [*Reber*, 1955a]. The refractive index over the sea of the standard atmosphere chosen is given in Table 1. This was obtained by using the first 1000 meters altitude at ocean station Union and attaching thereto the higher levels secured from detailed soundings at Honolulu. The maximum refractive bending occurs in the region of 1750–2000 meters altitude, where it is 0.580 of the earth's curvature. Thus, no duct normally exists, even approximately. However, ducts near this level do form at rare intervals, as demonstrated by 144 Mc/s communication during July and August, 1957, between California and Hawaii. These events were examined and a duct was found near two kilometers altitude all the way from the California coast to west of Hawaii. This rare phenomenon may be neglected for all practical purposes. The stability over the ocean is such that when the source passes through the horizontal H_2, one half of the observations will fall within ±0.014 degree.

TABLE 1—*Standard atmosphere over the ocean near Hawaii*

(Inverse logarithmic above 7000 meters)

Altitude in meters	Refractive index in 10^{-6} above unity	Altitude in meters	Refractive index in 10^{-6} above unity
2	348	3000	209
100	343	3066	207
200	338	3500	197
300	332	4000	185
500	322	4500	175
750	311	5000	165
1000	299	6000	146
1250	288	7000	130
1500	276	8000	116
1750	262	10000	92
2000	245	12000	73
2250	233	13000	64
2500	223	15000	50
2750	216	18000	31

Figure 3 shows the ray paths through the troposphere. Using this figure, the standard atmosphere of Table 1, the geography of Kole Kole, and 6381 km for the radius R of the earth, calculations were made of the expected performance. The results are given in Figure 4.

The ray path reflected from the sea is longer than the direct ray path for two reasons. The geometric path difference is $\Delta 1 = 2R \sin \beta_1 \sin^2 \theta$. The sea-reflected ray passes through a more dense region of the atmosphere where the index of refraction is significantly larger than unity. Thus the sea-reflected ray has a slower velocity and is retarded in comparison with the direct ray. The extra path length due to index of refraction is computed for both rays. Each level contributed a small amount to the excess path length. All levels are summed to get total retardation. The results are plotted in Figure 4d. At near grazing angles this retardation due to the refractive index is the determining factor. Using the above analysis, it is possible to determine very closely where the rays come from below the ionosphere. Considerable effort was expended on the above tropospheric analysis in order to be sure that such variations would be suitably small and predictable. However, as is often the case, other unknown factors may dominate a situation.

Sea surface—At wave lengths from 3 to 15 meters and near grazing angle, the sea is always a smooth mirror, as the height of the irregularities is much less than $\lambda/\sin \theta$. However, due to the curvature of the earth, the reflected ray has a larger solid angle than the incident ray. This divergence weakens the reflected ray according to the relation $D = (1 + \beta_1/\theta)^{-1/2}$. Figure 5 shows the envelope of the interference pattern where the maxima meet the line of $1 + D$ and the minima meet the line of $1 - D$. Consequently

the pattern gradually fades in near rising and out near setting. By using Figures 4d and 5 it is possible to predict the position and magnitude of the various maxima and minima at any chosen wave length. It must be remembered that a 180° phase reversal of the reflected ray occurs at the sea surface. Thus the first maximum appears at a path difference of $\lambda/2$. As the source rises, the pattern speeds up, approaching a period equal to that expected for antennas 6 km apart. By counting the observed fringe numbers, the actual ray path difference can be found. Any discrepancy between actual and theoretical path difference may be attributed to the ionosphere.

Ionospheric fluctuations—When these experiments were undertaken, the picture of the ionosphere seemed to be merely a mirror which receded below the horizon when the vertical incidence critical frequency f_0F_2 was less than a quarter of the observing frequency f. The ionograms taken at Kihei, Maui, during 1944 and 1945 showed that during winter nights the value of f_0F_2 usually hovered between two and four megacycles. Thus it was anticipated that a clear ionosphere would be encountered at 20 Mc/s almost every winter night during the middle 1950's. Unfortunately, this turned out to be a naive idea. When observations were closed in October, 1954, the results had been

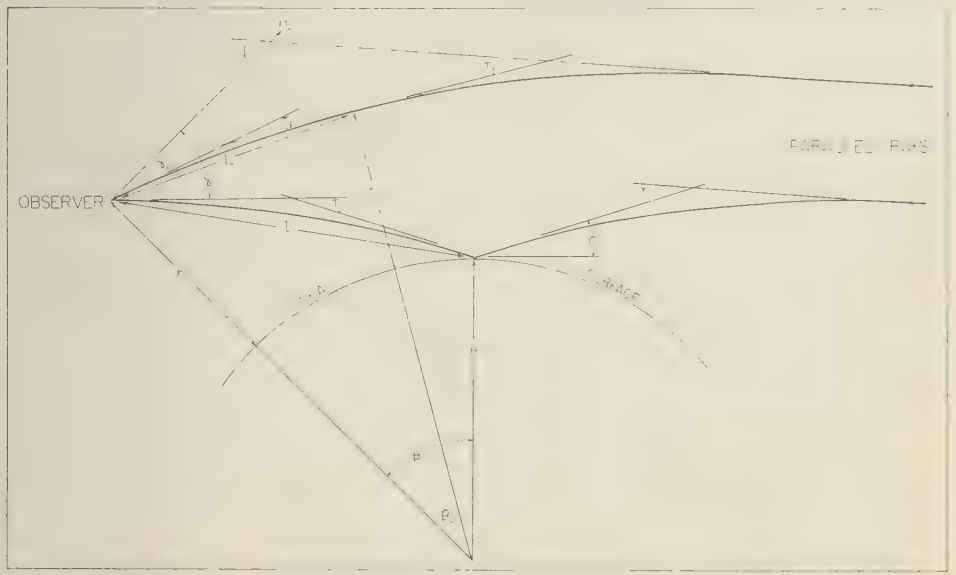

FIG. 3—Path of rays in troposphere; vertical scale above sea surface exaggerated 1385 times

DEFINITIONS OF FIGURE 3

R = radius of earth
h_1 = height of observer
h_2 = height of closest approach of direct way
l_1 = distance from observer to sea reflection point
l_2 = distance from observer to closest approach of direct ray
H_2 = horizontal at observer
θ = angle between reflected ray and sea surface
ϕ = angle between rays from source above troposphere and horizontal at observer
β_1 = angle between vertical at observer and vertical at point of sea reflection
β_2 = angle between vertical at observer and vertical at closest approach of direct ray
τ_1 = angle of refractive bending of reflected ray from above troposphere to sea reflection point
τ_2 = angle of refractive bending of reflected ray from sea reflection point to observer
τ_3 = angle of refractive bending of direct ray from above troposphere to point of closest approach
τ_4 = angle of refractive bending of direct ray from point of closest approach to observer
γ_1 = angle between direction of arrival of reflected ray and horizontal at observer
γ_2 = angle between direction of arrival of direct ray and horizontal at observer

looked at only in a cursory way. It was clear that fluctuations dominated the situation and that the fluctuations had their source in the ionosphere. However, the details of the matter were unknown. Much of the following discussion is the result of ideas relating to the ionosphere and holes therein generated as a by-product of the work in Tasmania.

The ionosphere appears to have considerable similarity to terrestrial clouds. The observations show that when f_0F_2 is greater than f, the sky is thickly overcast and little celestial energy comes through. At best there is a feeble illumination over most of the sky due to forward scattered energy. When f_0F_2 is slightly less than f, a small hole opens overhead, probably a bit north of the zenith near Hawaii. As f_0F_2 decreases, the hole becomes larger and the edge

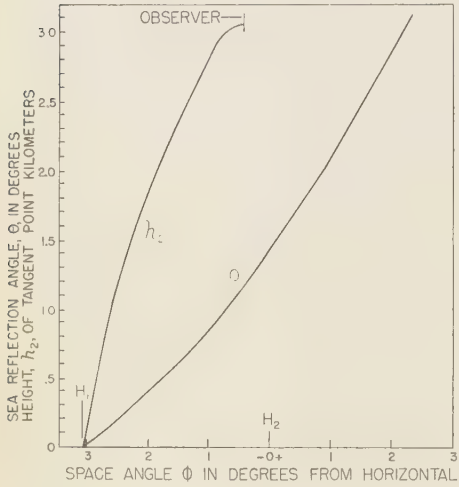

FIG. 4(a)

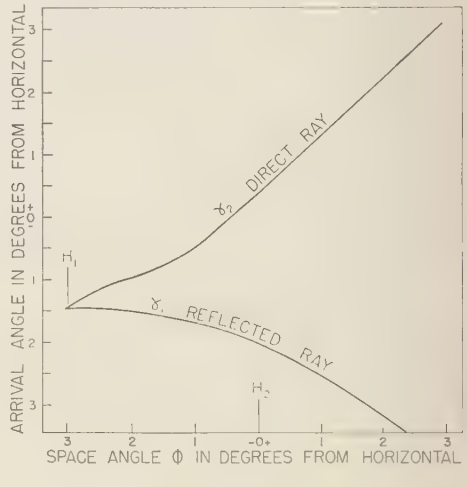

FIG. 4(b)

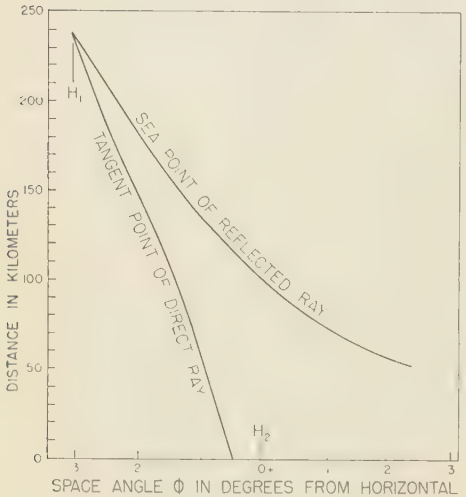

FIG. 4(c)

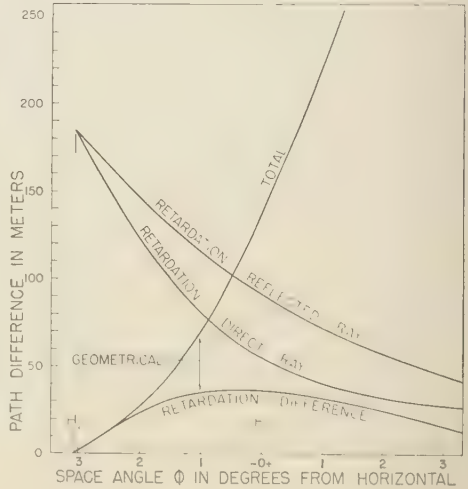

FIG. 4(d)

FIG. 4. Performance of rays in troposphere for top of Haleakala

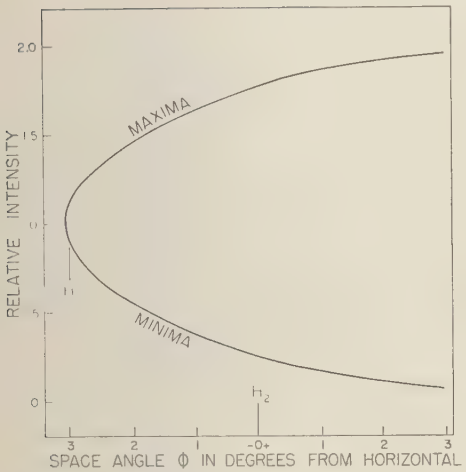

FIG. 5—Envelope of maxima and minima for interference patterns taken from top of Haleakala

descends toward the horizon. The edge forms an ionospheric horizon which is fuzzy and ragged, much like distant clouds. When a visual star sets into such clouds, it appears first to move about erratically, it twinkles, then weakens, changes color, and is finally extinguished. A radio star setting into or rising out of the ionospheric horizon is beset by quite similar phenomena.

High above the horizon only a few large and weak stratifications similar to high cirrus clouds appear. These may be seen as long swells on the records. They merely displace the fringes of an interference pattern, if such is present. As the distortion of the pattern becomes worse, groups of fringes will be compressed and others expanded in an accordion fashion. The amplitude of the pattern will gradually increase and decrease in a fading manner, and the average base level may slowly rise and fall. These three variations are incoherent and independent. The accordion action may be explained by large cylindrical lenses or ridges in the ionosphere which displace the source in position. The fading of pattern is caused by differential changes in the relative amplitudes of the direct ray and sea ray when one or the other is prevented from fully reaching the observer due to scattering in the ionosphere. The changes in base level are merely a more aggravated manifestation of ionospheric back scattering which affects both rays simultaneously. Examination of the traces shows that a fringe of abnormally large amplitude is often preceded or followed by a fringe or fringes of low amplitude. This is to be expected, as the excess energy of the strong fringe must be taken from another place on the wavefront. As the source descends into the horizon, the pattern breaks up into irregular fluctuations. Still lower, the fluctuations weaken due to the increasing amount of cosmic static being reflected back into space. Finally the fluctuations die out and the radio star disappears. No energy is lost by absorption. A change merely occurs from dominant forward to backward scattering. In a few cases, spurious patterns were produced, apparently by reoccurring cylindrical lenses similar to washboard effect. They were readily detected, as the period did not change in the characteristic manner of a true pattern. Good reliable observations may be secured only if the ionospheric horizon is well below the terrestrial horizon.

Reality of the pattern—An interesting psychological situation exists with relation to the breaking up of the pattern. Initially the maxima and minima are well shaped and regular. Then, as the fluctuations begin, the shape of the pattern becomes distorted in that some maxima are large, others small, some spaced close, others apart. As circumstances deteriorate a maximum or minimum will be omitted; then the pattern will recover for a few fringes. Still later the trace degenerates into irregular fluctuations which at times seem to cohere into a pattern for a short period. Finally the fluctuations weaken and die out. Throughout this sequence, the eye is trying to see regularity in randomness. It skips over the part not wanted and pieces together the wanted. I am convinced that the situation is rather similar to forming lines out of irregular detail when viewing Mars. It seems to be a fundamental limitation of interferometric observations near the edge of system sensitivity. This will be true whether the randomness is due to external causes in the ionosphere or to internal causes in the equipment. To assess the matter, several charts of the same source taken under mediocre conditions have been scaled. These are all averaged. The average deviation in position of each fringe δ is computed along with the fringe spacing Δ. A place is usually found where $\delta > \Delta$. At this place it is well to assume that

the positional accuracy of the pattern has become lost in randomness and significant directional results are at an end. However, useful amplitude determinations may usually be carried out far beyond this place.

Observed ionospheric horizon—All observations at the various frequencies were marked for time when the fluctuations began, reached maximum, and died out whether or not any coherent pattern existed on the trace. These were organized on a statistical basis (see Table 2). No significant difference was found between observations of rising in east or setting in west; therefore they are combined. However, there is a marked azimuth effect, and the horizon is lower at the higher frequencies. At 20 Mc/s and 30 Mc/s only night observations are included when the ionospheric horizon should have been below the terrestrial horizon as deduced from f_0F_2 observations at Kihei. At 50 Mc/s and 100 Mc/s day observations also satisfy this condition and are included. No significant difference appeared between night and day. The peculiarly high horizon near the east may be due to a local turbulent effect in the outer parts of the earth's atmosphere [*Reber*, 1955b]. A more probable explanation is that the turbulence is associated with the ring current [*Mitra*, 1952] supposed to be circulating in a toroid in the plane of the earth's equator. This toroid is estimated to have a center radius of 5.5 earth radii and an internal radius of 2 earth radii. If the geometry is even approximately correct, such an ion stream might satisfy the ionospheric horizon observations of Table 2.

TABLE 2—*Ionosphere horizon*
(The angle of source above the horizon and average deviation of observations, both in degrees)

Azimuth	Fluctuations appear	Fluctuations maximum	Fluctuations change to swells	Number of observations
		Twenty Megacycles		
N 23 E	0.0 ± 0.7	3.6 ± 1.5	11.3 ± 3.9	13
NE	3.7 ± 2.3	9.4 ± 3.0	15.3 ± 1.7	9
E 24 N	5.2 ± 1.1	9.6 ± 3.3	16.2 ± 5.5	3
E to S	Total backward scattering			25
				total 50
		Thirty Megacycles		
N 23 E	−0.4 ± 0.2	4.0 ± 1.5	6.1 ± 1.6	17
NE	0.6 ± 0.7	6.1 ± 1.9	10.3 ± 2.2	22
E 24 N	2.1 ± 0.8	6.8 ± 1.3	10.1 ± 1.7	24
E 14 N	4.0 ± 1.5	8.5 ± 1.6	13.8 ± 3.5	30
E 12 S	2.0 ± 0.7	5.3 ± 1.1	9.3 ± 2.6	18
SE	1.6 ± 1.0	4.4 ± 1.4	5.6 ± 1.9	25
				total 136
		Fifty Megacycles		
N 23 E	−0.7 ± 0.3	1.9 ± 0.8	3.7 ± 0.9	29
NE	−0.4 ± 0.4	6.3 ± 0.9	9.1 ± 2.6	28
E 14 N	0.8 ± 0.8	5.1 ± 1.1	9.9 ± 3.6	10
E 12 S	0.3 ± 0.6	4.0 ± 0.9	7.1 ± 2.4	5
SE	0.4 ± 0.6	3.1 ± 1.0	6.1 ± 1.6	3
				total 75
		Hundred Megacycles		
N 23 E	−0.1 ± 0.2	3.7 ± 0.6	5.0 ± 0.8	48
NE	0.0 ± 0.4	4.2 ± 1.0	7.5 ± 1.4	46
E 24 N	1.2 ± 1.0	3.8 ± 0.6	6.2 ± 1.1	10
E 14 N	1.5 ± 0.4	3.5 ± 0.9	6.6 ± 1.9	20
SE	0.7 ± 0.4	4.3 ± 0.8	5.2 ± 1.2	16
				total 140

Ray acceleration in the ionosphere—By counting fringe numbers the total path difference between the direct and reflected rays may be determined. At the horizontal there is always a deficiency in path difference. This descrepancy increases at higher angles and is zero at the horizon. The ionosphere may be considered a sphere concentric with the earth. Thus the sea-reflected ray makes a slightly greater angle with the ionosphere than the direct ray. The refractive index of the ionosphere is less than unity. Consequently, the path length of the reflected ray will be somewhat

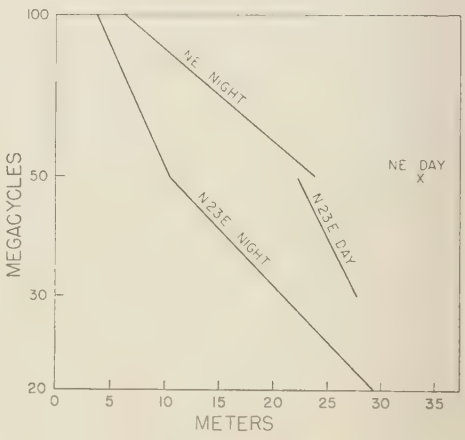

FIG. 6—Ionospheric acceleration for rays arriving from horizontal

less than the direct ray. The phenomenon becomes more pronounced as the two ray paths separate as the source rises. It is quite analogous to the retardation of the sea-reflected ray near the horizon caused by the tropospheric refractive index being greater than unity. The ionospheric acceleration is greater during the day, at lower frequencies, and toward the east, as shown in Figure 6. If these results are associated with the fluctuations, it would appear that the fluctuations are due to something much closer to the earth's surface than the ring current.

The small radio sources, their patterns, and their interpretation will be discussed in Part II.

References

Bolton, J. G., and G. J. Stanley, Source of cosmic radio radiation in Cygnus, *Australian J. of Sci. Research*, Series A, 1, 58–69, 1948.

Mitra, *Upper Atmosphere*, 2nd Edition, Figure 14, pp. 467, 473–5. Asiatic Society of Calcutta, 1952.

Reber, Grote, Tropospheric refraction near Hawaii, *IRE Transactions*, **AP-3**, 143–144, 1955a.

Reber, Grote, Radio astronomy in Hawaii, *Nature*, **175**, 78–79, 1955b.

(Manuscript received August 15, 1958.)

Part II: Celestial Sources

Abstract—Observations were secured at 20, 30, 50, and 100 Mc/s. Fluctuations are greatly reduced by averaging data. Cassiopeia is found to be an elliptical ring 2.3′ by 1.5′ inside a halo, a few minutes of arc in diameter. The halo increases in size and intensity relative to the pairing at lower frequencies. Cygnus contains a nucleus $< 1'$ wide by 2′ long in a halo about 4′ diameter. Hydra contains a source about 5′ wide. Observations of the sun confirm that the maximum obscuration is toward the east. Surges from Jupiter at 30 Mc/s are discussed.

Apparatus—Observations were made at 20 Mc/s from March 24 through April 28, 1953. The antenna was a pair of three-element Yagis, side by side, spaced ¾ wavelength between centers and ½ wavelength above ground. Observations were made at 30 Mc/s from July 20, 1953 through February 8, 1954. The antenna was a pair of five-element Yagis, side by side, spaced 1¼ wavelengths between centers and ¾ wavelength above ground. Observations were made at 50 Mc/s from March 29 through June 7, 1954. The antenna was a pair of horizontal rhombics, one above the other, spaced ¼ wavelength and 1½ wavelengths above ground. Each leg was 2½ wavelengths long. Observations were made at 100 Mc/s from June 15 through October 13, 1954 and November 20, 1957 through March 1, 1958. The same physical antenna made all dimensions twice as large in wavelengths. All antennas used horizontal polarization. This removed difficulties from Brewster angle absorption which affects only vertically polarized radiation. Helical antennas are not suitable for a sea interferometer because of the reversal of polarization sense at sea reflection. The above antennas were supported by a wooden framework mounted on a steel turntable which runs on a track 82 ft in diameter.

The receiver is a simple total power apparatus and is susceptible to long term drift. Provided the trace remains on scale during an observation, the drift is not important. Only short-time comparisons are desired and the general background is neglected. The bandwidth was 50 kc/s at 20 Mc/s where some difficulty was encountered finding clear channels even this wide. At 30, 50, and 100 Mc/s the bandwidth was 100 kc. The integrator is three stages of RC with ascending orders of impedance. Each stage RC = 1 sec. This is the same kind of system as was used in Tasmania [*Reber* 1958a] and provides markedly better discrimination against very short transients. The highest order of fringe measured is 130 with a period of about 14 sec. Thus, the ratios of frequency/bandwidth $\gg$ 130 and total RC $\ll$ period insure that the observed patterns are not materially affected by the apparatus constants.

Techniques—The observations were not confined to, but mainly conducted upon six prominent sources chosen over a variety of declinations. The celestial positions were taken from the literature [*IAU* catalog, 1957], Table 3 gives the computed elements at rising for observations from Kole Kole. All traces of a given source which showed a significant pattern were

TABLE 3 —*Elements of celestial sources*

Source	Cassiopeia	Cygnus	Taurus	Virgo	Hydra	Centaurus
Declination	+58°32′	+40°36′	+21°59′	+12°40′	−11°55′	−42°46′
Right Ascension	23h 21.2m	19h 57.7m	05h 31.5m	12h 28.3m	09h 15.8m	13h 22.5m
Rising azimuth east from north	21°02′	45°48′	65°06′	75°24′	101°35′	134°59′
Time in minutes from horizon H_1 to horizontal H_2	34.1	18.5	14.4	14.0	13.4	20.3
Celestial position angle in degrees east from north						
rising	140–320	121–301	114–294	112–292	110–290	116–296
setting	40–220	59–239	66–246	68–248	70–250	64–244

combined. The low order fringes were individually scaled. High order fringes were scaled every fifth or tenth fringe. The amplitude of high order fringes was taken as the average of three fringes centered upon the desired one. The standard error in both amplitude and position was computed for each scaled fringe. Consequently any smooth curve which passes through two thirds of the standard error bars should be significant. This process greatly reduces, but does not eliminate, the ionospheric fluctuations which are presumed to be random in phase and amplitude.

As explained in Part I, the system is a variable spacing interferometer. When the source is on the horizon, the height of the observer is zero. As the source rises, the effective height of the observer gradually increases to 3.066 km when the source reaches about three degrees elevation. Thus the spacing of the interferometer changes from zero to 6 km in about one half-hour. The source makes a pattern which starts out slowly. The period of the pattern gradually decreases through all possible values and ends quite fast. At any given frequency of observation the ratio of pattern periods changes by a factor of ten or more.

If the amplitude of pattern goes through a minimum during this apparition, the cause is two small sources which partially cancel each other. Their spacing is equal to an odd number of half periods of the pattern at the minimum. Their relative intensities may be determined from the depth of the minimum. If the pattern goes through a maximum, the two small sources are spaced an even number of half periods of the pattern at the maximum. If the pattern changes from a large amplitude to a small amplitude in a few fringes, it means that a large part (halo) of the source has been resolved, leaving only the nucleus. The ratio of amplitudes before and after the change determines the ratio of intensities of halo to nucleus. If the data is sufficiently accurate, a source may be sliced up into several different levels of intensity and width. When these are recombined, a detailed picture is secured of the intensity cross section. A trial and error process is used. The limits within which a given proposed model can be made to fit the observations are usually quite narrow. The intensity is on a relative basis at a given frequency. It is the peak intensity of the shape curve. The shape curve is chosen [*Wild* and *Sheridan*, 1958], as one period of a sine wave. The width is the angle between half intensity points on the shape curve. Time on all charts and drawings advances from right to left. The drawings are not corrected for divergence. This was done only for the particular fringes used in the analysis. Diagonal crosses are single observations.

Cassiopeia—Figure 7 shows the results at 20, 50, and 100 Mc/s for rising. Only three daytime observations showing any pattern were secured at 30 Mc/s. These confirm but add little to the above figure because of severe fluctuations. Fig-

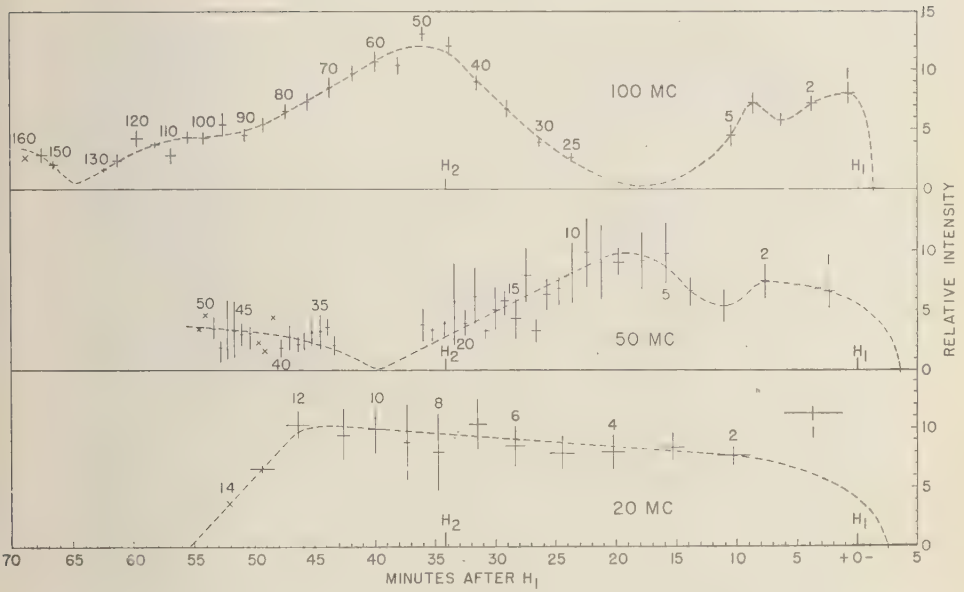

FIG. 7—Relative intensity versus time for selected fringes of Cassiopeia rising

ure 8 shows the results at 30, 50, and 100 Mc/s for setting. No 20 Mc/s observations were secured because the source set during the day. The 100 Mc/s rising pattern of Figure 7 is most interesting. The amplitude goes through a minimum near 18 minutes (of time), a maximum near 36 min. and a minimum near 65 min. The fringes spacings are respectively 4.6′ (minutes of arc), 2.3′, and 1.5′. At 18 min. the two sources are offset one half fringe so that they cancel; at 36 min., one full fringe so that they add; and at 65 min., 1½ fringes so that they cancel again. The analysis of Figures 7 and 8 is as follows.

Rising:

100 Mc/s: Halo is <3.4′ wide. Nucleus is a pair, each 1.8′ wide spaced 2.3′ on centers. Atop pair are nibs, <0.5′ wide spaced 2.3′ on centers. The pair have equal intensities within 5 pct, the nibs are equal within 40 pct. The ratio of intensities of Halo:Sum of pair:Sum of nibs is <0.1:1.0:0.1.

50 Mc/s: Halo is 6′ wide. Nucleus is a pair, each 1.8′ wide spaced 2.2′ on centers. The pair have equal intensities within 25 pct. The ratio of intensities of Halo:Sum of pair is 1.3:1.0.

30 Mc/s: No significant data.

20 Mc/s: Halo is 9′ wide. The pattern fringes are spaced too far to detect the nucleus.

Setting:

100 Mc/s: Halo is 4.3′ wide. No detectable nucleus, as halo may be the same as nucleus.

50 Mc/s: Halo is 5.5′ wide. Nucleus 3.0′ wide. Ratio of intensities of Halo: Nucleus is 0.85 : 1.0.

30 Mc/s: Halo is 7.5′ wide. Nucleus 3.0′ wide. Ratio of intensities of Halo : Nucleus is 1.2 : 1.0.

20 Mc/s: No observations.

These detailed conclusions may represent an over-extrapolation of the data. However, the fundamental properties are beyond doubt. These are a nearly equal pair inside a halo. The halo increases in size and intensity relative to the pair at lower frequencies. Small dips may be seen in the low order fringes of Figures 7 and 8. At 20, 30, 50, and 100 Mc/s, these occur at rising when the fringe spacing is 14.0′, 13.0′, 16.1′, 12.2′; at setting—, 18.4′, 16.8′, 15.2′. If these small dips have significance, they may be interpreted as a small unrelated source about 15′ north of Cassiopeia A. Sample recordings are shown in Figure 14.

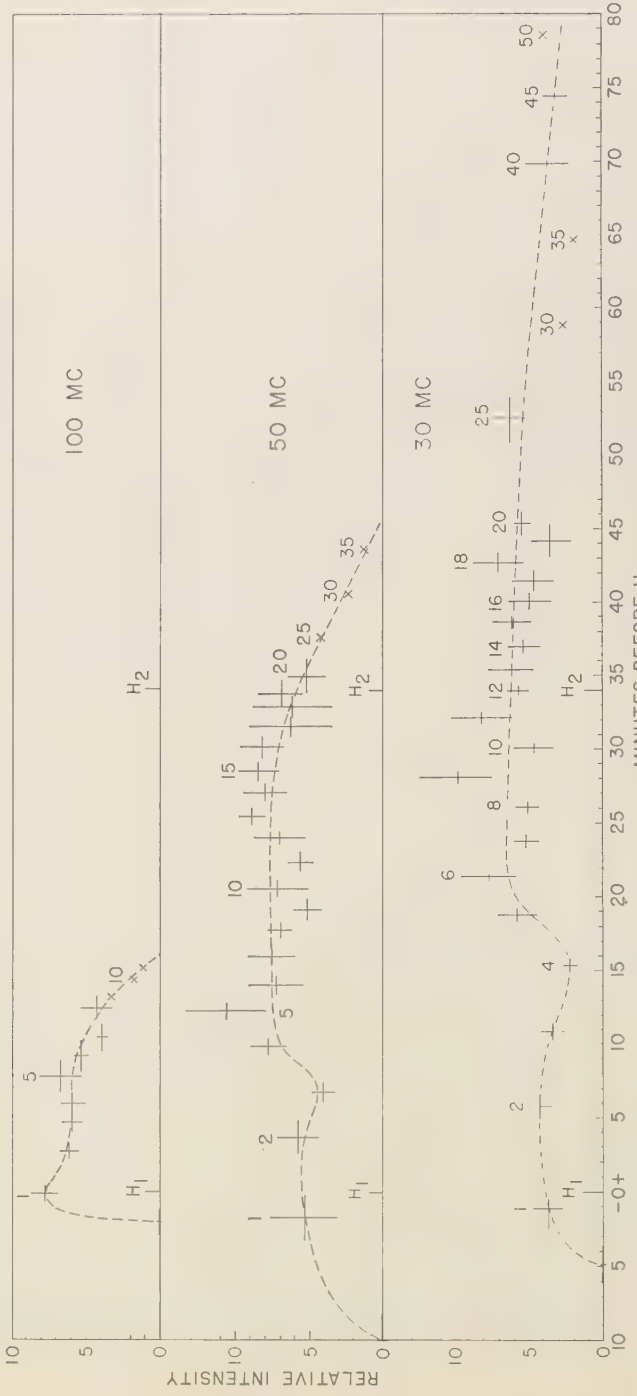

FIG. 8—Relative intensity versus time for selected fringes of Cassiopeia setting

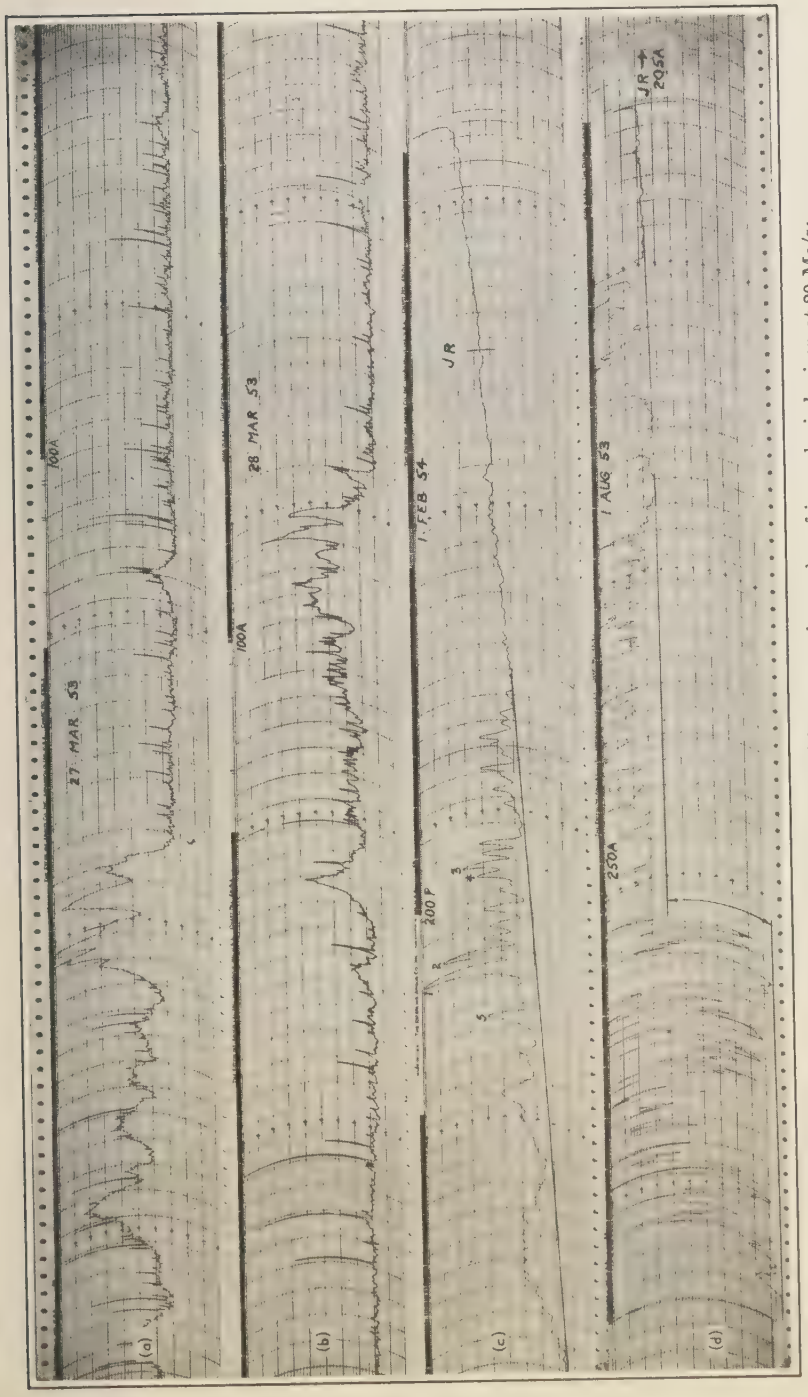

FIG. 9—Sample recordings; (a), (b) Cygnus rising over a sharp edge of ionospheric horizon at 20 Mc/s; (c), (d) Jupiter surges at 30 Mc/s; Jupiter rises at JR

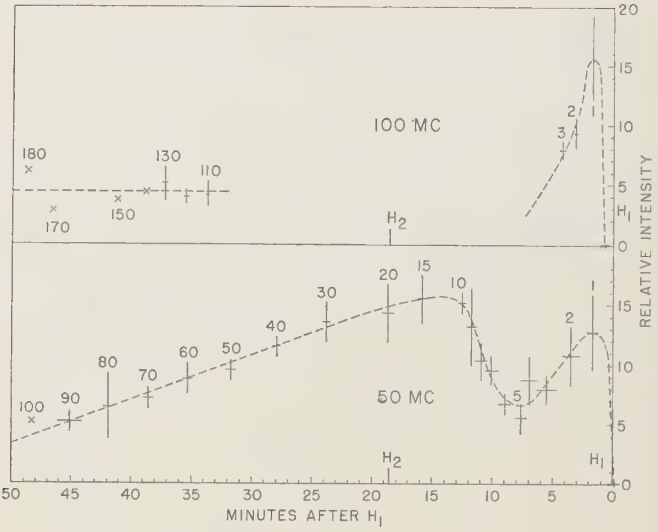

FIG. 10—Relative intensity versus time for selected fringes of Cygnus rising

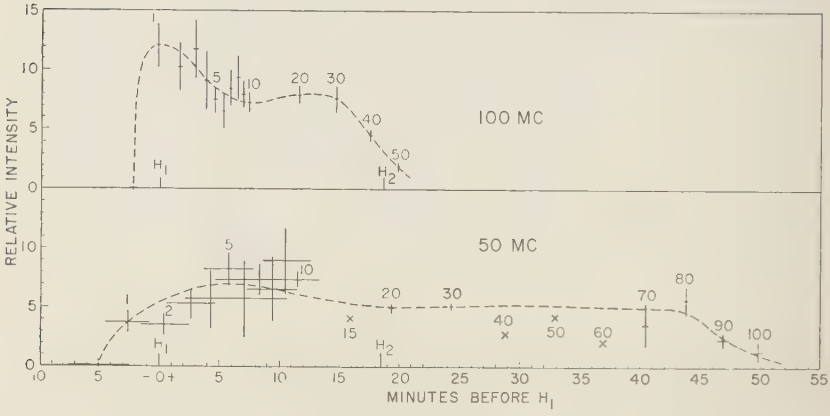

FIG. 11—Relative intensity versus time for selected fringes of Cygnus setting

Cygnus—Considerable effort was expended on this source at 20 and 30 Mc/s. No significant patterns were secured even during the most auspicious hours from midnight to dawn because of severe fluctuations. On March 27 at 20 Mc/s the ray path came abruptly over a sharp edge of an ionospheric ridge with a high gradient of refractive index. A short and very fast pattern developed for six cycles as shown in Figure 9a. Cygnus was 6.6° above the horizon and $f_0F_2 =$ 4.8 Mc/s at Kihei. No sporadic E was present. Such an apparition occurs from time to time. Only this once were both ray paths sufficiently stable to produce a pattern. Usually the phenomenon appears merely as the sudden onset of fluctuations as in Figure 9b. During two-20 Mc/s observations, the distant atmospherics were strong at first and the base line of trace was straight. Then as the atmospherics died, the fluctuations began weakly and built up. Obviously this is complete control by the ionosphere, as the maximum usable frequency dropped and

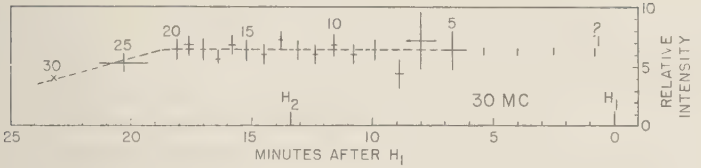

FIG. 12—Relative intensity versus time for selected fringes of Hydra rising

passed through the operating frequency. The Kihei values of f_0F_2 were respectively 3.8 and 4.5 Mc/s at the time the atmospherics died. In both cases Cygnus was about five degrees elevation above the horizon. The lack of pattern on Cygnus is not related to particular nights because often a significant pattern was secured from Cassiopeia on the same night. Figures 10 and 11 show the results at 50 and 100 Mc/s for rising and setting respectively.

Near the rising azimuth a cinder cone called Red Hill, about a half mile away, just touches the horizon. The width of the obstruction is about 300 ft. Apparently it accounts for the marked dip in the 50 Mc/s patterns and complete loss of middle fringes in the 100 Mc/s pattern. The low order fringes come over the top, while the high order fringes come around the south side of cone. Considering this limitation, the data may be construed as

Rising:
100 Mc/s Halo $<4'$ wide; nib $<1.0'$ wide. The ratio of intensities 8:1.
50 Mc/s: Halo $4.0'$ wide; center $2.8'$ wide; Nib $<1.0'$ wide. The ratio of intensities is 5:6:1.

Setting:
100 Mc/s: Halo $3.8'$ wide; center $1.8'$ wide. The ratio of intensities 3:1.
50 Mc/s: Halo $3.9'$ wide; center $2.2'$ wide. The ratio of intensities 2:1.

The manner in which the amplitude builds up, when the setting pattern first appears, suggests that the pattern is coming out of a null, even though no pre-null fringes may be seen. If this is true, the small source could be a pair with a center-to-center spacing of $1.0'$ and $1.2'$ respectively at 100 Mc/s and 50 Mc/s.

The Cygnus data is markedly poorer than the Cassiopeia data. About all that can be said with certainty is that a pair of coincident sources exist. The small one is probably the colliding galaxies. It seems to be enveloped in a halo. The pictures at 50 and 100 Mc/s appear quite similar. In both cases the structure appears sharper in the rising direction. Sample recordings are shown in Figure 15.

Taurus and Virgo—A wide variety of observations was made as noted in Table 2. Only fluctuations were secured. Usually these began when the sources were considerably above the horizon. About 10 additional observations above the 97 tabulated produced only straight lines. These may be interpreted as complete backward scattering into the sky.

Hydra—At 30 Mc/s fifteen rising observations produced patterns with from five to 19 fringes. In no case were any of the first four fringes visible due to obscuration toward the east. The results are shown in Figure 12. The source is a single object $4.7'$ wide. The small standard errors suggest that no appreciable systematic changes in amplitude were encountered from day to day [*Slee*, 1955]; if so, they were markedly less than the fluctuations. At 50 Mc/s only weak fluctuations were encountered.

Puppis, Fornax, and Centaurus—These sources all rise near SE and set near SW. They are treated in a combined fashion in Table 2. Not even fluctuations were found at 20 Mc/s due to complete backward scattering. At 30, 50, and 100 Mc/s weak fluctuations but no coherent patterns were found on two thirds of the traces. The remaining ones were blanks for the same reason.

Sun—Attempts to detect the sun at 30 Mc/s were failures because this object was below the system sensitivity. A few observations at 50 Mc/s confirmed its existence but the traces were quite weak. It produced long swells roughly ten minutes apart. Rising and setting observations were quite similar. These long swells are probably a diffraction effect [*Rice*, 1954]. The sun may be considered an extended source rising over an obstacle in the form of horizon. This

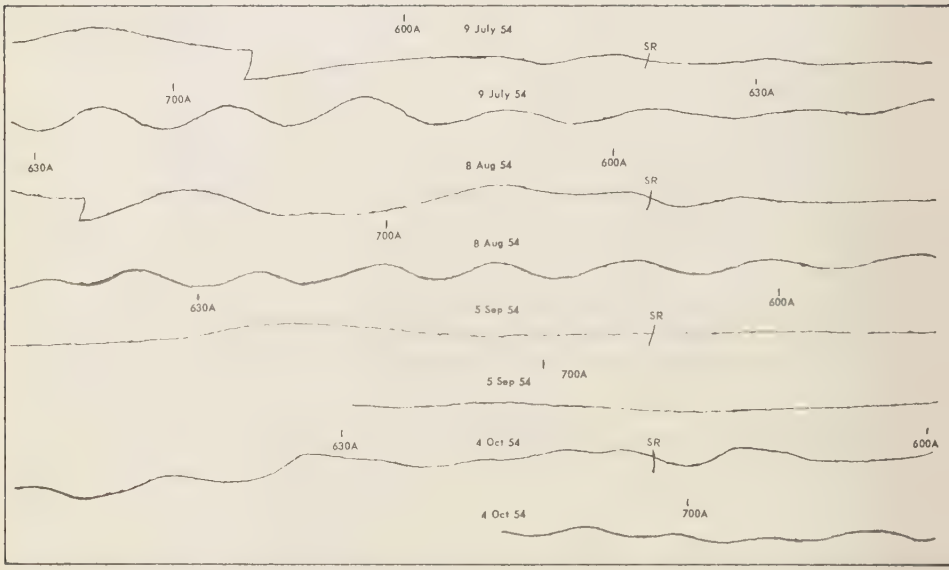

FIG. 13—Recordings of 100 Mc/s sunrise at azimuths 64°, 72°, 82°, 94° east of north; center of optical sun on horizon at SR

concept seems to apply to the sun only. No attempt has been made to assess the matter in a quantitative manner due to the great complexities. No solar transients or patterns due to bright solar spots were found.

A long series of solar observations was made at 100 Mc/s. The same long swells were encountered but were spaced about half as far apart. These observations were near solar activity minimum. Consequently, the solar background was very nearly the same for months at a time, and it was possible to test the idea of obscuration toward the east by noting what happened as the sun's apparent position moved south from summer to winter. Figure 13 shows four traces taken when the sun rose at different azimuths. Note the late start, short apparition, and very weak pattern when the sun rose near the east. This confirms the obscuration already inferred from the fixed celestial sources. The situation at setting was similar to that at rising (Figs. 14 and 15).

Jupiter—All 20 Mc/s observations were made while Jupiter was far below the horizon. At 30 Mc/s various cases of a peculiar interference were encountered, mostly when observing Taurus. Two examples are shown in Figure 9c and d. The sound was a smooth hiss which varied through wide ranges in an irregular manner. No snaps, pops, or cracks were heard. Thus there were no sharp wavefronts, which is confirmed by the gradual increase and decrease of the surges. The sound was quite similar to solar transients except that these occurred between midnight and dawn. At first it was thought that a rapidly fading carrier had come on the observing frequency. However tuning the receiver showed the interference to be a continuum impossible to remove by merely changing frequency. Also a beat oscillator failed to produce any whistle even on strong examples. Changing the antenna direction showed that the energy was coming from the east where very few people live. Likewise it was impossible to think of any man-made device which would produce this kind of a disturbance free from low pitch sounds associated with mains frequency or commutators. One visitor remarked that the sound was much like the sound of a small boat going through choppy waves. The phenomenon was quite mystifying. Fortunately, this difficulty was infrequent. When the discovery of transient radiation from Jupiter was announced [*Burke* and *Franklin*, 1955], I recalled these circum-

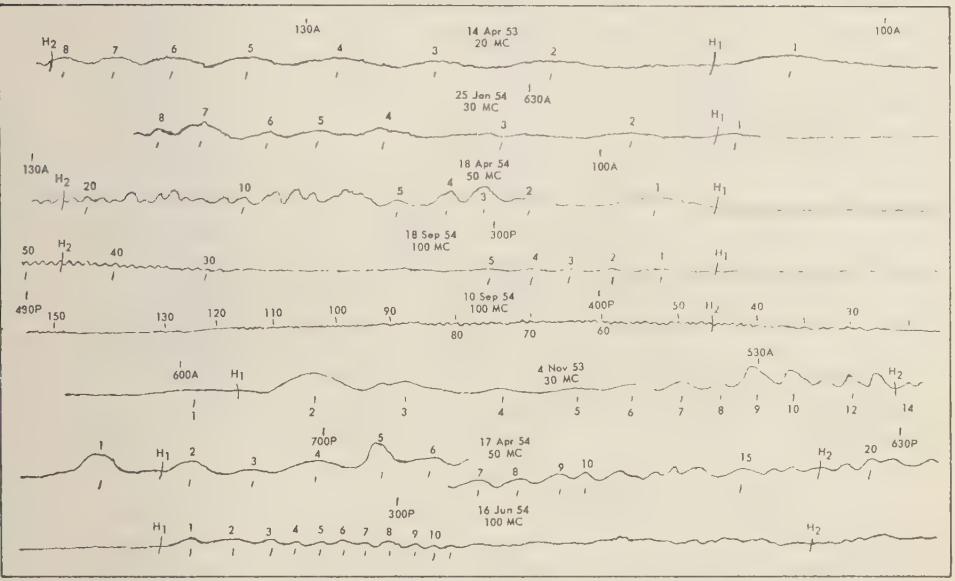

FIG. 14—Sample recordings; (a), (b), (c), (d), (e) Cassiopeia rises, (f), (g), (h), Cassiopeia sets

stances. All major occasions when Jupiter was in an auspicious position are given in Table 4. The intensity is given as an average of the five largest surges in terms of the average fluctuations produced by Taurus. This assumes that the two separate radiations were similarly affected in their transit through the earth's atmosphere. No phenomenon remotely similar to this was ever encountered at 20, 50, or 100 Mc/s.

TABLE 4—*Probable radiations from Jupiter*

Date	GCT time	Intensity times Taurus
8/1/53	1238–1258	≫30
8/15/53*	1114–1117	10
8/17/53	1210–1221	8
8/17/53	1240–1300	12
8/27/53	1104–1117	7
9/16/53	1433–1452	9
9/24/53*	0829–0831	8
11/11/53	1228–1301	>35
11/28/53	1417–1429	6
1/14/54	0122–0133	8
2/1/54	2356–	
2/2/54	0004	11
2/2/54	2347–2354	2

*Observation doubtful because Jupiter was a degree or less below the horizon

100 Mc/s Observations of Winter 1957-8—These are mostly rather poorer than those taken during the summer of 1954. Useful patterns were secured on Cassiopeia rising and setting, also Cygnus setting. The results confirmed the data described above insofar as an interpretation is possible. Even though poorer with larger standard errors, the second group, when combined with the first group, produced somewhat smoother curves than those shown in Figures 7, 8, and 11 because the randomness is still further reduced by averaging larger numbers of observations.

The ionosphere was exceptionally stable between 4 a.m. and 5 a.m. on November 22, 1957. This one observation of Cassiopeia setting produced true and unmistakable fringes Nos. 51–35 and Nos. 13–1 with a gap centered on about fringe No. 22. The high order fringes are quite weak, but their presence demonstrates that Cassiopeia has very small components. These cancel near fringe No. 22. A complete analysis gives an equal pair each 0.5′ wide, spaced 1.5′ on centers inside a halo 4.9′ wide. The ratio of intensities of Halo: Sum of pair is 10:1. Thus

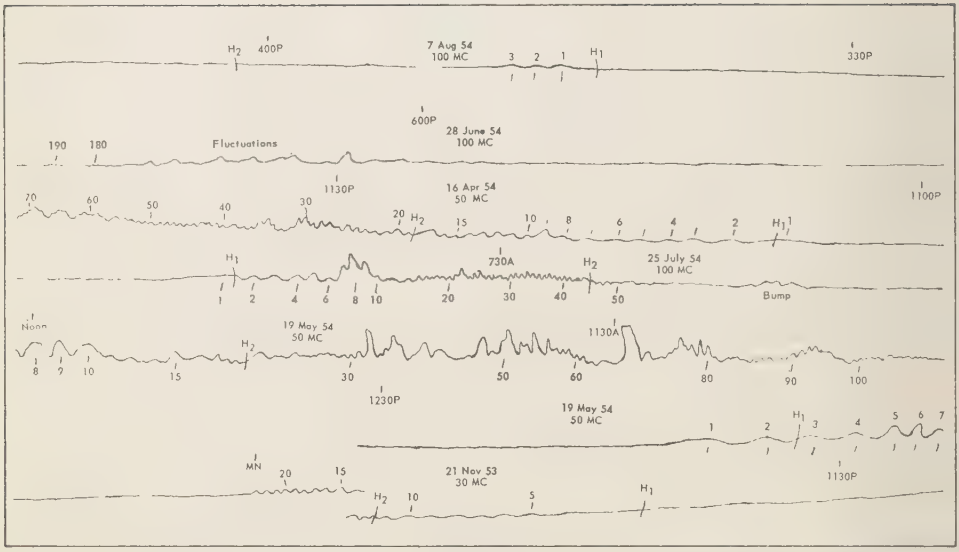

FIG. 15—Sample recordings; (a), (b), (c) Cygnus rises, (d), (e), (f) Cygnus sets, (g) Hydra rises

Cassiopeia is double in both cross sections. Apparently there is some kind of an elliptical ring inside the halo with the halo extending more in the 40°-220° position angle.

Only weak fluctuations were secured on 12 observations of Cygnus rising. Two out of 14 traces secured on Taurus and Virgo produced weak fluctuations. The remainder are blanks due to total obscuration. Eight traces on weaker sources farther south were all blanks. Only five of 17 sunrise observations provided traces on which the solar background could be measured. These confirmed the results of 1954. The remaining traces were badly cut up by solar transients due to the present high solar activity.

Spread F—The spread *F* [*Reber* 1958b] during winter of 1957–1958 at solar activity maximum is less than one tenth that during summer 1954 at solar activity minimum. However the cosmic static traces during 1957–1958 are nearly all far weaker and poorer. Even the fluctuations are weaker. This is directly contrary to the original observations that the fluctuations were proportional to spread *F* magnitude. My present opinion is that the 1957–1958 fluctuations are introduced far out beyond the *F* layer by irregularities in the ring current. Near solar activity minimum the ring current was feeble or absent. Thus the sky was clearer. When a weak burst of solar particles appeared, they penetrated down to the *F* layer causing spread *F* and the associated strong fluctuations. Near solar activity maximum the ring current is strong and nearly continuous. This shields the low latitude regions of the ionosphere from the effects of bursts of solar particles and spread *F* is reduced. Also the ring current keeps out the cosmic static due to much greater back scattering.

Addenda—In addition to the natural limitations imposed by the ionosphere, a large amount of man-made electrical disturbance was encountered. This was due to the exposed position of the observer and the fact that the technique required looking at the horizon. The two main centers of disturbance were the local industrial area of Kahului - Puunene at a distance of 20 miles NNW, and Honolulu - Pearl Harbor at a distance of 120 miles WNW. Consequently the quadrant from north to west was frequently unusable. Radio astronomy observatories should not be located atop high mountain peaks.

Local atmospherics are hardly known. However, much distant atmospherics were encountered at 20 Mc/s especially over quadrant southeast to southwest.

The continuously variable spacing interferometer is a powerful instrument for measuring the fine structure details of celestial radio sources. Unfortunately this particular application leaves considerable to be desired. The situation could be greatly improved by observing at a higher latitude. Also a vertical incidence type of equipment with one collector on a continually adjustable track would be very desirable.

References

Burke, B. F., and K. L. Franklin, Observations of a variable radio source associated with the planet Jupiter, *J. Geophys. Research,* 60, 312–317, 1955.

International Astronomical Union, *Transactions,* IX, Commission 40, 579–581, 1957.

Reber, Grote, Between the atmospherics, *J. Geophys. Research,* 63, 109–123, 1958a.

Reber, Grote, Solar activity cycle and spread *F, J. Geophys. Research,* 63, 869, 1958b.

Rice, S. O., Diffraction of plane radio waves by a parabolic cylinder, *Bell Syst. Tech. J.* 33, 417–504, 1954.

Slee, O. B., Apparent intensity variations of the radio source Hydra-A, *Australian J. Phys.,* 8, p. 498, 1955.

Wild, J. P., and K. V. Sheridan, A swept frequency interferometer for solar radiation, *Proc. Inst. Radio Engrs.,* 46, 168–169, 1958.

(Manuscript received August 15, 1958.)

A Study of the Morphology of Ionospheric Storms

S. MATSUSHITA*

High Altitude Observatory
University of Colorado
Boulder, Colorado

Abstract—A study was made of the variations of the maximum electron number density in the ionospheric $F2$ layer during magnetic storms. Fifty-one strong storms and 58 weak storms were studied. The data were collected during the ten-year period 1946–1955, at 38 ionospheric stations between 60.4°N and 60.4° geomagnetic latitudes. The ionospheric stations were put into eight zones according to their geomagnetic latitudes. Storm-time variations in the maximum electron number density (Dst) and disturbance daily variations during each six-hour period (DS) were obtained for each of the eight zones.

The Dst variation in higher middle-latitudes was characterized by an initial short increase followed by a much larger decrease, the amplitude of the decrease being accentuated in summer. In the equatorial region, however, the phase of the variation was the opposite of that in higher latitudes. There was generally an increase after an initial short decrease, with no seasonal effect. The Dst variation at intermediate latitudes resembled that at higher latitudes in summer and that at the equatorial region in winter, with the average over all seasons being relatively flat.

The diurnal component of the DS variation for each six-hour period indicated, on the harmonic dial, a change in the clockwise sense except in the equatorial region. The maximum amplitude of the diurnal component of the mean of the DS variations showed a gradual decrease from higher toward lower latitudes, with a subsequent increase in the equatorial region. A remarkable change of the phase of the diurnal component also occurred from higher toward lower latitudes.

1. INTRODUCTION

It has long been known that the ionospheric $F2$ layer changes its density and height during magnetic storms. In 1935, *Appleton* and *Ingram* [1935] reported that the $F2$ layer critical frequency ($foF2$) at Slough, England, was reduced during magnetic storms, while conversely *Berkner* and others [1939, 1940] found that $foF2$ at Huancayo, Peru, increased with increase of geomagnetic activity. Since 1949 more detailed investigations of these phenomena have been carried out by many researchers. *Appleton* and *Piggott* [1950, 1952] found changes of the noon values of $\Delta foF2$ (average departures of $foF2$ from monthly mean noon values) during the period from four days before to four days after "the day of major depressions of $foF2$ associated with magnetic storm conditions." They also found changes with latitude and season, and discussed the diurnal control of ionospheric storminess. *Martyn* [1953] obtained the disturbance daily variations (SD) and storm-time variations (Dst) of $\Delta foF2$ and $\Delta h'F2$ for seven ionospheric stations and tried to explain the results by the drift theory ($h'F2$ is the $F2$ layer minimum virtual height, and $\Delta h'F2$ means departures of $h'F2$ from monthly mean values). Several Japanese workers also contributed greatly in this field. *Fukushima* and *Hayasi* [1952] showed seasonal changes in Dst ($\Delta foF2$) variations for Japanese ionospheric stations. They concluded that in middle latitudes the $F2$ electron density during disturbances decreased in local summer and increased in local winter. *Uyeda* and *Arima* [1952] investigated latitudinal changes of the storm-time variation of $foF2$ and $h'F2$ or $hpF2$ (the height of the maximum density of the $F2$ layer) and classified them for individual storms into four different types of northern, southern, polar, and equatorial maximum variation. However, the average latitudinal changes of storm-time variation seem to occur in the way described by Appleton and Piggott, and by Martyn. Disturbance daily variation (SD) and storm-time variation (Dst) of $\Delta foF2$ and $\Delta h'F2$, and their seasonal and latitudinal changes, were also investigated by *Obayashi* [1952, 1954], *Sinno* [1953, 1954,

* On leave from Kyoto University, Japan

1955], *Matsushita* [1953, 1954], and *Nagata* [1954].

Instead of studies of the average behavior of several or more storms, some workers [*Meek*, 1952; *Lawrence*, 1953; *Sato*, 1956, 1957; *Miya* and *Wakai*, 1952] have analyzed single storms or a few selected storms. This procedure is essential for studies of ionospheric storms in the auroral zone and over the polar cap. However, in order to know the general behavior of ionospheric *F*2 storms in middle and low latitudes, we must analyze a large amount of data taken at many stations in the world. As mentioned above, various people have made morphological studies of *F*2 storms. Their results, however, are not always consistent. This seems to be due to having insufficient data from too few stations.

Here we have studied *foF*2 hourly data collected over a ten-year period from 38 ionospheric stations, a much larger volume of data than has been studied previously. Accordingly the results here may be more reliable, and may give a more consistent picture of *F*2 density changes during storms. Special efforts are also made in this report to obtain the detailed behavior of the disturbance daily variation. The virtual height *h'F*2 or a simply calculated *hpF*2 are not treated in this report, because these are quite unreliable, particularly during storms. Various results concerning the apparent height change obtained by the above-mentioned workers are not reliable for the purpose of interpretation of true height variations during storms. The morphological study of height variation must be made on the basis of true height values found by a method such as *Budden's* [1954].

2. Method of Analysis and Data Used

2.1 *Method of analysis*—First of all, we must define an ionospheric storm; in other words, we must decide which *foF*2 values should be selected from all the hourly *foF*2 data as representing ionospheric *F*2 storms. Any large deviations of *foF*2 from its average value, regardless of the geomagnetic situation, might be considered an ionospheric storm or disturbance. *Mednikova* [1957] studied storms in this way. However, it is difficult to decide what value of deviation of *foF*2 may be considered as being due to storms, because this value depends on time of day, season, and latitude; and once this is decided, it is embarrassing to discuss the causes of the ionospheric storm. As a second method, the five international magnetically disturbed days of each month might be selected as ionospherically disturbed days. Differences of *foF*2 on these days from the mean *foF*2 values on the international five or ten quiet days would then give the amount of *foF*2 change due to storms. In this method, however, strong and weak storm effects are mixed, and also separation of local time and universal time variations is difficult.

The following method, which seems to be better than the preceding two, was used in this study. First, an ionospheric storm was defined as an ionospheric variation accompanied by a geomagnetic storm. In order to know reliably the starting time of the geomagnetic storms, only storms with sudden commencement, SC, were selected. Since we had only hourly values, the starting time of the ionospheric storm was considered to be the hour closest to the SC time; it was treated as zero hour (0 h) in the storm time.

To obtain the deviation of *foF*2 during storms from the normal value, the usual index $(f - \bar{f})/\bar{f}$ was used, where f is *foF*2 during the storm, and $\bar{f}$ is the monthly median value (including storm days) of *foF*2 corresponding to the local time of f. Since the maximum electron number density N of the *F*2 layer is proportional to the square of the critical frequency, $200\,(f - \bar{f})/\bar{f}$ is approximately $(N - \bar{N})/\bar{N}$ in per cent, where $\bar{N}$ is the mean value of N. All final results in this study are expressed in terms of *change in the maximum electron number density in per cent, derived from statistical calculation of* $(f - \bar{f})/\bar{f}$.

Let the suffixes i, j, and k indicate the storm time, the storm number, and local time, respectively; we may put $(f_{ijk} - \bar{f}_{ijk})/\bar{f}_{ijk} = \Delta_{ijk}$. In this study, ionospheric variations during the 72 hours following the storm commencement were analyzed and compared with those during the six hours preceding the storm. Hence, the suffix i varies from -6 h to $+71$ h. As will be shown, the storm number j varies from one to 51 for strong storms, and from one to 58 for weak storms. Local time k goes from 0 h to 23 h. These Δ_{ijk} variations contain both the universal time and the local time variations. The former is called the storm time variation Dst and the latter, the disturbance daily variation DS. (For this notation, see

paragraph 3.2.) These two variations had to be separated.

The local times of the SC's of the magnetic storms are rather evenly distributed over the day, since the number of storms is large (51 strong and 58 weak storms). By forming the sum of Δ_{ijk} over j (storm number) for each storm time i, the local time effects are almost entirely averaged out. Thus the storm-time variation Dst of the $F2$ density was obtained from $(\sum_{j=1}^{n_i} \Delta_{ijk})/n_i$ for each i, where n_i was the number of Δ_{ijk} in each storm time i.

Geomagnetic DS variations for each six-hour period were obtained by *Sugiura and Chapman* [1956, 1957] in their work on the morphology of magnetic storms. Following their scheme, we found DS ionospheric density variations for every six hours. Let each six-hour period be designated by an index m, $+1 \leq m \leq 12$. For each m, differences were obtained between Δ_{ijk} and Dst values corresponding to their storm time i. The process may be expressed by $\Delta_{ijk}{}^m - (\mathrm{Dst}^i)^m = \delta_{ijk}{}^m$. The Dst variation should be thoroughly eliminated by this process. Now $\delta_{ijk}{}^m$ was arranged according to local time k. Then the mean value of $\delta_{ijk}{}^m$ for each local time was considered as the DS variation for each six-hour interval m, and harmonic analysis of $\delta_{ijk}{}^m$ was undertaken. The IBM 650 computer was used for all of these calculations.

2.2 *Selection of storms and data used*—During the ten years from January, 1946, to December, 1955, 109 magnetic storms with SC occurred. If, during the succeeding 72 hours, the maximum value of the magnetic A_p-index was larger than or equal to 50, that storm was classified as a strong storm, and if A_p was smaller than 50 it was classified as a weak storm (see Table 1). During the period treated, there occurred 51 strong storms (December Solstice 13, Equinox 24, and June Solstice 14) and 58 weak storms (December Solstice 16, Equinox 20, and June Solstice 22). The analysis of ionospheric storms followed this division.

The names and locations of the 38 ionospheric stations from which data were used in this study are shown in Figure 1 and Table 2. As mentioned in the introduction, *fo*$F2$ hourly values in higher latitudes were doubtful in many cases during magnetic storms. Hence, the 38 stations all lie between 60.4°N and 60.4°S geomagnetic latitude. These stations were divided into eight groups according to their geomagnetic latitudes as shown in Table 2. The number of stations in each zone, and the number of storms actually used for all stations in each zone for each season and for each intensity class are listed in Table 3.

3. Statistical Results

3. *Storm time variations Dst*—Storm time variations of the $F2$ density associated with strong and weak magnetic storms are shown in Figure 2. As seen in the figure, the variation was greater during strong storms than during weak. After an initial short increase of about 10 per cent, the Dst decreased in Zones 1 to 5 for the strong storms and in Zones 1 to 4 for the weak storms. Sometimes an increase occurred even before the onset of the magnetic storm. As expected, the amount of main decrease was larger toward higher latitudes. These variations may be called the "decrease type." In the equatorial region (Zone 8), however, the Dst showed an opposite phase, an initial short decrease followed by an increase. This will be called the "increase type." These results agree with the earlier work of several researchers which was mentioned in the introduction. However, it must be emphasized that variations in Zones 6 and 7 for the strong storm and in Zones 5 to 7 for the weak storm were rather flat. Accordingly, the Dst may be classified as of decrease, flat, and increase types, appearing at higher middle-latitude, intermediate latitude, and the equatorial zone, respectively.

The above results were obtained in the average over the year. But these Dst values show remarkable seasonal changes, as will be seen in Figure 3. In Zone 2 of the figure, the largest decrease occurred in summer. In Zone 6, the decrease type occurred in summer, and the increase type occurred in winter; hence the Dst was flat in the average over the year as shown in Figure 2. In the equatorial region of Zone 8 no appreciable seasonal changes occurred. These results show that in summer the decrease type was predominant except in the equatorial zone, while in winter the decrease type was weak and occurred only in higher middle-latitudes. It must be noted that *Fukushima*'s result [1952] on seasonal change holds only in lower middle-latitudes. Also it must be added here that when the data were analyzed for each main individual

TABLE 1—*List of magnetic storms with SC, 1946 to 1955*

Strong storms							Weak storms						
Serial No.	Year	Month	Date and time of SC in GMT			Maximum A_p during 3 days	Serial No.	Year	Month	Date and time of SC in GMT			Maximum A_p during 3 days
1	1946	January	3d	08h	09m	70	1	1946	May	6d	22h	28m	41
2		February	7	10	19	125	2		June	7	07	39	47
3		March	10	01	52	64	3		July	18	09	04	36
4		March	28	06	36	215	4		August	13	19	02	48
5		April	22	07	00	115	5		November	5	09	24	23
6		July	26	18	47	150	6		November	15	07	54	18
7		August	30	22	40	52	7		November	24	03	46	25
8		September	21	17	13	200	8	1947	January	4	11	17	24
9	1947	January	24	06	20	61	9		January	16	03	29	36
10		March	2	04	00	130	10		February	7	08	14	27
11		March	7	05	36	90	11		February	16	02	59	44
12		March	15	08	42	74	12		April	8	21	50	33
13		March	27	04	28	75	13		June	5	07	26	32
14		April	17	12	25	100	14	1948	February	3	02	06	34
15		June	13	17	49	62	15		March	11	21	36	39
16		July	17	17	49	70	16		April	6	03	58	24
17		August	15	09	51	58	17		May	23	23	25	17
18		August	22	09	11	71	18		August	19	19	36	29
19		September	2	23	25	84	19		October	1	01	14	46
20		September	30	18	09	61	20	1949	February	17	12	26	28
21		November	9	08	57	62	21		February	21	15	16	46
22	1948	March	15	03	35	140	22		March	1	11	42	24
23		May	14	23	23	72	23		March	9	12	44	22
24		August	7	23	00	145	24		March	16	15	33	37
25		October	17	22	11	94	25		April	29	15	44	16
26		November	1	19	46	56	26		May	3	18	15	31
27	1949	January	24	18	28	155	27		May	30	12	30	36
28		March	21	21	27	90	28		June	6	21	14	27
29		April	7	19	22	83	29		October	27	04	49	35
30		May	12	06	40	150	30		November	1	09	54	34
31		June	3	21	53	59	31		November	28	23	16	38
32	1950	February	19	23	40	79	32	1950	February	23	10	43	49
33		March	19	05	45	84	33		June	23	18	02	44
34		August	7	10	55	71	34		June	29	08	22	39
35		September	30	17	47	79	35		July	24	01	51	40
36	1951	January	21	10	57	54	36		September	16	10	18	27
37		April	18	06	52	66	37		December	12	05	26	39
38		July	1	22	28	82	38	1951	March	6	07	50	38
39		September	19	08	42	105	39		May	25	18	48	42
40		October	28	11	54	98	40		June	14	17	51	27
41		December	27	21	36	68	41		June	25	04	28	37
42	1952	February	23	21	26	72	42		August	15	20	10	30
43		March	3	07	31	94	43		September	5	20	45	19
44		April	21	11	50	94	44		September	27	00	05	48
45		June	29	19	32	78	45	1952	January	29	15	27	35

TABLE 1 (*Continued*)—*List of magnetic storms with SC, 1946 to 1955*

Strong storms					Weak storms				
Serial No.	Year	Month	Date and time of SC in GMT	Maximum A_p during 3 days	Serial No.	Year	Month	Date and time of SC in GMT	Maximum A_p during 3 days
46	1953	January	5d 05h 46m	51	46		October	21d 10h 10m	25
47		August	23 00 24	58	47	1953	May	5 21 15	36
48		September	18 16 09	80	48		July	23 08 08	48
49	1955	January	17 03 22	59	49		September	15 02 59	19
50		April	27 16 24	54	50		October	15 08 45	46
51		November	19 13 19	65	51	1954	February	21 10 34	36
					52		March	22 17 16	42
					53		October	23 07 22	45
					54		October	27 07 47	17
					55	1955	May	25 14 34	39
					56		June	6 17 28	23
					57		June	22 10 39	18
					58		October	7 22 57	11

station, rather than for means in each zone, the results were quite similar to the above; this verified that the method of grouping stations was valid.

3.2 *Disturbance daily variations DS and SD—Chapman* and *Bartels* [1940] used the symbol S_D for the geomagnetic disturbance daily variation. The same symbol has often been used for the ionospheric disturbance phenomenon. However, the amplitude and the phase (the time of the maximum amplitude) of the S_D variation change during the course of the storm. Accordingly, that variation at a certain period during the storm has recently been called D_s or DS variation; hence S_D (or SD) is an average of D_s (or DS) variations. According to *Sugiura* and *Chapman*'s notation [1956], the symbol DS for the variation at a certain period and SD for the average were used here for the disturbance daily variation of the $F2$ density. As mentioned in paragraph 2.1, the DS was obtained for each six hours for each group of eight zones. In the harmonic analysis of these DS, the diurnal (24 hours) component was generally larger than other harmonic components. Accordingly, the diurnal component was mainly analyzed.

The phase and amplitude of the diurnal component of the DS for each six-hour period was expressed in the form of the harmonic dial shown in Figure 4. The distance from the origin of the dial to the point represents the maximum amplitude (in per cent) during the six-hour period, and the direction from the origin shows the local time at which the maximum variation occurred. The first point on each diagram shows the phase and amplitude of the DS diurnal component during the six hours preceding the SC, the second point shows those during the six hours succeeding the SC, and so on. Thus changes of the phase and amplitude every six hours for strong and weak storms in all eight zones can be seen in Figure 4. The points on the harmonic dial progress more or less in clockwise sense, and turn about twice during 72 hours. This result is different from those of weak and moderate magnetic DS variation obtained by Sugiura and Chapman. In their results for each magnetic component, the change is counterclockwise. The number of data in the present study might not be sufficient to get the DS variation every six hours. However, mean values of the SD for the first, second, and third 24 hours succeeding the SC (which are called SD_1, SD_2, and SD_3), and also the mean for all 72 hours (SD) may be reliable, particularly in Zones 1 to 5 and Zone 8 for strong storms. These mean values are plotted in Figure 4, and the probable error circles of the SD are also shown there. Except in Zone 8, changes of the

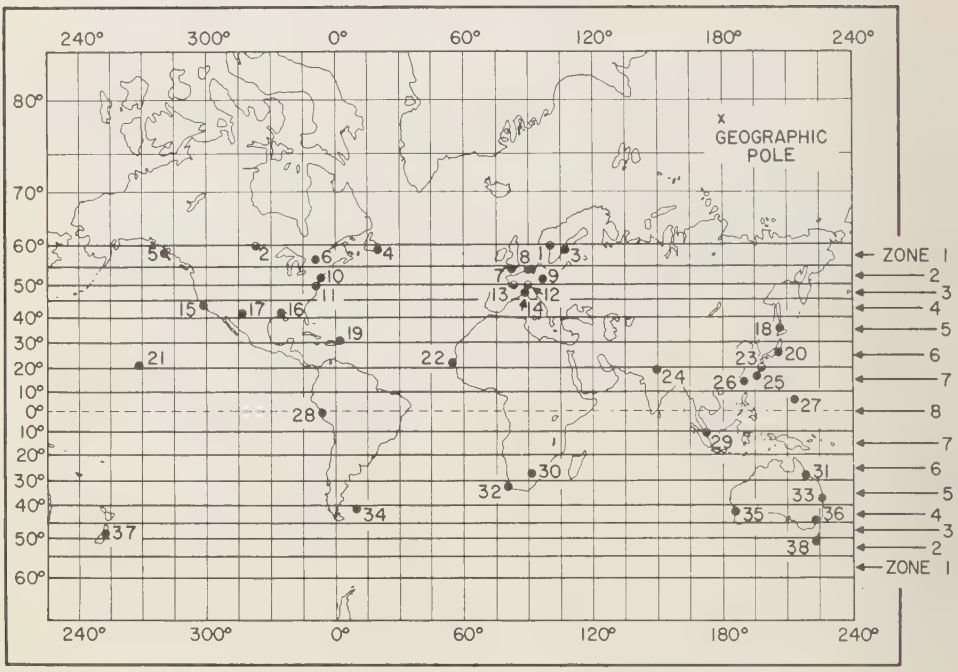

FIG. 1—Distribution of ionospheric stations in geomagnetic coordinates

SD_1, the SD_2, and the SD_3 in the harmonic dial are still clockwise. A clockwise change is also implicit in *Obayashi*'s [1954] and *Sinno*'s [1954] results.

In Figure 4 will be seen a remarkable latitudinal change of the SD, which is presented more clearly in Figure 5. In Figure 5 the local times of occurrence of the maxima of the diurnal component for the SD_1 (thin solid line), the SD_2 (broken line), the SD_3 (dotted line), and the SD (thick solid line) are indicated in each zone. These times show a remarkable phase change from higher toward lower latitudes which has not been suggested previously. The maximum amplitude of the diurnal component for the SD_1, the SD_2, the SD_3, and the SD in each zone are also shown on the left side of Figure 5; the maximum amplitude shows a gradual decrease from higher toward lower latitudes, with an increase in the equatorial zone. The following two points must also be emphasized from this amplitude distribution:

(1) The amplitude of the SD in Zone 2 is smaller than that in Zones 1 and 3. Also in Zone 2 during strong storms and in Zone 1 during weak storms, the amplitude of the SD_1 is smaller than that of the SD_2 and the SD_3. As will be discussed in Section 4, these seem to indicate the effect due to the shift of the focus of disturbance daily electric current system which flows in the ionosphere and which produces the magnetic DS and SD variations.

(2) The increasing amplitude in Zone 8 indicates the effect of larger SD and DS electric current [*Matsushita*, 1953, 1954] caused by the higher electric conductivity there. In Table 4, the present results in the equatorial region are compared with previously obtained results.

For application to the forecast of radio propagation conditions, the most probable hour for a large decrease of $F2$ density is shown in Table 5. In Zone A the maximum decrease of about $B\%$ in the $F2$ maximum electron number-density will occur at about C o'clock local time in the period from D to E hours after the onset of a strong magnetic storm with sudden commencement. The amount of B becomes larger in summer. Zones 6, 7, and 8 are ignored. The storm

TABLE 2—*Ionospheric stations in eight zones*

Zone		Station	Geomagnetic Latitude	Geomagnetic Longitude	Geographic Latitude	Geographic Longitude
	1	Oslo	60.0°	100.1°E	60.0°N	11.1°E
	2	Winnipeg	59.6	322.7	49.9 N	97.4 W
1	3	Upsala	58.6	105.9	59.8 N	17.6 E
	4	St. Johns	58.5	21.4	47.6 N	52.7 W
60.4°–55.5°	5	Prince Rupert	58.3	282.4	54.3 N	130.3 W
	6	Ottawa	56.9	351.2	45.5 N	75.8 W
	7	Slough	54.3	83.2	51.5 N	0.6 W
2	8	DeBilt	53.8	89.4	52.1 N	5.2 E
	9	Lindau Harz	52.4	93.9	51.7 N	10.1 E
55.4°–50.5°	10	Fort Monmouth	51.7	353.9	40.3 N	74.0 W
	11	Washington D.C.	50.3	350.1	38.9 N	77.1 W
3	12	Freiburg	50.3	89.9	48.1 N	7.8 E
	13	Poitiers	49.5	81.8	46.6 N	0.3 E
50.4°–45.5°	14	Schwarzenburg	48.4	88.8	46.8 N	7.2 E
	15	San Francisco	43.7	298.4	37.4 N	122.2 W
4	16	Baton Rouge	41.3	334.6	30.5 N	91.2 W
45.4°–40.5°	17	White Sands	41.2	316.5	32.4 N	106.7 W
5	18	Wakkanai	35.3	206.0	45.4 N	141.7 E
40.4°–29.5°	19	San Juan	29.9	3.3	18.4 N	66.0 W
	20	Kokubunji	25.4	205.4	35.7 N	139.5 E
6	21	Maui	20.9	268.1	20.8 N	156.5 W
29.4°–20.5°	22	Dakar	20.9	54.6	14.6 N	17.4 W
	23	Yamagawa	20.3	197.8	31.2 N	130.6 E
7	24	Delhi	18.9	148.9	28.6 N	77.2 E
	25	Okinawa	15.3	195.4	26.3 N	127.7 E
20.4°– 9.5°	26	Formosa	14.0	189.5	25.0 N	121.5 E
8	27	Guam	4.0	212.9	13.6 N	144.9 E
+9.4°– −9.4°	28	Huancayo	−0.6	353.8	12.0 S	75.3 W
7	29	Singapore	−10.0	172.7	1.3 N	103.8 E
6	30	Johannesburg	−26.9	91.3	26.2 S	28.1 E
	31	Townsville	−28.5	218.8	19.3 S	146.7 E
5	32	Capetown	−32.9	79.8	34.2 S	18.3 E
	33	Brisbane	−35.8	226.9	27.5 S	152.9 E
	34	Falkland Is.	−40.7	9.0	51.7 S	57.9 W
4	35	Watheroo	−41.7	185.8	30.3 S	115.9 E
	36	Canberra	−44.0	224.6	35.3 S	149.0 E
3	37	Christchurch	−48.1	252.7	43.6 S	172.7 E
2	38	Hobart	−51.7	224.6	42.9 S	147.3 E

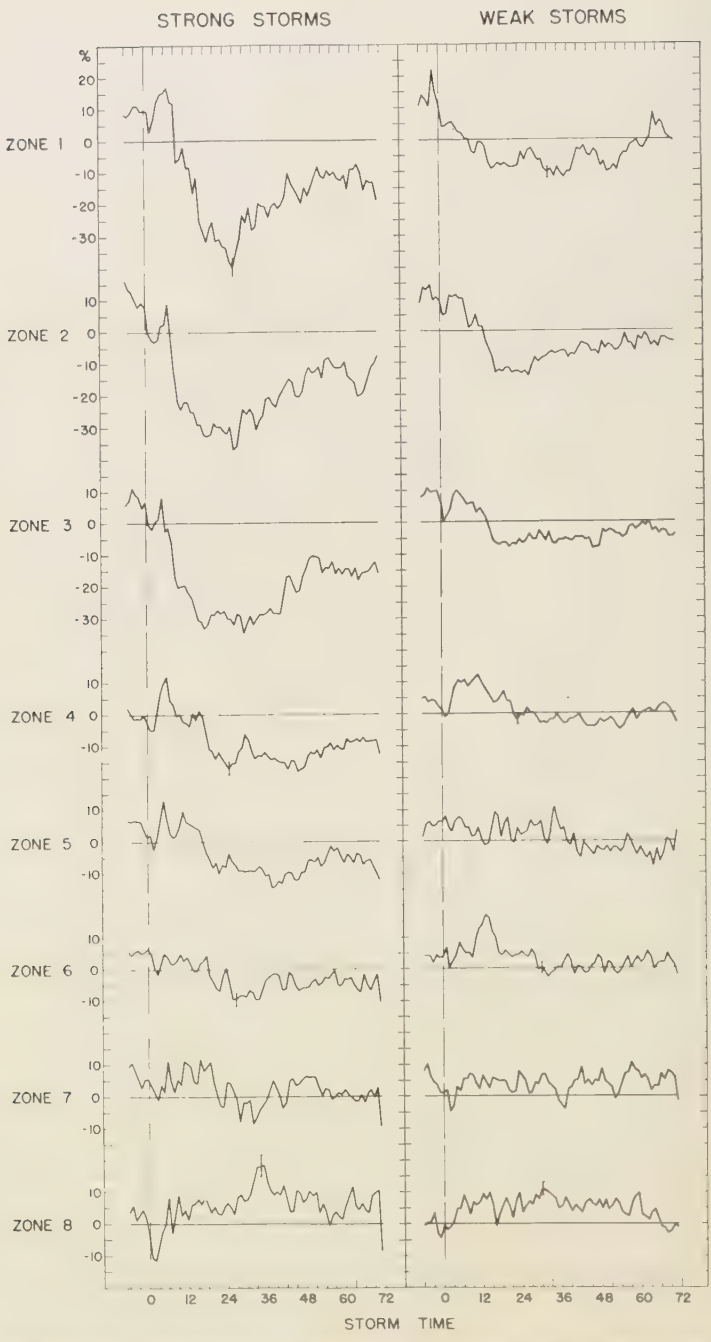

FIG. 2—Dst variations of the maximum electron number density of the $F2$ layer in each of the eight zones for strong and weak magnetic storms with sudden commencements; the abscissa is $200\ (f - \bar{f})/\bar{f}\%$; probable errors are shown in Zones 1, 4, 6, and 8

TABLE 3—*Number of stations, and number of storms actually used for all stations, in each zone*

Zone No.	Number of stations			Number of storms							
				Strong storms				Weak storms			
	N*	S*	Total	Summer	Equinox	Winter	Total	Summer	Equinox	Winter	Total
1	6	0	6	52	89	54	195	94	83	68	245
2	4	1	5	35	66	41	142	69	71	42	182
3	4	1	5	65	111	60	236	94	97	76	267
4	3	3	6	74	110	68	252	87	106	105	298
5	2	2	4	46	83	42	171	67	73	63	203
6	3	2	5	47	79	48	174	73	71	55	199
7	4	1	5	45	83	41	169	66	82	56	204
8	1	1	2	22	44	25	91	31	34	27	92

*Northern or southern hemisphere

time D h to E h was obtained from the time at which the Dst value was less than −20% in Zones 1 to 3, −10% in Zone 4, and −8% in Zone 5. B was obtained from the sum of the Dst values during D h to E h and the maximum amplitude of the SD, and C was decided from the mean time of the maximum amplitude and its standard deviation.

4. Discussion

During magnetic storms, solar charged particles, x-rays generated by these particles, and possibly shock waves or magnetohydrodynamic waves may arrive at the earth's upper atmosphere, particularly in the auroral zone. Ionospheric storms may be caused by these, either directly or indirectly. However, their theoretical explanation is not easy. From the statistical results of apparent $F2$ height increase, which were obtained by various workers mentioned in the introduction and others [*Lewis* and *McIntosh*, 1953], thermal expansion due to incoming energy has been suggested [*Nagata* and *Oguti*, 1953; *Kirby* and others, 1935; *Meek*, 1953]. *Parker* [1956] has also suggested the lifting of some parts of the ionosphere due to hydromagnetic forces. However, this mechanism seems to require an enormous rate of energy input to explain the apparently rapid height change during ionospheric storms. *Seaton* [1956] sug-

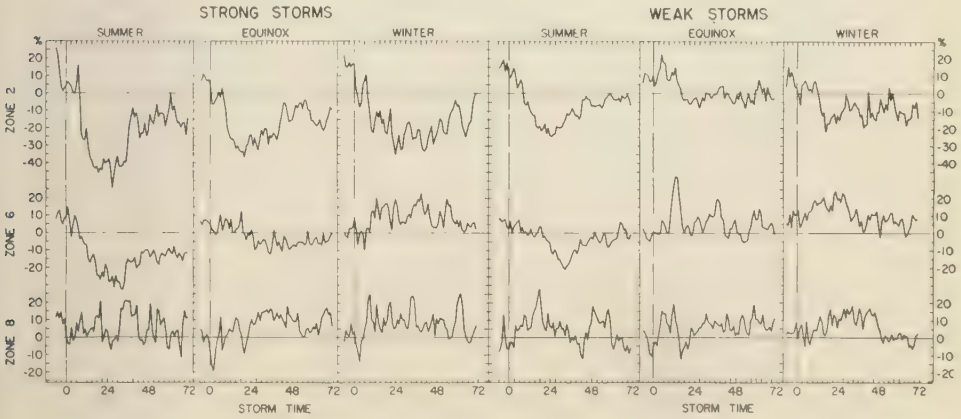

FIG. 3—Seasonal effect on the Dst variations of the $F2$ maximum density in Zones 2, 6 and 8

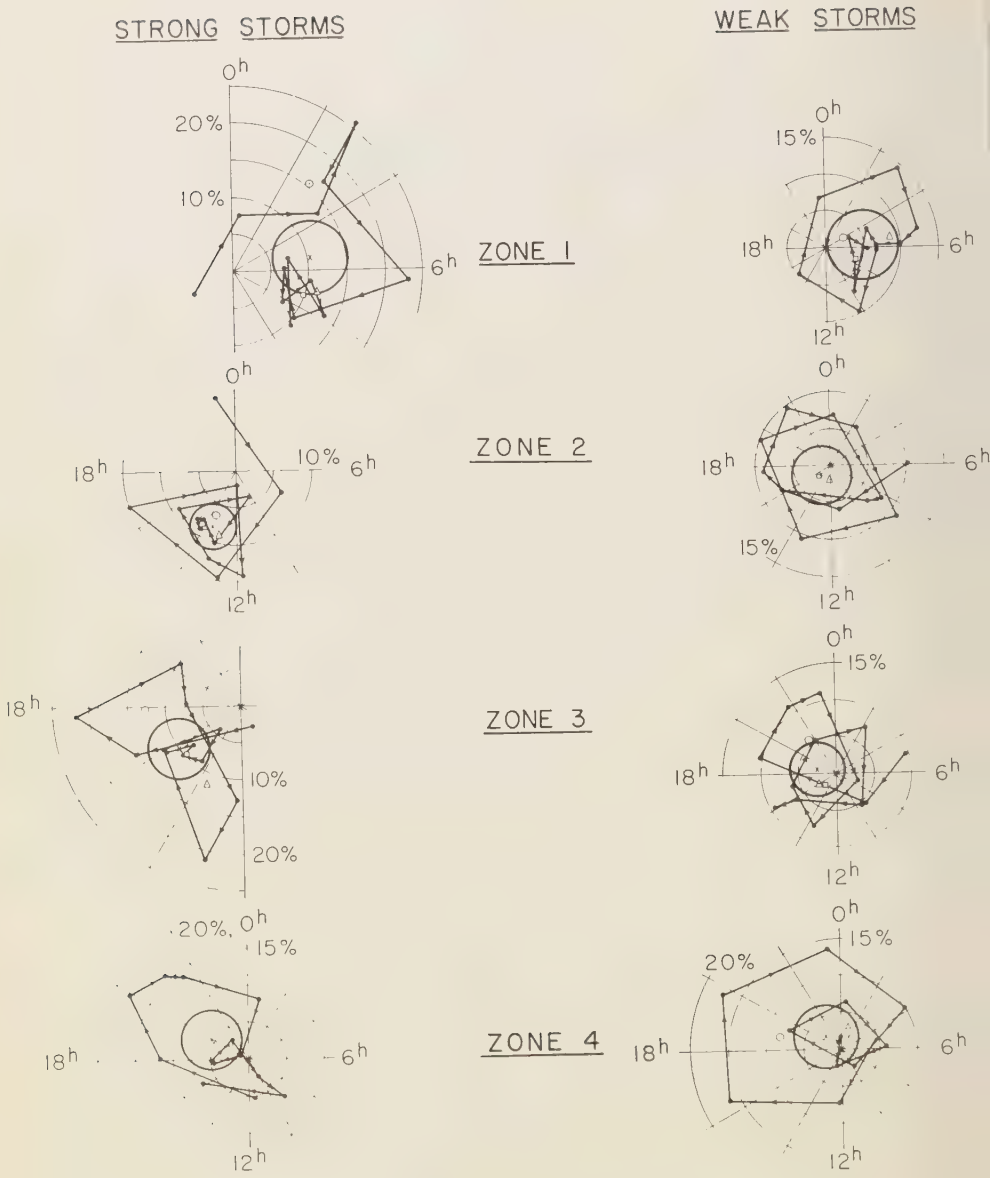

FIG. 4—(See title on p. 315)

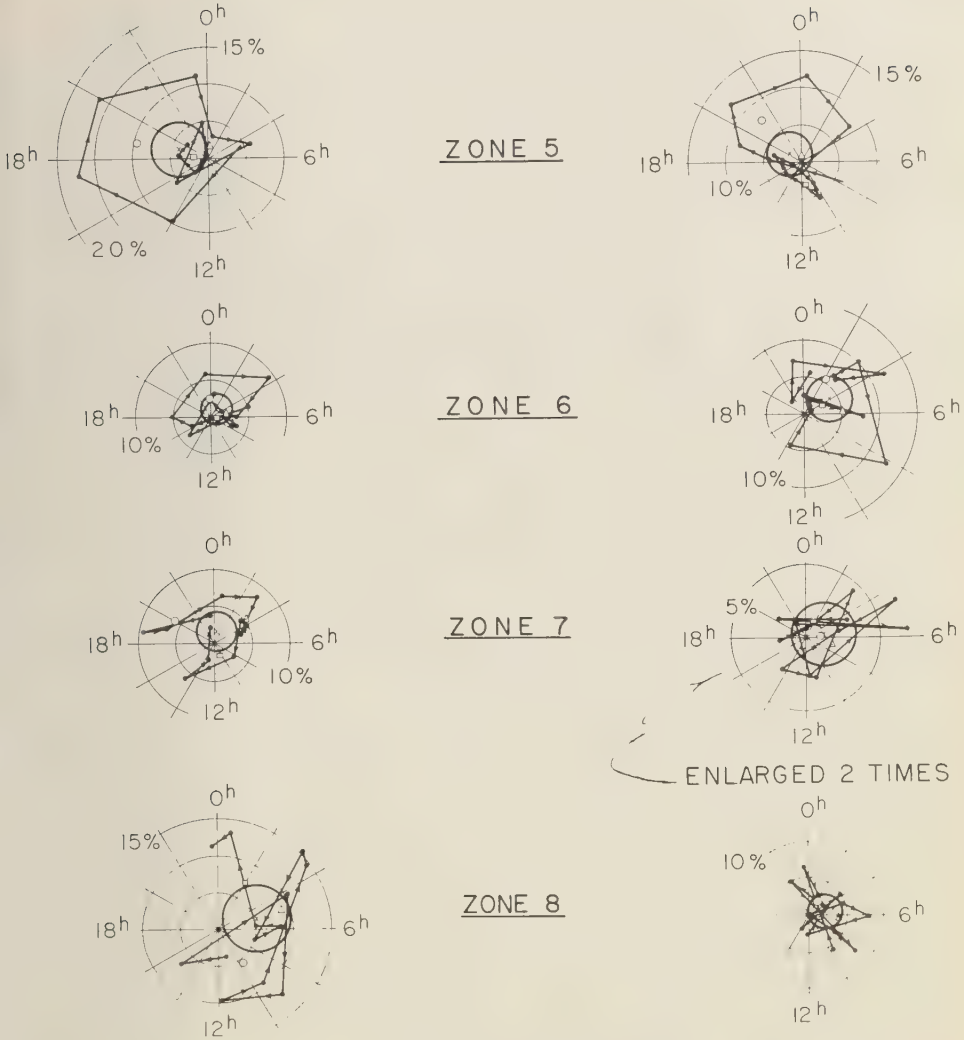

FIG. 4—Harmonic dials for the diurnal component of the DS variations of the *F*2 maximum density in each of the eight zones, for strong (left) and weak (right) magnetic storms with sudden commencements

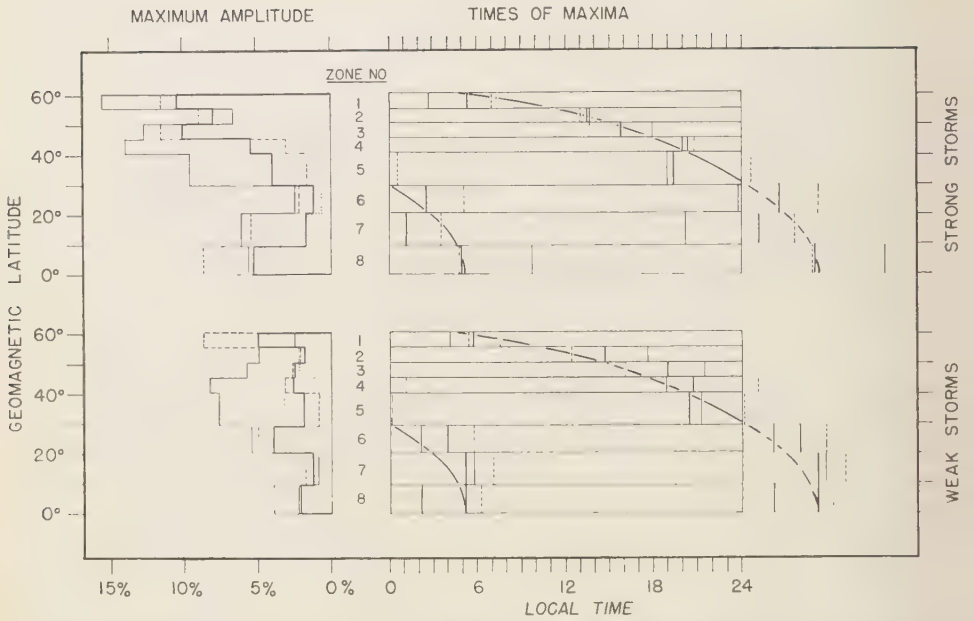

FIG. 5—Distributions of the maximum amplitudes (left), and of the local times of the maxima (right), for the diurnal component of the SD_1 (thin solid line), the SD_2 (broken line), the SD_3 (dotted line), and the SD (thick solid line) in each of the eight zones

gested that changes of atmospheric constituents, particularly an increase in the number of oxygen molecules in the *F*2 layer, may cause rapid recombination reactions such as

$$O^+ + O_2 \rightarrow O + O_2^+,$$

$$O_2^+ + e \rightarrow O^* + O^{**},$$

and hence the *F*2 density decreases. This idea might be applied to an explanation of the ionospheric *G*-condition [*Matsushita,* 1958]. It seems inadequate to explain all storm phenomena, however, since the *F*2 density *increases* in lower latitudes in summer and in the equatorial region in all seasons. The most reasonable idea at present seems to be the drift theory which has been developed by several workers [*Martyn,* 1953; *Matsushita,* 1953; *Sato,* 1956; *Maeda,* 1953, 1955; *Hirono* and *Maeda,* 1955]. However, many questions still remain in the assumptions of the theory, and their theoretical results do not agree well with the present statistical results. In the following paragraphs, further conclusions are derived from the statistical results which indicate a possibility of explanation by the drift theory, and the remaining questions to be solved are discussed.

Since *Chapman* and *Bartels* [1940] deduced the idealized SD electric current system, which seems to flow in the ionosphere and which is responsible for magnetic disturbance daily variations, many workers [*Vestine,* 1938; *Harang,* 1946; *Nagata* and *Fukushima,* 1952] have modified the current pattern, particularly in high latitudes. *Matsushita* [1953] pointed out that the SD current system in the equatorial region was intensified and shifted about three hours earlier in local time than Chapman and Bartels reported. Thus the SD current system during strong magnetic storms may be drawn schematically as in Figure 6. In the present results for the ionospheric SD during strong storms, the maximum amplitude in Zones 6 and 7 is very small. The probable error circle in the harmonic dials of Figure 4 also shows the insignificance of the SD variation in these zones. The phase of the SD in these zones merely means that it occurred between that in Zone 5

TABLE 4—*Diurnal component of the SD for the F2 density in the equatorial region*

Station	Period	Max. amplitude				Time of max. amplitude				
		SD_1	SD_2	SD_3	SD	SD_1	SD_2	SD_3	SD	
Ibadan	Jan.-Dec. 1952				10.5%				16.9h	*Skinner* and *Wright** [1955]
Huancayo	Jan. 1942 to Oct. 1948				4.3%				2.2h	*Martyn** [1953]
		Mc/s	Mc/s							
	Jan. 1951 to July 1952	0.35	0.27			14.2h	15.4h			*Matsushita* [1953]
Huancayo	Jan. 1946 to	2.9%	7.2%	8.5%	4.7%	11.8h	5.1h	3.0h	4.7h	Strong storm
	Dec. 1955	4.5	2.6	4.9	1.7	3.6	11.5	12.9	9.2	Weak storm
Guam	Jan. 1946 to	9.2	11.2	6.9	6.4	8.9	4.9	0.7	5.3	Strong storm
	Dec. 1955	2.8	6.4	6.8	3.5	12.0	7.0	2.7	5.7	Weak storm
Zone 8	Jan. 1946 to	5.6	8.8	7.3	5.3	9.7	4.8	2.0	4.9	Strong storm
	Dec. 1955	2.3	4.0	1.3	2.2	2.2	6.2	6.6	5.1	Weak storm

*These authors did not show numerical values; the above values were calculated by *Maeda* [1955] from their graphs. *Sinno*'s [1953, 1954] and *Sato*'s [1956] studies of Huancayo gave the SD curve alone.

and Zone 8. Accordingly, ignoring these two zones, the time at which the maximum of the SD occurred is shown in Figure 6. Now it will be noticed that the SD variation of the *F*2 density has its maximum when an *eastward* electric current is flowing in equatorial region, and while a *westward* electric current is flowing in other zones. This suggests that the SD variation of the *F*2 density may be due to the drift effect caused by coupling of the electric field of the SD current and the earth's magnetic field; the *F*2 height variation may first occur because of the drift force, then the *F*2 density change follows. We must notice that the electric *field* of the SD current can affect the *F*2 layer in this way, even if the SD electric current itself flows in the lower ionosphere. The above relations between the direction of the current and the *F*2 density change indicate that the drift effect due to interaction of the westward electric field of the SD current and the earth's magnetic field causes an increase-phase of the SD variation of the *F*2 density except in the equatorial zone. (The increase in the equatorial zone is caused by an eastward field.) Likewise the reversal of the direction of the electric field may cause the decrease of the *F*2 density of the SD variation.

As mentioned above, the direction of the electric field seems to give a key to the phase of the ionospheric SD variation. If this is the case, then the maximum amplitude must depend on the amount of the electric field. This seems to agree with our results for the following reason. The SD current flows most intensely in the auroral zone. During strong storms, this intense auroral current also flows in Zone 1, as shown in Figure 6, and sometimes even in Zone 2. The current in middle and low latitudes is a leak current from the auroral current; hence the current intensity decreases toward lower latitudes, with an increase in the equatorial region during daylight hours because of the larger electrical conductivity. This change of current intensity is quite similar to the change of the maximum amplitude of the ionospheric SD. The relatively smaller maximum amplitude of the SD_2 and the SD_3, compared with that of SD_1, in Zones 4 and 5 (Fig. 5) is also understandable from this viewpoint, because the SD electric current in these

TABLE 5

Zone *A*	Decrease *B*%	Local time *C* h	Storm time *D* h to *E* h
1	30–50	14–22	17–42
2	30–45	22–4	10–41
3	30–45	1–7	10–42
4	15–25	3–13	19–55
5	15–20	3–13	20–48

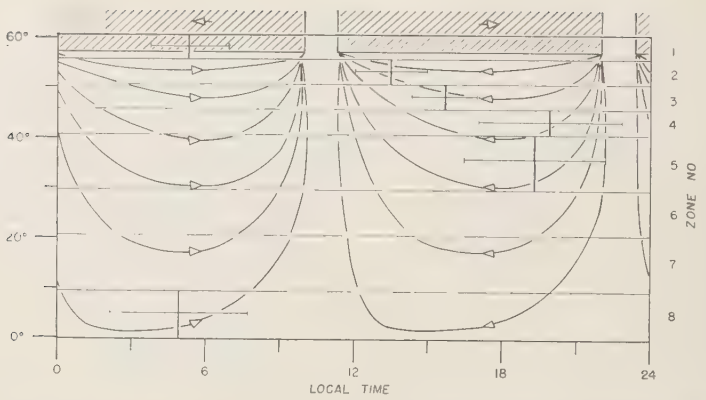

FIG. 6—Relationships between the direction of the SD electric current system and the time of the maximum of the diurnal component of the mean disturbance daily variation of the $F2$ maximum density for 72 hours (with probable errors)

zones usually becomes weaker in the second and third 24 hours after the SC than that in the first 24 hours. Moreover, the explanation of the smaller amplitude in Zone 2 than in Zones 1 and 3 is that Zone 2 is usually situated near the focus of the SD current system. If a magnetic storm is very strong, the auroral current may flow even in Zone 2; hence the ionospheric SD variation there becomes similar to that in Zone 1. If a storm is not very strong, the SD in Zone 2 becomes similar to that in Zone 3. Then the phase lies between that in Zone 1 and Zone 3, and the amplitude becomes smaller. (In the cases of weak magnetic storms, the current focus is usually situated in Zone 1 or 2.) Thus it may be concluded that the SD variation in $F2$ density is due to the drift effect of the SD electric current system, the density increasing with the eastward current (hence electric field) in the equatorial region and with the westward current in other zones.

Before further discussion of the reason why the electric current causes these $F2$ density changes, we will consider whether this relation also holds in the Dst variation. For the same explanation to hold for the ionospheric Dst variation, we may deduce from Figure 2 that a westward electric current must initially flow in the ionosphere all over the earth (causing the density to decrease in the equatorial zone and to increase in other zones), and then an eastward main current has to flow (causing the density to increase in the equatorial zone and to decrease in other zones). It is not easy to explain these kinds of electric currents in the ionosphere. However, one possible explanation for these currents may be an induced electric current due to the electric current which is responsible for the magnetic Dst variation and which seems to be located in the outer atmosphere [*Chapman* and *Bartels*, 1940]. In order to show this relation, Table 6 is provided. As will be seen in the table, the direction of the electric current system responsible for the magnetic Dst variation is eastward during the initial phase and westward during the main phase. If an induced current due to those currents flows

TABLE 6—*Relations between directions of the electric currents and variations of the F2 density*

Magnetic Dst variation	Dst electric current system	Induced electric current in the ionosphere	Dst of $F2$ density
Initial phase	Eastward	Westward	Increase in Zones 1 to 5 Vague in Zones 6 and 7 Decrease in Zone 8
Main phase	Westward	Eastward	Decrease in Zones 1 to 5 Vague in Zones 6 and 7 Increase in Zone 8

in the ionosphere, the direction of the induced current is westward during the initial phase, and eastward during the main phase of the magnetic storm. By these directions of electric currents, we may expect the observed storm-time variation of the $F2$ density, the same as for the DS variation.

If this is the case, the seasonal variation of the ionospheric Dst variation mentioned in paragraph 3.1 may also be explained to some extent. In summer, the electric conductivity in the ionosphere should become larger than in winter, according to the seasonal change of the current system which is responsible for the quiet day magnetic variation [*Chapman* and *Bartels*, 1940]. The induced Dst current system has to be larger in summer, and the density decrease becomes predominant. The situation is just opposite in winter. This is merely a speculation, and since many questions still remain on the induced current in the ionosphere, further study must be made.

For the SD variation, however, it may not be meaningless to consider further how the drift effect due to interaction of both the SD electric field and the earth's magnetic field can produce the $F2$ density change, and why for a given direction of the electric field the change of the $F2$ density is in the opposite sense in the equatorial region, compared with other zones. In the $F2$ region, as is well known, the following equation holds:

$$\frac{\partial N}{\partial t} = q - \beta(z)N - \operatorname{div}(NV), \qquad (1)$$

where N is the electron number density, q is the ion production rate, $\beta(z)$ is the attachment coefficient which varies with height z, and V is the drift velocity. This drift velocity is due to the coupling of the earth's magnetic field and the electrostatic field of the current (the SD current in this case). It has three components, southward, eastward, and upward. These components of the drift velocity were obtained theoretically by *Maeda* [1955]. Among these three components, the most effective for the change of N is the vertical component w, which does not change with height in the $F2$ layer [*Hirono* and *Maeda*, 1955]. Then (1) may be written as

$$\frac{\partial N}{\partial t} = q - \beta(z)N - w\frac{\partial N}{\partial z}. \qquad (2)$$

This equation can be solved by *Millington's* method [1932], with an assumed distribution of $\beta(z)$ with height, and a given density distribution of the $F2$ layer. That is a possible way to discuss the density change due to the drift effect. Qualitatively speaking, from the present relation between the direction of the current and the density change, the vertical upward drift seems to give a density increase in the equatorial region, and a decrease in other zones. The solution of the equation must also have this behavior. However, in order to solve (2) properly, we must know reliably the height variation of the $F2$ layer on both quiet and stormy days, as well as the distribution of β with height and the density distribution. Unfortunately values of the minimum virtual height, $h'F2$, or simply calculated values of the height of the maximum density, $hpF2$, are useless for this purpose, as mentioned in the introduction. That is why previous theoretical studies using unreliable height values would not account for the present statistical results. In the Boulder Laboratories of the National Bureau of Standards, true height values are being calculated [*Wright* and others, 1958] using *Budden's* method [1954]. When those calculations are finished, reliable changes of the $F2$ height during both quiet and disturbed periods will be known and a detailed quantitative discussion may be possible.

As to the opposite behavior of the ionospheric SD variation in the equatorial region from the other zones, it must be pointed out that the theoretical form of the vertical drift velocity is different [*Maeda*, 1955] in the equatorial zone, because of the anisotropic electric-conductivity in the ionosphere, but this is not enough to explain the opposite phase. There must be other differences between the equatorial region and other zones, such as the height distribution of β and diffusion or other physical behavior. It can be concluded that the present statistical results might be explained by the drift theory but that many problems still remain to be solved.

Acknowledgments—The work reported here was principally supported by the Air Force Cambridge Research Center under contract AF 19(604)-2140.

It was originally started in the Boulder Laboratories of the National Bureau of Standards at M. Sugiura's suggestion. The author completed this work in collaboration with Sugiura, who was unable to take a more active part because of illness.

The author wishes to express his sincere gratitude to W. O. Roberts, A. H. Shapley, T. E. Van Zandt, and R. W. Knecht for their kind help and valuable advice, and to R. B. Norton for his assistance with laborious numerical calculations. He wishes also to thank the Boulder Laboratories of the National Bureau of Standards for an appointment as guest worker and for use of ionospheric data, for the IBM 650 computer time involved in the study, and for extending to him the use of other facilities of the Boulder Laboratories.

References

Appleton, E. V., and L. J. Ingram, Magnetic storms and upper-atmospheric ionisation, *Nature,* **136**, 548–549, 1935.

Appleton, E. V., and W. R. Piggott, World morphology of ionosperic storms, *Nature,* **165**, 130–131, 1950; The morphology of storms in the *F*2 layer of the ionosphere, *J. Atmospheric and Terrest. Phys.,* **2**, 236–252, 1952.

Berkner, L. V., and S. L. Seaton, Systematic ionospheric changes associated with geomagnetic activity, *Terrestrial Magnetism and Atmospheric Elec.,* **45**, 419–423, 1940.

Berkner, L. V., H. W. Wells, and S. L. Seaton, Ionospheric effects associated with magnetic disturbances, *Terrestrial Magnetism and Atmospheric Elec.,* **44**, 283–311, 1939.

Budden, K. G., A method for determining the variation of electron density with height ($N(z)$ curves) from curves of equivalent height against frequency ((h',f) curves), *Phys. Soc., Rep. 1954 Cambridge Conference on Phys. of Ionosphere,* pp. 332–339, 1954.

Chapman, S., and J. Bartels, *Geomagnetism,* Oxford University Press, vol. I, 1940.

Fukushima, N., and T. Hayasi, A relation between *F*2-layer disturbance and geomagnetic condition, *Rept. Ionosphere Research Japan,* **6**, 133–136, 1952.

Harang, L., The mean field of disturbance of polar geomagnetic storms, *Terrestrial Magnetism and Atmospheric Elec.,* **51**, 353–380, 1946.

Hirono, M., and H. Maeda, Geomagnetic distortion of the *F*2 region on the magnetic equator, *J. Geophys. Research,* **60**, 241–255, 1955.

Kirby, S. S., T. R. Gilliland, E. B. Judson, and N. Smith, The ionosphere, sunspots, and magnetic storms, *Phys. Rev.,* **48**, 849, 1935.

Lawrence, R. S., Continental maps of four ionospheric disturbances, *J. Geophys. Research,* **58**, 219–222, 1953.

Lewis, R. P. Waldo, and D. H. McIntosh, Diurnal and storm-time variations of geomagnetic and ionospheric disturbance, *J. Atmospheric and Terrest. Phys.,* **3**, 186–193, 1953; Geomagnetic and ionospheric relationships, *J. Atmospheric and Terrest. Phys.,* **4**, 44–52, 1953.

Maeda, K., A theory of distribution and variation of the ionospheric *F*2 layer, *Rept. Ionosphere Research Japan,* **7**, 81–107, 1953; Theoretical study on the geomagnetic distortion in the *F*2 layer, *Rept. Ionosphere Research Japan,* **9**, 71–85, 1955.

Martyn, D. F., The morphology of the ionospheric variations associated with magnetic disturbance, *Proc. Roy. Soc. London, A,* **218**, 1–18, 1953; Geomorphology of *F*2-region ionospheric storms, *Nature,* **171**, 14–16, 1953.

Matsushita, S., Ionospheric variations associated with geomagnetic disturbances, *J. Geomag. Geoelect.,* **5**, 109–135, 1953; Ionospheric *F*2 variations associated with geomagnetic disturbances at the equatorial zone, *Phys. Soc., Rep. 1954 Cambridge Conference on Phys. of Ionosphere,* pp. 265–269, 1954.

Matsushita, S., Some studies of the upper atmosphere in the auroral zone, *Ann. géophys.,* **14**, 483–491, 1958.

Mednikova, N. V., Ionospheric perturbations in the middle latitudes, *Physics of solar corpuscular flows and their effect on the upper atmosphere of the earth,* Academy of Science USSR, pp. 183–244, 1957.

Meek, J. H., Ionospheric disturbances in Canada, *J. Geophys. Research,* **57**, 177–190, 1952.

Meek, J. H., Correlation of magnetic, auroral, and ionospheric variations at Saskatoon, *J. Geophys. Research,* **58**, 445–456, 1953.

Millington, G., Ionization charts of the upper atmosphere, *Proc. Phys. Soc. London,* **44**, 580–593, 1932.

Miya, K., and N. Wakai, Characteristics of ionospheric disturbances during severe magnetic storms, *Rept. Ionosphere Research Japan,* **6**, 137–146, 1952.

Nagata, T., Ionospheric storms in high latitudes, *Rept. Ionosphere Research Japan,* **8**, 39–44, 1954.

Nagata, T., and N. Fukushima, Constitution of polar magnetic storms, *Rept. Ionosphere Research Japan,* **6**, 85–97, 1952.

Nagata, T., and T. Oguti, Ionospheric storms in the auroral zone, *Rept. Ionosphere Research Japan,* **7**, 21–28, 1953.

Obayashi, T., Some characteristics of ionospheric storms, *Rept. Ionosphere Research Japan,* **6**, 79–84, 1952; On the world-wide disturbance of the ionosphere, *Rept. Ionosphere Research Japan,* **8**, 135–142, 1954; On the world-wide disturbance in *F*2-region, *J. Geomag. Geoelect.,* **6**, 57–67, 1954.

Parker, E. N., On the geomagnetic storm effect, *J. Geophys. Research,* **61**, 625–637, 1956.

Sato, T., Disturbances in the ionospheric *F*2 region associated with geomagnetic storms, I, II, and III, *J. Geomag. Geoelect.,* **8**, 129–135, 1956; **9**, 1–22 and 94–106, 1957.

Seaton, M. J., A possible explanation of the drop in *F*-region critical densities accompanying major ionospheric storms, *J. Atmospheric and Terrest. Phys.,* **8**, 122–123, 1956.

Sinno, K., On the variation of the *F*2 layer accompanying geomagnetic storms, I and II, *Rept. Ionosphere Research Japan,* **7**, 7–14, 1953; **8**, 127–

133, 1954; Studies on the disturbances in *F2* layer associated with geomagnetic disturbances, *J. Geomag. Geoelect.*, 6, 120–126, 1954; On the disturbances in *F2* layer associated with geomagnetic disturbances, *Rept. Ionosphere Research Japan*, 9, 166–173, 1955.

Skinner, N. J., and R. W. Wright, Some geomagnetic effects in the equatorial *F2*-region, *J. Atm. Ter. Phys.*, 6, 177–188, 1955.

Sugiura, M., and S. Chapman, A study of the morphology of magnetic storms, *Repts. Geophys. Inst., Univ. of Alaska*, pp. 1–126, July, 1956; pp. 1–54, June, 1957.

Uyeda, H., and Y. Arima, Classification of *F2*-layer storms with respect to their world-wide distribution and characteristics of them, *Rept. Ionosphere Research Japan*, 6, 1–12, 1952; Studies on ionospheric storms, *Rept. Ionosphere Research Japan*, 6, 169–177, 1952.

Vestine, E. H., Asymmetrical characteristics of the earth's magnetic disturbance-field, *Terrestrial Magnetism and Atmospheric Elec.*, 43, 261–282, 1938.

Wright, J. W., T. E. Van Zandt, and G. H. Stonehocker, Data on ionospheric electron densities —I, *Natl. Bur. Standards Rept. no. 5590*, pp. 1–68, 1958.

(Manuscript received September 15, 1958.)

Excess Radiation at the Pfotzer Maximum during Geophysical Disturbances*

Robert R. Brown

Department of Physics, University of California
Berkeley, California

Abstract—Observations of the counting rate of a single Geiger counter at the Pfotzer maximum (~50 gm/cm² atmospheric depth), when compared with nucleonic intensity data obtained with a sea-level neutron monitor, indicate the temporary presence of radiation in excess of normal cosmic radiation during geophysical disturbances at a latitude well below the auroral zone. In the absence of such disturbances, the total intensity variations at the intensity maximum were found to be 2.2 times larger than variations of the nucleonic intensity at sea level.

Introduction—Recently, from observations obtained with cosmic ray detectors at small atmospheric depths, *Winckler* and others [1957, 1958] have clearly demonstrated the presence of bursts of x-rays during visible auroral storms. In addition, observations of soft x-radiation at balloon altitudes have been obtained by *Anderson* [1957] during daylight hours following the onset of a geomagnetic storm. These x-rays have been interpreted as resulting from the bremsstrahlung of low energy electrons high in the atmosphere, possible sources of the electrons being solar corpuscular streams bombarding the earth or local electrons accelerated by the interaction of solar streams with the geomagnetic field. The close time correlation of these events with the geophysical disturbances, however, suggests that the electrons are not of solar origin but obtain their energy locally.

The x-ray observations reported to date have been obtained at latitudes in or near the auroral zone; in addition, with the exception of one intense x-ray burst observed [*Winckler* and others, 1958] at 47 gm/cm², the soft radiation has been found mainly at atmospheric depths of about 10 gm/cm². In the present paper, observations of the total radiation intensity at the Pfotzer maximum during a recent intense geophysical disturbance are reported. These observations, as well as others obtained earlier, indicate the temporary presence of radiation in excess of that to be expected from cosmic radiation at a latitude well below the auroral zone. While the nature and energy of this radiation cannot be determined directly from these observations, the similarity of the geophysical conditions under which the observations were made with those cited above suggests that the excess radiation may be attributed to x-rays.

Apparatus—For the purpose of measuring the total intensity of radiation at high altitudes, many balloon-borne instruments, each containing a Victoreen Type 1B85 Geiger counter and a FM telemetering system, were constructed. Individual counter pulses were scaled by a factor of 16 at the ground receiving station and recorded at one minute intervals during flights.

The instruments were not equipped with pressure-measuring devices, and thus intensity observations, from flight to flight, could be compared only at one depth in the atmosphere, the Pfotzer maximum at approximately 50 gm/cm². The instruments were carried aloft by three neoprene balloons, each inflated to provide 2 kg free lift. The flight characteristics of these balloon clusters were found to be quite similar in the lower atmosphere, the intensity maximum being reached from 62 to 66 minutes after launching. Beyond the maximum, the rate of ascension varied, depending on the condition and number of the balloons remaining inflated.

The construction and arrangement of components in the instruments were identical, and the characteristics of the electronics, from unit to unit, differed only slightly. The counters were placed in styrafoam boxes with walls one inch thick and mounted with their axes vertical. The high voltage power supplies and all high voltage connections were potted in paraffin. The instru-

* Supported in part by the joint program of the U. S. Office of Naval Research and the U. S. Atomic Energy Commission.

TABLE 1—*Details for Flights 34 to 39, July 7 to 12, 1958*

Date	Flt. Unit No.	Rate/Rate A	Launch (UT)	Intensity maximum (UT)	Maximum rate (counts/sec)
7/7	34 13	0.940 ± .009	2100	2202 2300	22.3 ± 0.4 22.2 ± 0.4
7/8	35 22	0.938 ± .009	2100	2204 2308	22.3 ± 0.4 21.9 ± 0.4
7/9	36 5	1.030 ± .010	2100	2206 2324	19.5 ± 0.3 19.5 ± 0.3
7/10	37 17	1.024 ± .010	2100	2202 2310	20.1 ± 0.3 20.1 ± 0.3
7/11	38 28	0.992 ± .010	2100	2206 2236	21.0 ± 0.3 21.4 ± 0.3
7/12	39 18	0.998 ± .010	1630	1732 1828	21.1 ± 0.3 20.7 ± 0.3

ments were enclosed in styrafoam boxes for thermal and mechanical protection.

Two units were set aside as standards against which the remaining units were compared for differences in effective counter dimensions. Each instrument used in the flights listed below was calibrated against standard unit A to better than one per cent statistical accuracy; in addition, each instrument was placed in a bell jar and pumped down just prior to launching for a corona check of the pulses coming from the counter.

Solar activity and related geophysical disturbances—A class 3+ solar flare was reported at 0040 UT on July 7, 1958. The flare was located in the NW quadrant of the sun, at 10° longitude from the central meridian and 25° latitude from the equatorial plane. The flare maximum occurred at 0113 UT and ended at 0214 UT. A geomagnetic storm was reported on July 8, approximately 31 hours after the flare. At the Tuscon Magnetic Observatory, the storm began at 0748 UT with a sudden commencement in horizontal intensity of +182γ and −30′ in declination. The total range during the storm was 503γ in H, 147γ in Z, and 40′ in D. In addition, an aurora of strong intensity was reported on the night of July 8, auroral observations coming from as far south as 39° north geographic latitude.

Observations—A series of six balloon flights carrying instruments of the type described above were launched from Berkeley, California, on successive days after the flare, starting July 7. All flights successfully passed through the Pfotzer maximum twice, once on ascent and again on descent, and the counting rate at the maximum was obtained from the telemetering records after correction for counting loss (approximately 2.5% for all units) and variations in the effective dimensions of the counters. The details of the flights are given in Table 1.

All six instruments were recovered promptly and upon examination found to be in excellent electrical and mechanical condition. Each instrument was compared again with standard unit A, and the normalization factors after recovery agreed, within statistics, with those obtained prior to launching.

The first five instruments flown were recovered within a circle of 10 miles radius whose center was located 55 miles northeast of the launching site. The sixth instrument was recovered 30 miles northeast of the launching site. Because of a 135° change in wind direction at high altitudes during this six-day period, the instruments probably passed through the intensity maximum in the vicinity of the midpoints of the lines connecting the launching site and the impact points.

Results—The total intensity observations summarized in Table 1 show that the intensity at the Pfotzer maximum 14 to 15 hours after the onset of the sudden-commencement geomagnetic storm was not appreciably lower than that observed on the previous day, 22 to 23 hours after the 3+ flare and 8 to 9 hours before the onset of the magnetic storm. On the next day, July 9, 38 to 39 hours after the sudden commencement of the magnetic storm, the intensity was approximately 12% below the pre-storm value; in the days that followed, the intensity rose again toward the initial value.

Examination of the record of the Berkeley neutron monitor, located at sea level, shows that a Forbush decrease of the nucleonic component began with the onset of the magnetic storm on July 8. The neutron data indicate that the nucle-

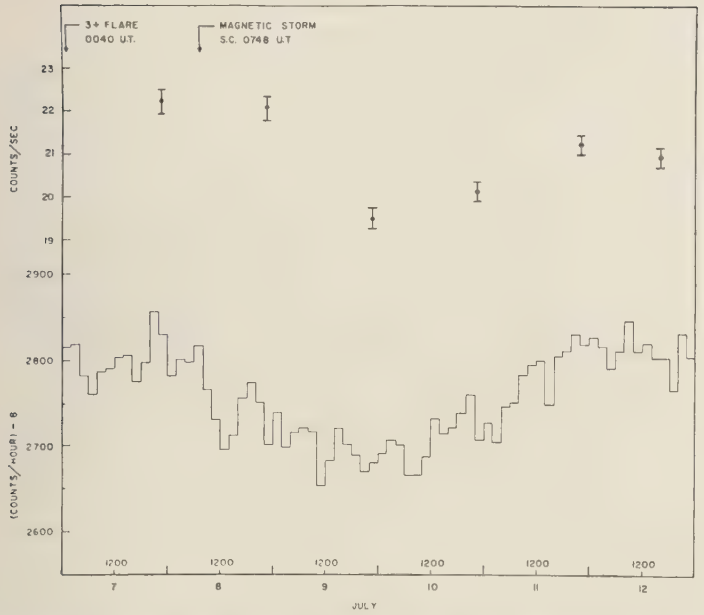

FIG. 1—The average counting rate obtained with a single Geiger counter at the Pfotzer maximum and the two-hour average of the nucleonic intensity observed with a sea-level neutron monitor for period July 7-12, 1958

onic intensity had decreased 3.6% by 1300 UT, increased again to 1.6% below the pre-storm value by 1700 UT, and then decreased again to 3.6% below the initial value by the time the instrument launched that day was passing through the intensity maximum. The nucleonic intensity then followed a further downward trend and began to recover again, starting late on July 9. The average counting rate observed at the intensity maximum on each flight and the neutron data are shown in Figure 1.

From a series of similar flights conducted earlier in the year, it has been determined that total intensity fluctuations at the Pfotzer maximum at this latitude are about 2.2 times larger than the nucleonic intensity fluctuations at sea level. On this basis, the intensity at the maximum on July 8 should have been 8% below the level actually observed if the radiation encountered at that level in the atmosphere consisted only of normal cosmic radiation. This is shown more clearly in Figure 2 where the average counting rate observed at the maximum on each flight is plotted against the nucleonic intensity for the corresponding two-hour time interval.

The dashed line in Figure 2 represents the relation of such observations expected in the absence of geophysical disturbances. The data on which this is based were obtained during a series of 15 flights from April 9 to May 10, 1958; the observations for these flights are shown in Figures 3 and 4. The one point removed from the others in Figure 4 was obtained on April 17 during a geomagnetic storm of gradual commencement; as such, it represents another example of excess radiation at the Pfotzer maximum. Except for this one day, the period during which these flights were conducted was free from magnetic storms. Aurora of strong intensity were reported on the two days surrounding the magnetic storm, April 16 and 18, as well as April 28 to 30. (The displacement of the dashed line in Figure 2 from that in Figure 4 is due partly to a rearrangement of the neutron monitor structure between the two series of flights and to the latitude effect at high altitudes, the high spring winds carrying the instruments much greater distances and in the southeasterly direction.)

Discussion—The two observations of excess

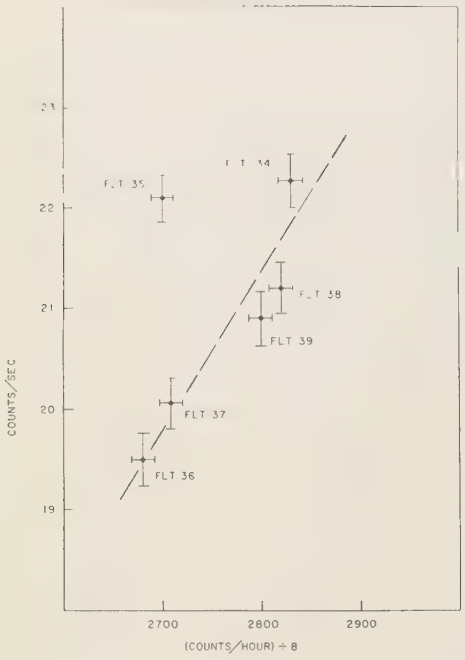

FIG. 2—The average counting rate of a single Geiger counter at the Pfotzer maximum during the period July 7-12, 1958, as compared with the nucleonic intensity for the corresponding two-hour intervals

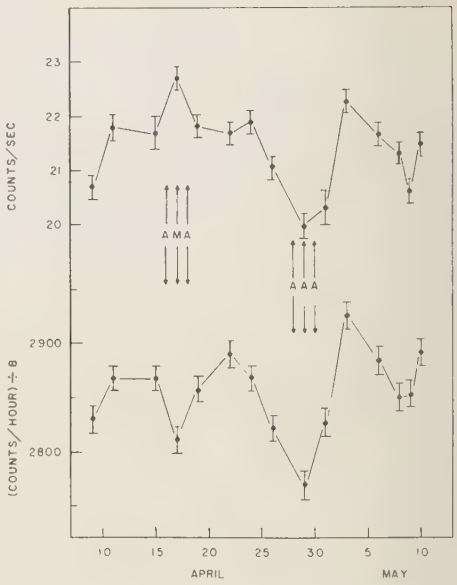

FIG. 3—The average counting rate obtained with a single Geiger counter at the Pfotzer maximum and the two-hour average of the nucleonic component observed with a sea-level neutron monitor for the period April 9 to May 10, 1958; (days on which aurorae and magnetic storms were observed are indicated by A and M, respectively)

radiation at the Pfotzer maximum, on July 8 and April 17, were both obtained during daylight hours. Since magnetic storms and aurorae were associated with the periods during which these flights were conducted, it is of interest to examine the circumstances of each event in order to determine, insofar as possible, the source of the radiation.

A. *July 8 event*—Flight 35, launched at 2100 UT on July 8, passed through the Pfotzer maximum at 2204 and 2308 UT, 14 to 15 hours after the onset of a geomagnetic storm and several hours before an aurora of strong intensity. The total intensity observations for this flight are shown in Figure 5. This flight record is typical of those obtained with these instruments in that it shows the ascent and descent through the intensity maximum at approximately 50 gm/cm^2 atmospheric depth. However, it differs in one respect from others obtained in the absence of geophysical disturbances: starting at about 2148 UT, the rate of change of intensity increased briefly instead of decreasing as the counting rate approached the maximum value. This suggests a burst of radiation superimposed on the intensity variation due to increasing altitude. No additional fluctuations, aside from those of statistical origin, were evident during the remainder of the flight.

Examination of magnetograms from the Tuscon Magnetic Observatory show that Flight 35 was aloft during the last rapid field changes of the magnetic storm and the earliest part of the slow recovery of field toward normal. The field variations for this period are shown in Figure 6; the largest variation during this period involved a change in the horizontal component of 160γ from 2200 to 2206, coinciding with the passage of the instrument through intensity maximum on ascent. While the largest individual fluctuation in the horizontal component during the entire storm amounted to approximately 225γ, the change in the horizontal component

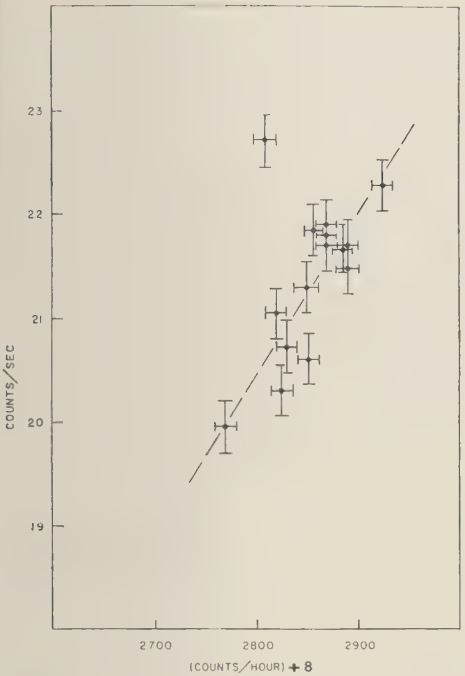

FIG. 4—The average counting rate of a single Geiger counter at the Pfotzer maximum during the period April 9 to May 10, 1958, as compared with the nucleonic intensity for the corresponding two-hour intervals

from 2200 to 2206 represents the largest time rate of change of the horizontal component following that at the sudden commencement of the storm.

For the strong aurora reported on July 8, preliminary estimates (G. Sprague, IGY Auroral Data Center, private communication) of L, the geomagnetic latitude of the southern edge of auroral arc forms, based on the three-hour magnetic $K(L_K)$ index and the North Atlantic Radio Quality Figure $R(L_R)$ are given in Table 2. These estimates indicate a southern movement of the auroral arc, bringing it within six to seven degrees magnetic latitude from the trajectory of Flight 35.

B. *April 17 event*—Flight 17, launched at 1730 UT on April 17, passed through the maximum at 1834 and 1936 UT, 17 to 18 hours after the onset of a geomagnetic storm of gradual commencement. The flight record on this occasion showed no intensity fluctuations beyond those expected from statistical considerations.

TABLE 2—*Preliminary estimates of L, the geomagnetic latitude of the southern edge of auroral arc forms, for six-hour intervals on July 8, 1958*

Date	Time (UT)	L_K	L_R
7/08	00	58	56
	06	52	55
	12	51	52
	18	50	51

Magnetograms from the Tuscon Magnetic Observatory show that the initial disturbance on April 17 was a slow decrease in the horizontal component of about 72γ, starting at approximately 0220 UT. A second disturbance of a similar nature began at approximately 1424 UT, the horizontal component of the field decreasing 60γ by 1530 UT. The first disturbance was accompanied by a 5′ change in declination and essentially no change in the vertical component, while the second disturbance was accompanied by a 15′ change in declination and a small change in the vertical component of the field.

Strong aurora were reported on April 16 and 18; preliminary estimates (G. Sprague, private communication) of the position of the southern edge of the auroral arc forms indicate that for the period of observation of excess radiation the position of the aurora was nearly constant and five to six degrees magnetic latitude farther north than the most southern excursion of the aurora of July 8.

General remarks—The two examples of excess radiation reported here were obtained during periods in which magnetic storms and aurorae were observed. These conditions resemble those associated with the observations of *Winckler* and others [1957, 1958] and *Anderson* [1957], and thus, lacking direct observations of the nature of the radiation in the present experiments, it can only be assumed that x-rays, similar to those found at more northern latitudes, were responsible for the effects.

The excess radiation at this latitude appeared to be fairly quiescent; as such, the present observations resemble more those of Anderson, where the radiation also appeared fairly quiescent and persisted for long intervals of time,

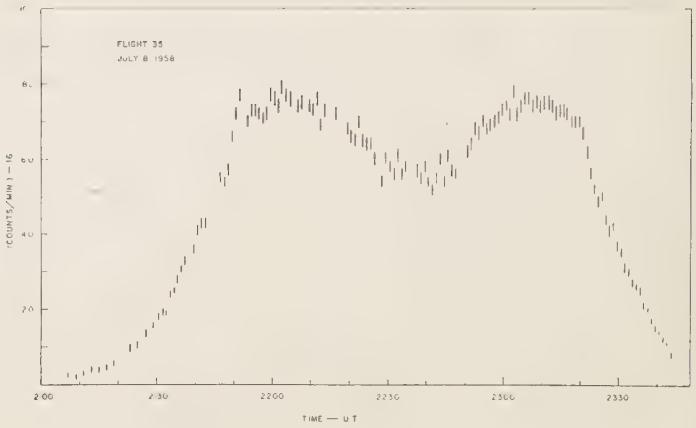

FIG. 5—The counting rate of a single Geiger counter during Flight 35, July 8, 1958

rather than those of Winckler, where the radiation appeared as short bursts associated with auroral arcs developing a strong ray structure, or when existing rays increased in intensity.

Observations of the auroral x-rays [*Winckler* and others, 1958] indicate that this type of radiation lies in the 50-100 kev range, while for x-rays associated with geomagnetic storms [*Anderson,* 1957] indications are that the radiation is either in the same range of energy or possibly higher by almost a factor of ten (a clear-cut distinction between the two cases cannot be made). The present observations at this latitude cannot distinguish between the two possibilities either; however, in view of the greater atmospheric depth, more energetic radiation than that associated with auroral displays appears to be required (unless observations from more northern latitudes indicate that the disturbances on these occasions were of very great intensity).

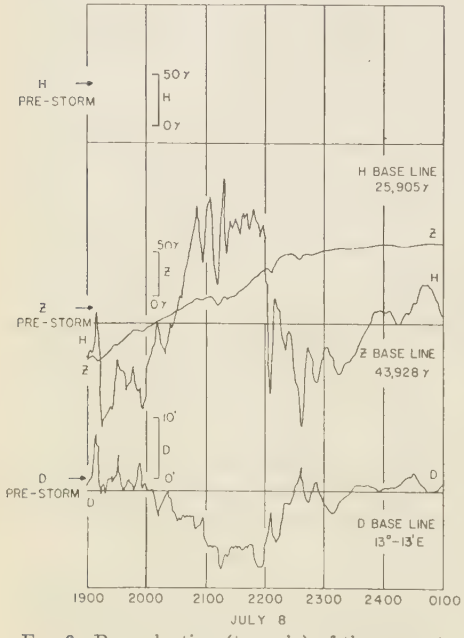

FIG. 6—Reproduction (to scale) of the magnetogram from the Tuscon Magnetic Observatory for the period during which Flight 35 was aloft

Possible origins of these x-rays involve local mechanisms, either through the acceleration [*Winckler* and others, 1958; *Anderson,* 1957] of electrons, with subsequent bremsstrahlung in the vicinity of the earth, from the interaction of solar corpuscular streams and the geomagnetic field, or through nuclear interactions [*Colgate,* 1955; *Singer,* 1956] of protons in these streams and N^{14} in the upper atmosphere. While the electron acceleration mechanism remains to be examined in detail, this mechanism will certainly produce x-radiation over a wide range in energy; in contrast to this, the nuclear mechanism produces radiation in the Mev region, characteristic of such reactions, and would be expected to propagate to fairly low altitudes the effects of auroral protons.

The excess radiation at the Pfotzer maximum

might be attributed to the effects of geomagnetic disturbances, since storms were present on both occasions. Auroral disturbances could be the source of these observations, but it would be necessary to assume that the corpuscular bombardment responsible for these effects extends much farther toward equatorial latitudes than the visible effects would indicate. To explore this question further, balloon flights at equatorial latitudes during geomagnetic storms and periods of strong auroral activity would be required.

Altitude variation of fluctuations—The comparison of intensity fluctuations at the Pfotzer maximum with those of the nucleonic component at sea level gives a factor of 2.2 at this latitude. This is comparable to the factor of 2.3 reported by *Neher* and *Forbush* [1952]. However, in that case, the comparison was between ionization chamber observations at 50 gm/cm^2 over Bismarck, North Dakota, and neutron observations at Climax, Colorado.

Acknowledgments—The author is indebted to the Radio Warning Service, Ft. Belvoir, Va., for the WASHCAL teletype messages advising of solar flares of class 3; the High Altitude Observatory and the National Bureau of Standards for the Weekly Preliminary Report of Solar Activity; the U.S. Coast and Geodetic Survey for the magnetograms from the Tuscon Magnetic Observatory; and the IGY Auroral Data Center for preliminary estimates of auroral positions. In addition, the author wishes to express his appreciation to the members of the Cosmic Ray Group, especially John Creedon and Wayne Hughes, for their generous assistance with the preparation and launchings of the balloon flights.

References

Anderson, K. A., Occurrence of soft radiation during the magnetic storm of 29 August 1957, *J. Geophys. Research*, 62, 641–644, 1957.

Colgate, S. A., Prediction of auroral gamma rays (abstract), *Phys. Rev.*, 99, p. 665, 1955.

Neher, H. V., and S. E. Forbush, Correlation of cosmic-ray ionization measurements at high altitudes, at sea level, and neutron intensities at mountain tops, *Phys. Rev.*, 87, 899–890, 1952.

Singer, S. F., *Phys. Dept. Tech. Rept. no 52*, Univ. of Maryland, 1956.

Winckler, J. R., and L. Peterson, Large auroral effect on cosmic-ray detectors observed at 8 g/cm^2 atmospheric depth, *Phys. Rev.*, 108, 903–904, 1957.

Winckler, J. R., L. Peterson, R. Arnoldy, and R. Hoffman, X-rays from visible aurorae at Minneapolis, *Phys. Rev.*, 110, 1221–1231, 1958.

(Manuscript received October 7, 1958.)

An Apparent Relationship between Geomagnetic Disturbances and Changes in Atmospheric Circulation at 300 Millibars

David D. Woodbridge,*[1] Norman J. Macdonald,** and Theodore W. Pohrte*

** Department of Physics, Colorado School of Mines, Golden, Colorado, and*
*** High Altitude Observatory of the University of Colorado, Boulder, Colorado*

Abstract—This paper describes a study of the average contour length changes and trough developments at the 300-mb level following geomagnetic disturbances from October 1956 through March 1957. A 'contour length index' and a 'trough index' were developed to measure the degree of disturbance of the 300-mb circulation over western North America and the eastern Pacific Ocean and the intensity of troughs in this circulation. Three trough classifications were defined and the development of all troughs appearing in the Aleutian Island - Gulf of Alaska area were analyzed by class.

The results suggest that troughs which appeared in the Aleutian Island - Gulf of Alaska area a few days after an abrupt increase in geomagnetic activity subsequently developed a stronger average cyclonic curvature than other troughs. The largest trough developments and the maximum contour lengths occurred, on the average, eight to nine days after the magnetic disturbance. Added studies will be needed to determine whether the suggested relationships are general ones.

Introduction—There is considerable evidence that the earth intercepts, from time to time, streams of electrified particles from the sun. When these clouds of particles encounter the earth's magnetic field they are presumably channeled into the upper atmosphere in the vicinity of the poles. Their impact on the atmosphere, it is usually postulated, gives rise to such effects as northern lights, irregularities in long distance radio communications, and disturbances of the earth's magnetic field. Several recent studies [*Shapiro*, 1956; *Woodbridge* and others, 1958] suggest that such solar corpuscular emission may influence atmospheric circulation. The present paper independently tests the existence of such a solar effect on the weather.

A qualitative study [*Woodbridge* and others, 1957] of 300-mb half-hemisphere charts from late September 1956 through early March 1957 suggested that disturbances of the earth's magnetic field, as reflected in the A_{GH} index, were followed in four to ten days by major perturbations in the circulation at the 300-mb level. These circulation changes were more frequent and of larger scale over the quadrant from 90°W to 180°W as compared with the region from 0° to 90°W. The winter half-year of 1956-1957 was characterized by strong persistence of zonal circulations from 90°W to 0°. The work described below was carried out in an effort to test these qualitative observations in more objective fashion.

Data and analysis—Over twenty-five years ago, *Chapman* and *Ferraro* [1931] developed a corpuscular theory of magnetic storms. Since then more evidence has been found to link magnetic disturbances to solar activity. On a macroscopic scale, it has been shown by *Chapman* and *Bartels* [1940] that there exists a nearly one-to-one correspondence between the annual means of magnetic and solar activity. During times of low and declining solar activity magnetic disturbances and aurorae exhibit a strong tendency for 27-day recurrence—the period of synodic rotation of the sun [*Mitra*, 1947]. The nearly simultaneous onset of magnetic storms in both northern and southern hemispheres [*Ellison*, 1955] is difficult to attribute to any other than an extra-terrestrial source. On the shorter term, there is a definite tendency for geomagnetic disturbance to follow the largest solar flares, at least near the time of maximum of the sunspot cycle [*Ellison*, 1958].

The present study, covering the period from September 27, 1956 to March 31, 1957, has used the daily Cheltenham *A*-indices (A_{GH}) of geomagnetic-field fluctuations as a measure of the solar corpuscular energy received at the earth.

[1] *Now at Research Projects Office, Army Ballistic Missile Agency, Redstone Arsenal, Alabama*

(The A_{CH} index is the daily index of magnetic activity on a linear scale. It is the sum of the average values of a three-hourly index defined as one-half of the average gamma range of the most disturbed of the three force components at the Cheltenham and Belvoir measuring stations.) The A-index, because it is a linear measure of magnetic storminess, has been recommended by *Bartels* [1957] in preference to the K-indices. Cheltenham indices were used because they were more readily available than planetary A-indices (A_p). However, A_{CH} is highly correlated with A_p.

The length of constant-pressure contour lines between meridians separated by more than 60° is a good measure of the degree of the disturbance of the large-scale circulation. The contour lengths increase with the number and amplitude of wave perturbations. A latitude error in these lengths can be introduced by using, as was done here, uncorrected lengths from maps with conformal conic projections. Such errors are mostly induced by slowly changing, seasonal, north-south shifts of the mean latitude of the contour lines; this study is concerned with short term changes, so the daily changes of the mean latitude of I_{304} were not corrected for latitude error.

The contour-length index (I_{304}) was defined as the length of the 30,400-ft contour line from 90°W to 180°W. Daily measurements were made from the 15h 00m UT 300-mb charts. In cases where the 30,400-ft contour was closed due to blocking action in some area, the length of the unclosed line was determined and one half of the closed portion was then added to this value.

To study the perturbations in more detail a trough index (I_t) was also developed. Troughs that were classified as open, closing, or a cut-off low, and the method used for computing I_t are shown in Figure 1. The value of I_t used in the statistical analyses was the index obtained by averaging the 30,400-ft and the 29,200-ft contours.

Daily computations of I_t were made for all troughs from the day they first appeared in the Aleutian - Gulf of Alaska area (120°W to 180° and north of 40°N), until they either dissipated ($I_t = 0$) or moved out of the area covered by the charts (east of 0°). On this scale, large troughs reached values of over 0.70, moderate troughs centered at about 0.50, and troughs less than 0.35 could be considered small.

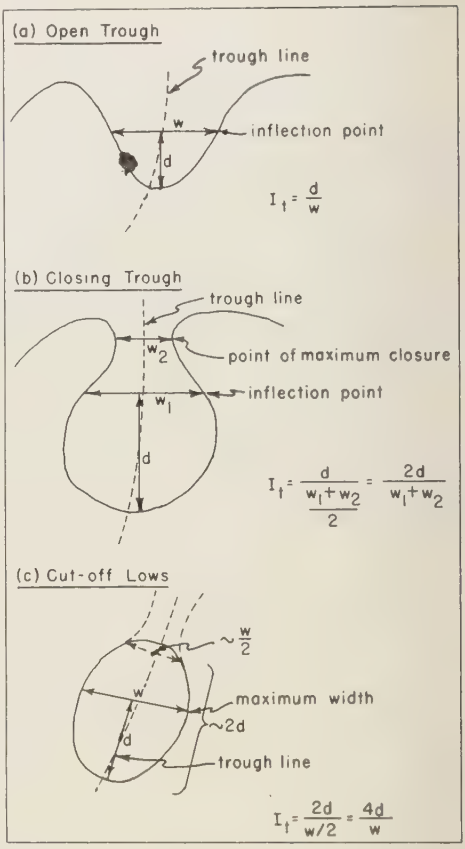

FIG. 1.—Method used to measure I_t; final I_t was determined by averaging the calculations using the 30,000-ft and 29,200-ft contours

Statistical analysis of I_{304}—The contour-length index changes were analyzed by the 'superposed epoch' method to determine whether abrupt increases in geomagnetic activity were related to major changes in this circulation index. The key day (day zero) was defined as any day when the value of A_{CH} reached or exceeded 23 and had increased by an amount equal to or greater than 12 from its value on the preceding day. During the period of time studied 19 key days occurred.

The mean value of I_{304} was then tabulated for days after (+) and days before (−) the 19 key days. The resulting average values of I_{304} are

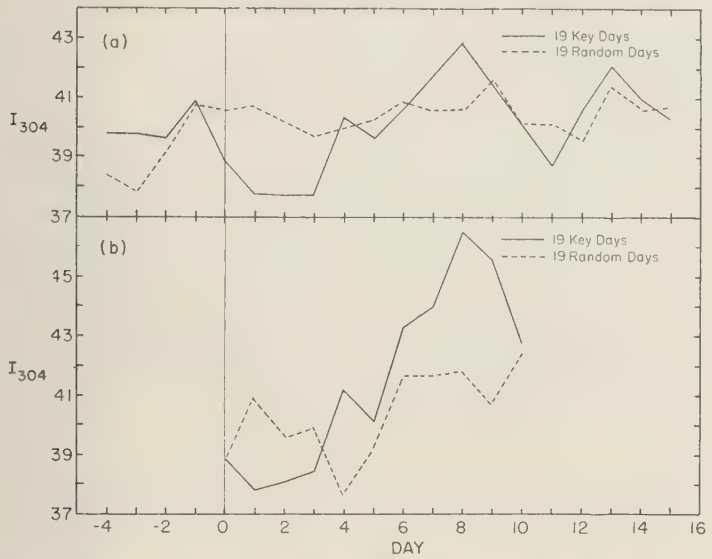

FIG. 2—Average value of the contour index (I_{304}) for days before (—) and days after (+) magnetically selected key days; dashed line represents means using randomly selected key days

plotted on a time graph and shown in Figure 2ab. The first of these shows the fluctuation of the mean value of I_{304} around the 19 key days with I_{304} values entering the mean even if key days were so close together that the individual values entered several different means. We called the graph so computed the 'overlapping data' graph, for obvious reasons.

Figure 2b is similar to 2a and uses the same 19 key days, but in this case the data were deleted from the means before they overlapped the next key day value. Here, thus, each value of I_{304} enters only once into the average. This procedure, we felt, would sharpen the apparent trends if they were real effects. Of course statistical fluctuations become bothersome as the number of points entering each mean diminishes.

The dashed lines show average values of I_{304} before and after 19 randomly selected key days. These lines give some measure of significance against which to compare the fluctuation in the geomagnetically selected data.

The result is a peak in both graphs eight days after the geomagnetic key day. This tends to support the preliminary conclusion that a more disturbed or meridional circulation became evident about a week or so following a large geomagnetic rise.

Statistical analyses of troughs—During the period of study, a total of 54 troughs appeared in the Alaskan - Aleutian area. The average interval between troughs was 3.4 days, and the average intensity at the time of maximum development was approximately 0.60.

The superposed epoch method was also used here to show the total number of troughs ap-

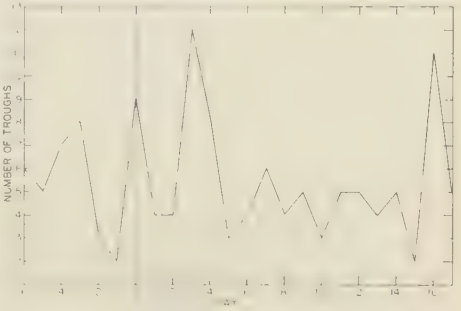

FIG. 3—Total number of troughs appearing in the Aleutian - Gulf of Alaska area before and after the 19 magnetically chosen key days

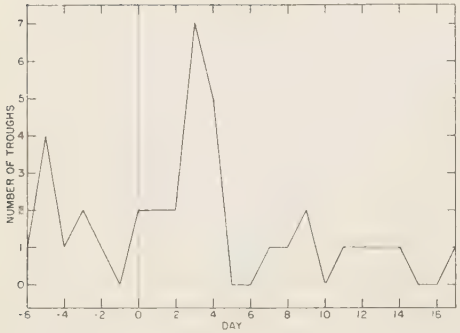

FIG. 4—Same as Figure 3 except showing only those troughs which reached or exceeded 0.7 at some later time

pearing from six days before to 17 days following the chosen key days. Although slightly more troughs of all sizes appeared three and four days after and abrupt increase in A_{CH} (Fig. 3), the number does not seem significantly greater than the mean. Figure 4, however, shows the results of a similar superposed epoch study of the frequency of occurrence of large troughs, that is, those whose index ultimately reached 0.7 or greater. Here the increased number of troughs that appeared three or four days after an abrupt increase in the A_{CH} index seemed considerably more marked.

In the next step, all troughs were divided into two groups: (1) those that appeared three or four days after an abrupt increase in geomagnetic activity ('key' troughs), and (2) those that appeared at any other time. During the six months in our study there were 18 key troughs, and 36 others in the Aleutian - Gulf of Alaska area. Figure 5a shows the average time variation of the trough index for the seven days after the first appearance of troughs in the Aleutian - Gulf of Alaska area. We included all troughs that did not move off our maps (east of 0°) during the seven days; there were 49 such troughs out of the total number of 54.

To test whether the difference between the average I_t of key troughs and 'not-key' troughs was caused by a few extreme cases, we computed new averages after deleting the three largest key troughs and the six smallest not-key troughs (Figure 5b). From these two graphs, it can be seen that the I_t of troughs appearing three or four days after magnetic disturbances

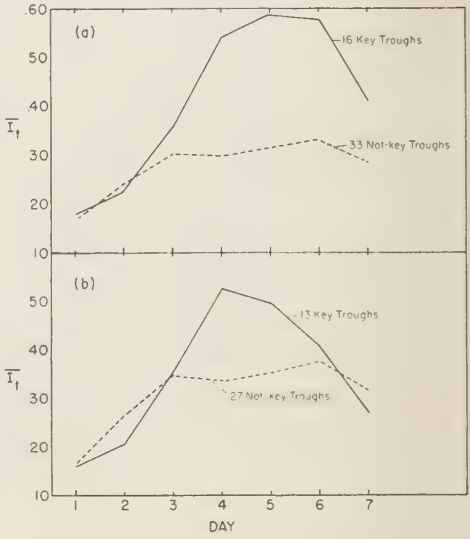

FIG. 5—Average I_t for (a) 16 magnetically chosen key troughs and 33 other troughs; only those troughs which did not move off the maps during the first seven days are shown; (b) three largest key troughs and six smallest not-key troughs deleted

on the average reached a larger amplitude than troughs that appeared at other times. By the fifth day the I_t of these key troughs was nearly twice the amplitude of other troughs.

Typical trough development—During the study period, the most intense troughs developed in one of two preferred patterns, which we have labelled Types A and B. Type A troughs reached their maximum intensity in the far western part of the United States during the first seven days of life. They sometimes caused a readjustment of the pre-existing long wave pattern. Type B troughs resulted in an intensification or formation of a long wave trough in the eastern United States, sometimes in association with slight retrogression of the long wave system. The B types also reached their maximum amplitude during their first seven days.

In order to show the typical development of the Type A and B troughs, two sets of composite synoptic charts were constructed by a method similar to that of *Pagava* and others [1940]. An example of the method (Figure 6) shows a composite of a number of the best cases of Type A patterns on the day of their first appearance

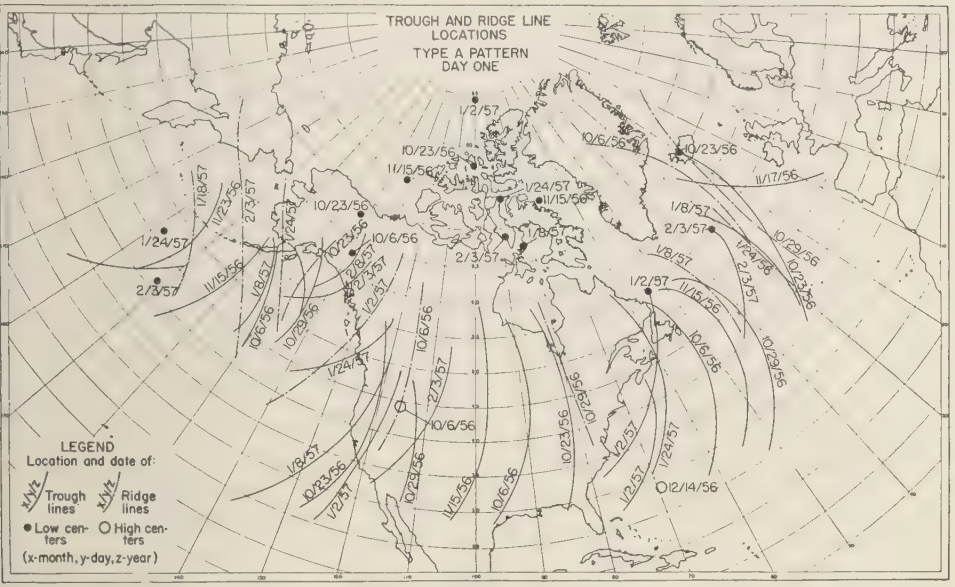

FIG. 6—An example of the method used in developing the typical patterns; the idealized chart for the first day of Type A was drawn from this composite chart

in the Aleutian Islands - Alaska area. Similar plots were made of the location and dates of all troughs, ridges, and centers of low and high pressure for the first five days of both types. From these composite charts we prepared simplified, idealized patterns showing the progressive development of each trough type. The first five days of development of Types A and B are shown in Figures 7 and 8.

Types A and B showed time variations in undergoing their typical developments. On the average, both types of troughs reached their maximum developments on the fifth day after first appearance, but on some occasions the delay was as short as four days and on others as long as seven. For this study we classified troughs as Type A or B if they behaved in a manner as shown in the idealized charts and if they reached maximum development in four to seven days. Otherwise we classed them as of Type C, an omnibus category. Our 54 troughs were distributed as follows: 16 Type A troughs, 9 Type B troughs, 29 Type C troughs.

Association of trough types and intensities with abrupt geomagnetic rises—A study of the frequency of occurrence of Types A, B, and C troughs appears in the contingency tables (Table 1), in which (a) shows that Type A troughs generally developed with large I_t values, since 13 out of the 16 Type A troughs developed a trough index of 0.7 or greater. Type B troughs (b) reached a value near or above the average maximum trough intensity in seven out of the nine cases. Type C troughs (c) were generally quite shallow; most of them had a trough index less than 0.5.

Table 1(d) is made up from (a), (b), and (c). The random expectation of the number of Types A and B following A_{CH} increases is about eight, but 14 were observed. Similarly Type C troughs rarely occurred after large geomagnetic increases, and in this showed about the same departure from random expectations as the troughs of Types A and B. A Chi-squared test applied to the contingency table to determine the significance of this result shows that the probability of occurrence of a distribution this far from random is about 10^{-8}. It should be noted that two ideal examples of Type A occurred *two* days after an A_{CH} key day during March 1957. These two cases are not included in the A_{CH} column, even though they probably should be thrown into the 'favorable' category by extending the lag criterion to days 2, 3, and 4

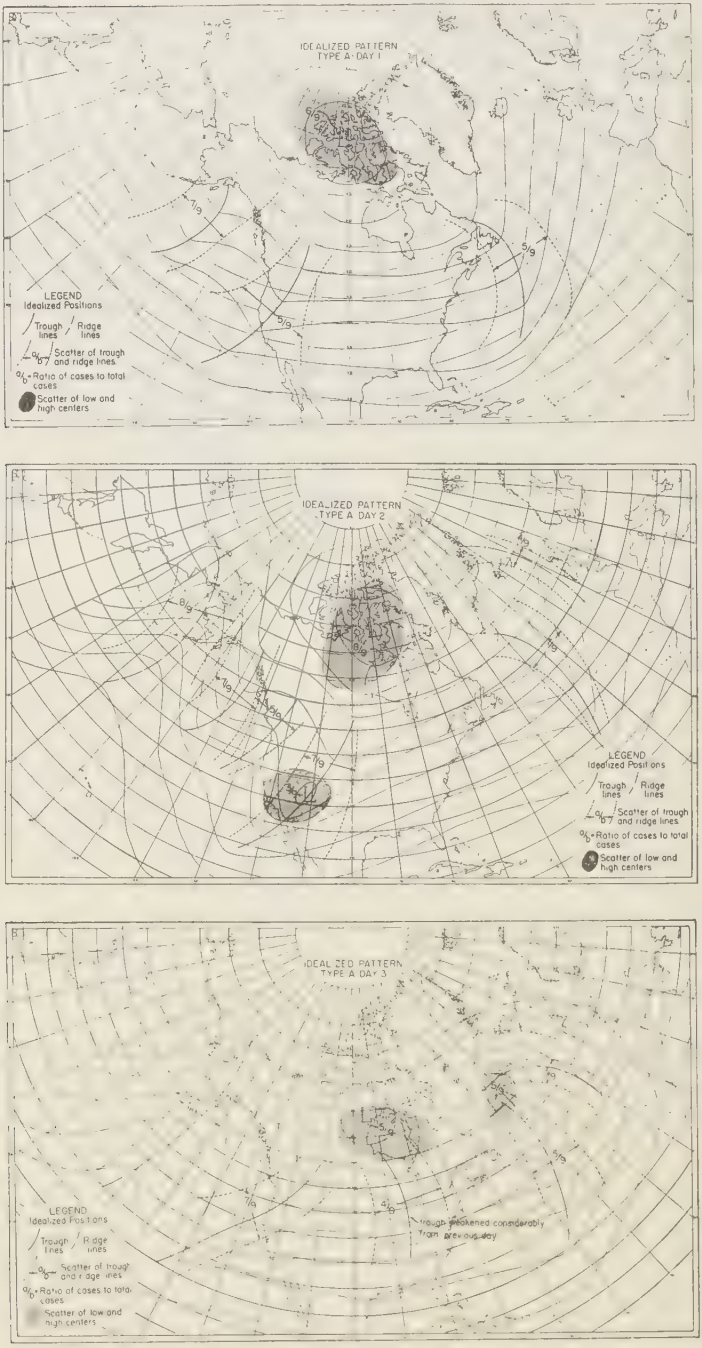

FIG. 7—(See title on p. 337)

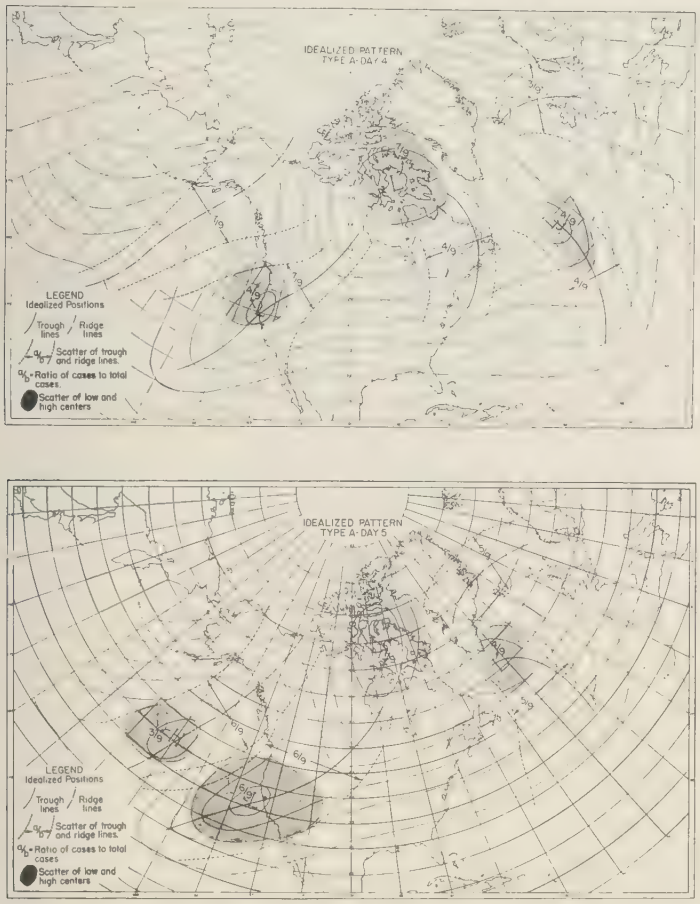

FIG. 7—Idealized pattern, Type A; (a) Day 1; (b) Day 2; (c) Day 3; (d) Day 4; (e) Day 5

after magnetic rise. We did not do this because we had set our limits for the study prior to March first and did not wish to change them until our evaluation was completed.

Figure 9, again, is a superposed epoch study showing the behavior of the A_{CH} index before and after key days chosen, this time, as the day of first appearance of a trough Types A and B (solid line) and Type C (dashed line) in the Aleutian - Gulf of Alaska area. The dashed horizontal lines approximately represent the 5.0, 1.0, and 0.1 pct confidence limits as computed by Student's t-test for the difference of each daily mean from the population mean. The result is a significant peak in the A_{CH} value three days before the first appearance of trough Types A and B. This result strengthens our confidence in the reality of the association of large troughs and abrupt increases in A_{CH}.

Conclusions—Within the restrictions imposed by the limited period of time covered by the study and thus the limited volume of data analyzed, there appears to be a significant relationship between geomagnetic activity and the subsequent development of wave phenomena at 300 mb. This association appears to be as follows:

(1) Troughs that appear in the Aleutian Island - Alaska area two, three, or four days after an abrupt increase in geomagnetic activity are

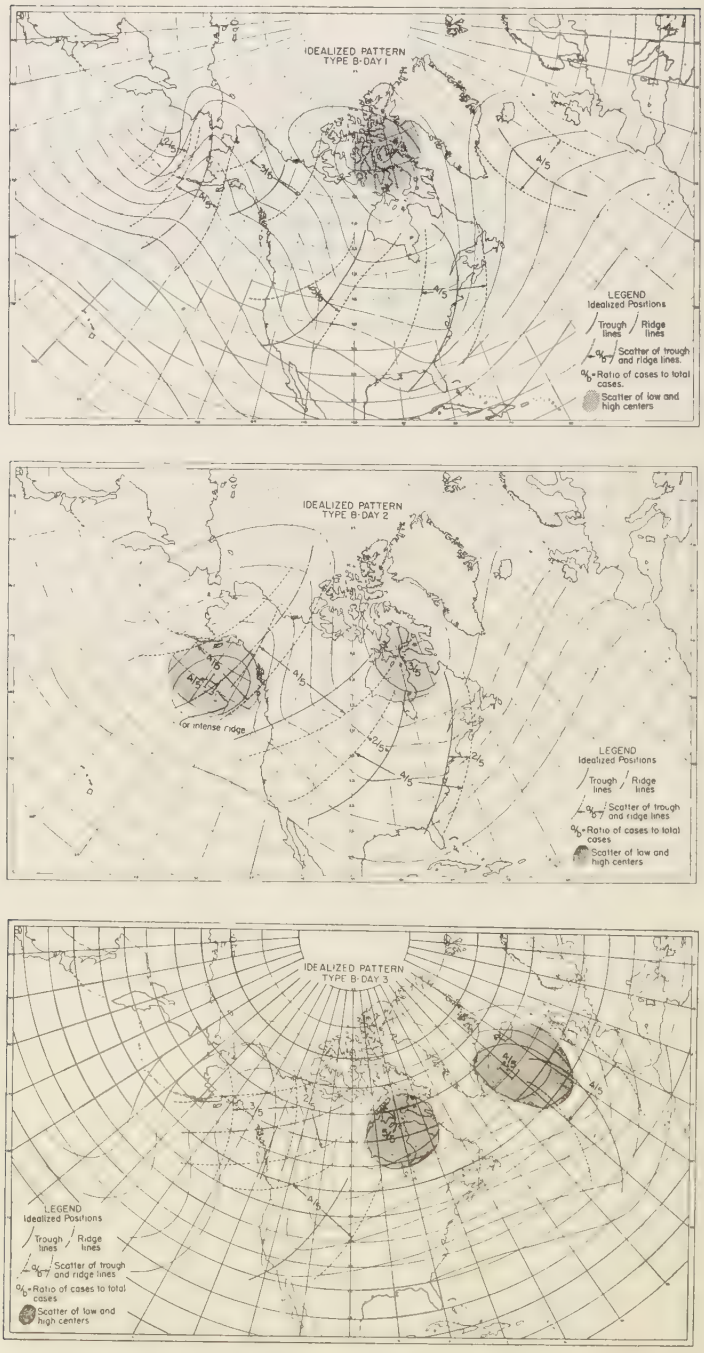

FIG. 8—(See title on p. 339)

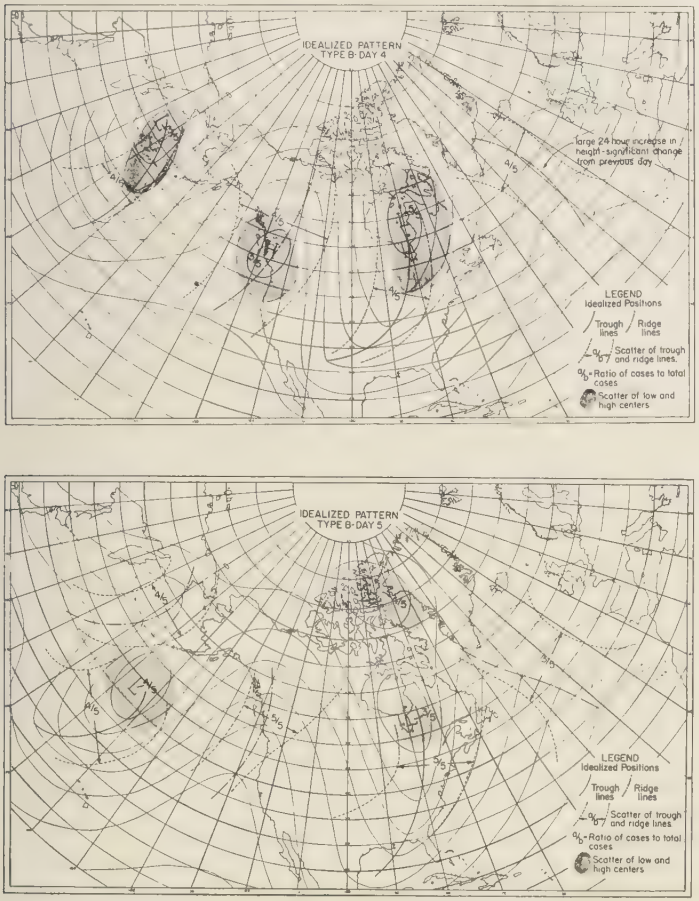

FIG. 8—Idealized pattern, Type B; (a) Day 1; (b) Day 2; (c) Day 3; (d) Day 4; (e) Day 5

likely to have, at full development, larger values of I, than troughs that appear in the same area at other times.

(2) The developing troughs and intensifying ridges reach a maximum about eight or nine days after the abrupt rise of geomagnetic activity, which results in maximum value of the I_{304} on these days.

(3) The maximum trough development is likely to be in the long wave trough position along the west or east coasts of North America about five days after first appearing in the Aleutian - Alaskan area.

Note that the period of study was not unusual, either with respect to the frequency of geomagnetic key days, considering the highly active state of the sun at this time, or with respect to the frequency distribution of troughs through the study area. Geomagnetic activity near the previous solar maximum, for example, was similar and a value of about two troughs per week appearing in upper levels in any selected area in the middle latitudes is about normal.

Acknowledgments—We wish to express our appreciation to P. D. McTaggart-Cowan and A. Thomson of the Canadian Department of Transport for the maps they have so generously supplied to us. We also express sincere gratitude to Robert Curtis of Continental Airlines and Henry Harrison

TABLE 1—*Frequency of occurrence of trough types*

(a) TROUGH TYPE A

I_t	A_{CH}	No A_{CH}	Total
>0.7	8	5	13
<0.7 ≥0.5	0	1	1
<0.5	1	1	2
Total	9	7	16

(b) TROUGH TYPE B

I_t	A_{CH}	No A_{CH}	Total
>0.7	3	1	4
<0.7 ≥0.5	2	1	3
<0.5	0	2	2
Total	5	4	9

(c) TROUGH TYPE C

I_t	A_{CH}	No A_{CH}	Total
>0.7	0	2	2
<0.7 ≥0.5	0	10	10
<0.5	4	13	17
Total	4	25	29

(d)

Trough Type	A_{CH}	No A_{CH}	Total	
A & B	14	11	25	From X^2 test with one degree of freedom P=0.001
C	4	25	29	
Total	18	36	54	

LEGEND

I_t = Maximum trough index

A_{CH} = Trough appearance 3 or 4 days following A_{CH} index ≥23 with 24-hour ΔA_{CH} ≥12.

Type C = All troughs not A or B

No A_{CH} = Trough appears on any day except 3 to 4 days after A_{CH} ≥23 with 24-hour ΔA_{CH} ≥12.

of United Air Lines for assistance in obtaining data and for the time they have taken to discuss this program during its progress. We are indebted to Walter Orr Roberts and the staff of the Observatory for the many helpful suggestions in the progress of this research. This study was supported by the High Altitude Observatory Institute for Solar-Terrestrial Research.

REFERENCES

BARTELS, J., The geomagnetic measures for the time variations of solar corpuscular radiation, described for use in correlation studies in other geophysical fields, *Ann. IGY*, 4, part 3, 227–236, 1957.

CHAPMAN, S., AND J. BARTELS, *Geomagnetism*, vol. 1, chap. 11, 370–372, Oxford Press, London, 1940.

CHAPMAN, S., AND V. C. A. FERRARO, A new theory of magnetic storms, *Terrest. Magnetism and Atmospheric Elec.*, 36, 77–171, 1931.

ELLISON, M. A., *The sun and its influences*, chap. 6, p. 148, Macmillan Co., New York, 1955.

ELLISON, M. A., Magnetic activity following a solar flare, *J. Atmospheric and Terrest. Phys.*, 12, 214–215, 1958.

MITRA, S. K., *The upper atmosphere*, chap. 8, 394–395, Roy. Asiatic Soc. of Bengal, Calcutta, 1947.

PAGAVA, S. T., AND OTHERS, *Basic principles of the synoptic method of long-range weather forecasting*, 3 vol., USSR Hydrometeorology Publishing House, Leningrad, 1940 (Translation by WIS, HDQTRS AAF, 1940).

SHAPIRO, R., Further evidence of a solar-weather effect, *J. Meteorol.*, 13, 335–340, 1956.

WOODBRIDGE, D. D., T. W. POHRTE, AND N. J. MACDONALD, A possible effect in 300-mb circulation related to solar corpuscular emission, *Tech. Rept. 3, Inst. for Solar-Terrestrial Res.*, High Altitude Observatory, 23 pp., 1957.

WOODBRIDGE, D. D., T. W. POHRTE, AND N. J. MACDONALD, A possible relationship of geomagnetic disturbances to 300-mb trough development, *J. Meteorol.*, 15, 247–248, 1958.

(Manuscript received June 5, 1958; revised October 13, 1958.)

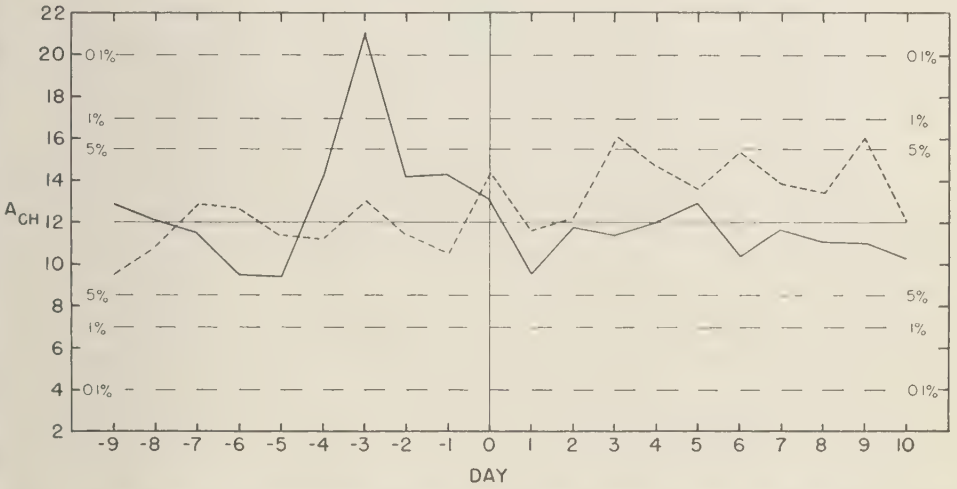

FIG. 9—Mean value of the geomagnetic index (A_{CH}) for days before (—) and days after (-|-) the 25 days when trough Type A or B (solid line) and the 28 days when Type C (dashed line) first appeared in the Aleutian - Gulf of Alaska area

On Some Limitations of Upper Wind Records

B. N. Charles

Sandia Corporation
Albuquerque, New Mexico

Abstract—Some effects of low-elevation-angle terminations of electronic wind soundings are indicated by statistics from two climatological projects. These effects bias mean values, standard deviations, and inter-level correlations. Examples are given, and the suggestion made that the climatic record of upper winds be routinely augmented by interpolated synoptic values.

Statistical deficiencies in available collections of upper wind data are generally recognized but frequently ignored, in the interests of necessity or expediency. The major part of these collections has been obtained by electronic tracking of a balloon-borne radio transmitter or radar reflector. The balloon rises in the atmosphere at a nearly constant rate; timed azimuth and elevation angles are recorded until the target merges with the horizon and can no longer be followed by the ground electronic equipment. At this time, 'low-elevation-angle termination' occurs and introduces a systematic bias, since it is associated with strong winds which are omitted from the data collection. The needs for statistics of upper winds are urgent, however, and the available data collections undergo routine statistical summarization in many countries. The results so obtained find wide application in air route planning, basic aircraft and missile design, and estimation of fallout deposition due to nuclear explosions.

In recent years the U. S. Weather Bureau has compiled serially complete collections of wind data for a five-year period for a large number of North American stations. The observational records of course had gaps because of missing data. To estimate missing values, Weather Bureau meteorologists used daily maps of constant-pressure surfaces and interpolated and extrapolated from pertinent arrays of the observational data. In brief, every conceivable justifiable means of inferring missing data was employed [*Ratner*, 1957], to produce once-daily (1500 GMT) winds for thirteen pressure surfaces ranging from the 950- to the 30-mb levels (or from about 1800 to 78,000 ft above mean sea level). The period of record was March 1, 1951 to February 29, 1957. Although it is not feasible to define the accuracies of the estimates (which apply, after all, to irretrievable, undocumented situations) in quantitatively precise terms, there are numerous grounds for believing the aggregate of these estimates to be at least as accurate, for statistical purposes, as are presently available measurements. These data collections were subsequently summarized in a joint venture of the Weather Bureau and Sandia Corporation [*Bull. Am. Meteorol. Soc.*, 1958].

In an independent project, the U. S. Air Force Air Weather Service prepared statistics of wind based entirely upon available observational records [Hqs. AWS, 1958, private communication]. No effort was made to 'enrich' the data collections; observational material exclusively was used in the usual manner. The periods of record ranged from five to ten years, and were seven to nine years for most stations. Many geographical studies of upper wind statistics published in recent years are based upon shorter periods.

A total of 18 stations was duplicated in the two projects described, and it thus was possible to compare the results. The comparison was made by plotting summer and winter vertical profiles of the west-to-east mean wind components, and their standard deviations. Differences in the summer season are not appreciable; in winter, however, serious disagreements occur. Figure 1 shows the profiles of mean west-to-east wind speed for a number of stations at which the differences exceeded 10 knots through large thicknesses of atmosphere. Figure 2 shows examples of differences in excess of 5 knots in the standard deviations through similar thicknesses of atmosphere.

The fact that in most of the 18 cases the Weather Bureau statistics are consistently larger, and especially so near the level of maximum tropospheric wind, indicates that some of the expected bias has been removed.

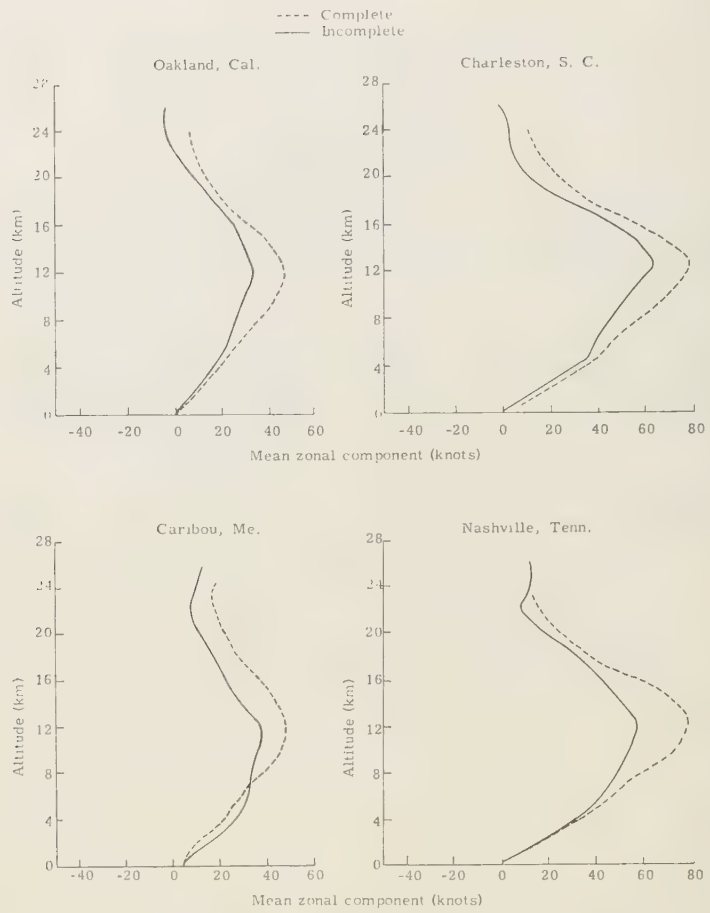

FIG. 1—Vertical profiles of mean zonal wind speed, computed from serially-complete and serially-incomplete data collections (winter season)

It is unfortunate that systematic errors in the statistical estimates occur in connection with the strongest winds. For many wind-dependent processes, in connection with which decisions may be based, on wind statistics the winds near jet-stream altitudes are frequently of major importance. In such cases, the use of conventional wind statistics may lead to serious underestimates of important phenomena.

Because of recent intensified interest in the statistical vertical coherence of wind [*Durst*, 1957, and *Court*, 1958, for example], interlevel correlation coefficients obtained from the two projects were also compared. Figure 3 shows the zonal interlevel correlation coefficients for Caribou in winter and Chanute Air Force Base in summer. The Caribou data were selected because of the large disagreements in both mean values and standard deviations as shown in Figures 1 and 2. The data for Chanute AFB were chosen because of the good agreement between the results of the two projects for this station. The left side of Figure 3 shows the inter-level correlation fields from the two data collections; those from the serially-incomplete collection appear above the diagonals. For perfect correspondence, the two charts would be symmetric about their diagonals. To facilitate comparison, the 0.8 and 0.6 isopleths have been extracted on the right-hand side of Figure 3. The disagree-

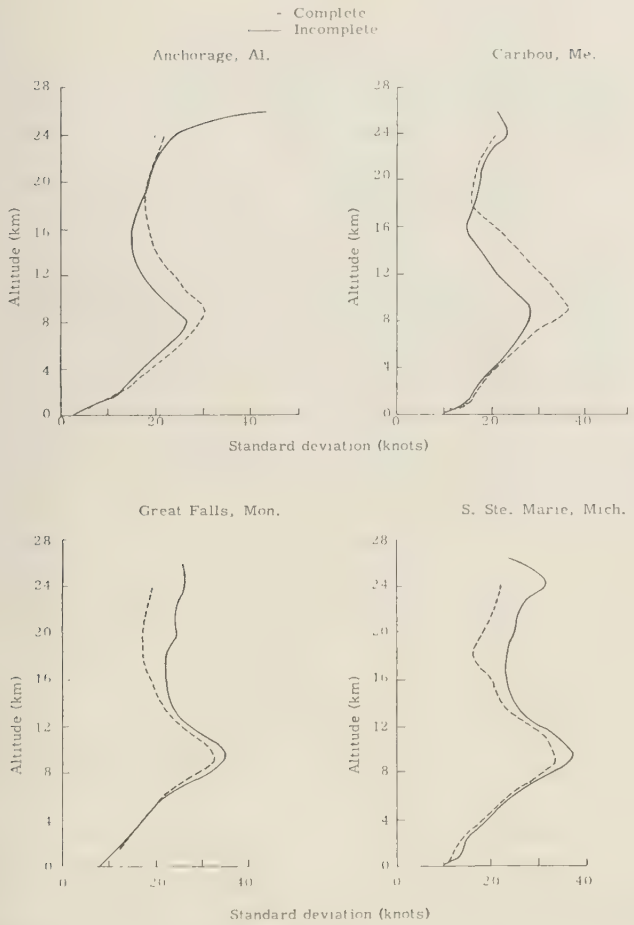

FIG. 2—Vertical profiles of the standard deviations of the mean zonal speed, computed from serially-complete and serially-incomplete data collections (winter season)

ment for the Caribou data is relatively extreme, while that for the Chanute data is not much greater than might result from artistic license.

It thus appears that the current method of summarizing available wind data collections to obtain information for planning and design purposes may be vulnerable to large error, especially for periods characterized by systematically large winds. Future developments will undoubtedly improve this situation. Fast-rising balloons, for example, will increase the mean altitude of low-elevation-angle terminations, and new airborne weather reconnaissance systems with improved electronics may avoid the difficulty entirely. The pressing problem of current requirements must be considered, however. The obvious corrective procedure of augmenting the available records with suitable estimates of missing data may be distasteful, on the grounds that objectively measured data are being contaminated by subjective guesses. It would be desirable to demonstrate the validity of inferred data obtained by methods similar to those employed by the U. S. Weather Bureau as described above, but this is not possible at present. However, the essential accuracy of the measured data is itself suspect [*Reitar*, 1958], so that for statistical sampling inferred data may well be as efficient as observed data.

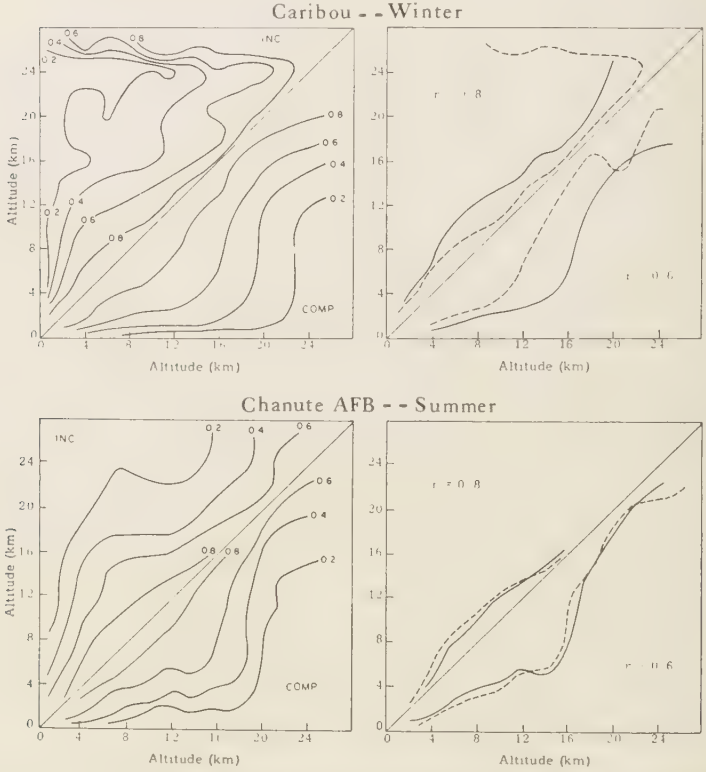

FIG. 3—Inter-level correlation coefficients of zonal wind speeds, computed from serially-complete and serially-incomplete data collections

To support the needs of modern aviation, our weather services routinely prepare synoptic weather charts for various altitudes up to the lower stratosphere. It is suggested that suitably interpolated synoptic values from these charts be used for the routine augmentation of upper air records. The program should also include the further extension of data to higher altitudes, consistent with knowledge concerning the validity of such estimates.

Acknowledgment—Appreciation is expressed to the Directorate of Climatology, Headquarters Air Weather Service, for permission to use their data.

REFERENCES

Bull. Am. Meteorol. Soc., Announcement, **39**, p. 557, 1958.

COURT, A., Wind correlations, U.S.A.F. Cambridge Research Center, Bedford, Mass. Tech. Rep. 58-229, 26 pp, 1958.

DURST, C. S., A statistical study of the variation of wind with height, Air Ministry, Meteorological Office, London, *Prof. Notes no. 121*, 10 pp, 1957.

RATNER, B., Areal climatic probabilities of radioactive fallout, U. S. Weather Bureau, Office of Climatology, unpublished manuscript, 1957.

REITAR, E. R., The layer of maximum wind, *J. Meteorol.*, **15**, 27–43, 1958.

(Manuscript received November 19, 1958.)

Preliminary Results of an Experiment to Determine Initial Precedence of Organized Electrification and Precipitation in Thunderstorms*

BERNARD VONNEGUT, CHARLES B. MOORE, AND ALEXANDER T. BOTKA

Arthur D. Little, Inc.
Cambridge, Massachusetts

Abstract—Observations of summer thunderstorms developing over Mt. Withington, New Mexico, show that electrification begins early in the cloud's development. Measurements within the cloud and above it show that electric charge accumulations similar in polarity to those of the mature storm begin to form before any echo can be seen with an x-band radar and before any electrical perturbations can be detected on the mountain summit beneath the cloud.

Measurements of potential gradient were made within the cloud with radiosondes supported on tethered balloons. It was found that the gradient within the cloud was far larger than that outside the cloud and that it reached values as high as 20 v cm^{-1} before the appearance of the radar echo. Measurements made from an airplane flying over the top of the growing cloud showed that here the fair weather potential gradient reversed before any radar echo could be seen. The development of the initial electrical activity appeared to be closely related to convective activity as indicated by tension on the line holding the tethered balloon and by the rapid rise of the cloud tops.

The initial radar precipitation echo within the cloud was frequently in the form of a hollow inverted cup that usually filled in and became solid in a few minutes.

A. Introduction

An assumption common to most speculations upon thunderstorms is that the falling of charged precipitation particles is responsible for their electrification. Though this assumption has on occasion been questioned, for example by *Gish* [1951], it has generally been uncritically accepted as self-evident and has not been subjected to test. During the summer of 1957 we made measurements on a number of thunderstorms at Mt. Withington, New Mexico, that bear on this problem and appear worth reporting at this time. Far from confirming the popular notion that precipitation causes electrification, these measurements indicate that electrification frequently precedes the formation of detectable precipitation and, as *Rayleigh* [1879] suggested,** that electrification may be a cause of precipitation, rather than a result.

* This work was made possible by the support of the Geophysics Branch of the Office of Naval Research, the Aerology Division of the Bureau of Aeronautics, U. S. Navy, the Atomic Energy Commission, and the Geophysics Research Directorate of the Air Force Cambridge Research Center.

** Excerpts pertinent to cloud physics from Rayleigh's little-known paper, *The influence of electricity on colliding water drops,* are given in the Addendum.

B. Design of the Experiment

The experimental program that we carried out is an extension of earlier work reported by *Workman* and *Reynolds,* [1953]; *Reynolds* and *Neill,* [1955]; and *Reynolds* and *Brook,* [1956], who made simultaneous measurements of the electric field and the radar echo from the summer thunderstorms that form almost daily over Mt. Withington. They measured the electric field beneath the cloud as a function of time, with field-measuring apparatus placed on the 3140-m summit of Mt. Withington. They measured the time of appearance of the first precipitation with an APQ-13, 3.2 cm radar 21 km north of the mountain. The conventional antenna scan in azimuth was used with a PPI presentation. An example of the data obtained is shown in Figure 1. All of their measurements showed that electrification of the cloud, as indicated by reversal of the normal fair-weather field, was preceded by the appearance of the first radar echo. On the basis of these observations, *Reynolds* and *Brook* [1956] concluded that "precipitation is a necessary but not sufficient condition for the onset of thunderstorm electrification."

The conclusion that precipitation precedes electrification certainly appears warranted from

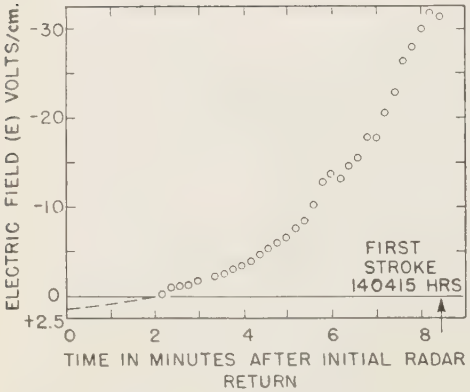

FIG. 1—Electric field increase preceding first lightning stroke in a growing New Mexico thunderstorm, September 5, 1952; the field meter was about 3 km distant from the cloud (after Reynolds and Neill)

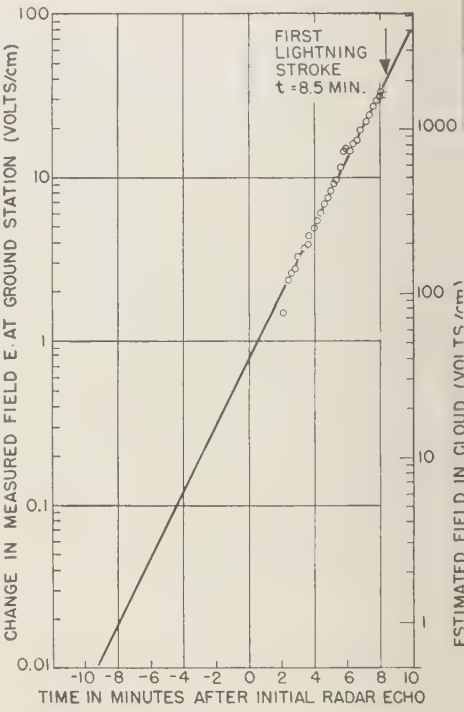

FIG. 2—Growth of the electric field with time at a station 3 km from a starting thunderstorm; the time data in Figure 1 has been replotted against the logarithm of the change in field; through the use of Gunn's observations discussed in the text, a new scale giving the electric field in the cloud is plotted; according to this extrapolation the cloud developed an internal field of 50 v cm^{-1} by the time the radar echo appeared; the observed field is increasing 10 times every 5 minutes

their data if 'onset of electrification' refers to significant changes in the electrical field on the ground beneath the cloud. On the other hand, because of several considerations, it appears that electrification might exist within the cloud for some time before it could be detected from the ground. First of all, one would expect that the electric field produced on the ground by electric charges in the cloud would be greatly attenuated because of distance. According to Reynolds' estimates, the closest charged region of the cloud would be 2 km or more from measuring equipment on the ground. Secondly, in the light of *Gunn's* [1955] observation that the electric field abruptly increased as he flew into a thundercloud, one might expect that measurements exterior to the cloud would be quite insensitive to electrification within.

Though, from one point of view, the data in Figure 1 appear to indicate that precipitation precedes electrification, the reverse can be argued. For example, if we replot the data on semilog paper as in Figure 2, we see that the growth of the electric field produced by the cloud is quite exponential and appears as a straight line. Now, the electric field within the cloud is doubtless far greater than it is on the ground. We can make an estimate of the ratio between the field observed by Reynolds on the ground and that existing within the cloud by comparing his field at the time of the first lightning stroke with the field that is probably necessary to cause lightning in a cloud. *Gunn* [1947] found that just prior to a lightning stroke, the electric field in a cloud was of the order of 1500 v cm^{-1}. According to Reynolds' data, the field on the ground was only 30 v cm^{-1} at the time of the first lightning stroke. On this basis we can estimate that the field produced by charge in the cloud was attenuated by a factor of about 50 at the ground. If we assume that this attenuation factor remained constant during the cloud's development, and that Reynolds' data can be extrapolated back in time according to the straight line in Figure 2, we find that the electric field in the cloud was already 50 v cm^{-1} at the time of the first radar echo.

The primary purpose of the experimental program carried out during the summer of 1957 was to determine which occurs first in the cloud, electrification or precipitation. We designed an experiment to extend Reynolds' earlier work by increasing the sensitivity of the radar precipitation detection and by making potential-gradient measurements as near as possible to the center of electrical activity. The primary components of the 3.2 cm radar were made available to us by Marx Brook and were the same that he and Reynolds had used in their work. We increased the sensitivity of the apparatus for detecting the initial echo by (1) carefully adjusting the components, (2) changing the antenna to give a zenith scan, and (3) bringing the equipment much nearer to the cloud by installing it on the mountain summit.

New, low-noise 1N23E crystals were used so that the measured receiver sensitivity of −105 dbm was attained repeatedly. TR tubes having a recovery time of less than 4 μsec to within 3 db of full sensitivity were used, so that precipitation could be detected at distances as small as 2 or 3 km. Our estimates of the smallest raindrops that could be detected in these clouds indicate that the initial precipitation echoes could be caused by raindrops with a median diameter for reflectivity of about 100 to 150 microns at these ranges.

The sensitivity of the detection of the initial electrification was increased by supplementing measurements made on the summit with potential-gradient measurements made within and above the cloud. Radiosondes to measure the vertical component of the potential gradient were suspended in the cloud on a tethered balloon, and an instrumented P-38 was flown over the top of the cloud with occasional passes through the cloud. The participation of Jim Cook, owner and pilot of the airplane, was made possible through the cooperation of the United States Weather Bureau and the Office of Naval Research. This aircraft not only measured the potential gradient above the cloud but also obtained information on the nature of precipitation in flights directed through the cloud by radioed instructions from the radar observer on the mountain summit.

C. Results

The measurements that we obtained during the summer of 1957 are in accord with those of Reynolds, Neill, and Brook in that on no occasion was reversal of the electric field observed on the mountain beneath the cloud before the first radar echo. On the other hand, the potential-gradient measurements within the cloud and directly over it show more often than not that the development of appreciable electrification occurs in a seemingly organized fashion before rather than after the first radar return. In summary, our results are as follows:

1. *Temperature and humidity structure*—The temperature and humidity distribution in this part of the United States during July and August was found to be quite similar from one day to another, although there was some variation due to effects of large-scale flow patterns elsewhere. To give some background for our other observations, at the risk of oversimplifying, we offer the data shown in Table 1 as representative of the conditions we found on and over Mt. Withington on many mornings.

Table 1—*Typical morning observations over Mt. Withington (July and August, 1957)*

Temperature (°C)	*Altitude Above Sea Level*		*Notes*
	In Clear Air (meters)	*In Cumuli** (meters)	
+13	3140	—	At 0900 MST at top of mountain
+ 7	3850	3850	Mean cloud base
0	4700	5100	
− 5	5450	6000	
−10	6150	6750	
−15	6900		

*The temperatures in the clouds were obtained by soundings with captive balloons, by aircraft, and by use of USWB radiosonde observations.

The moisture content of the air at the mountain top in the mornings varied between 9 and 12 gm kg^{-1} of dry air, averaging about 10 gm kg^{-1}. The air into which the cumuli grew was much drier, averaging perhaps 3 gm kg^{-1} at the 5 km level.

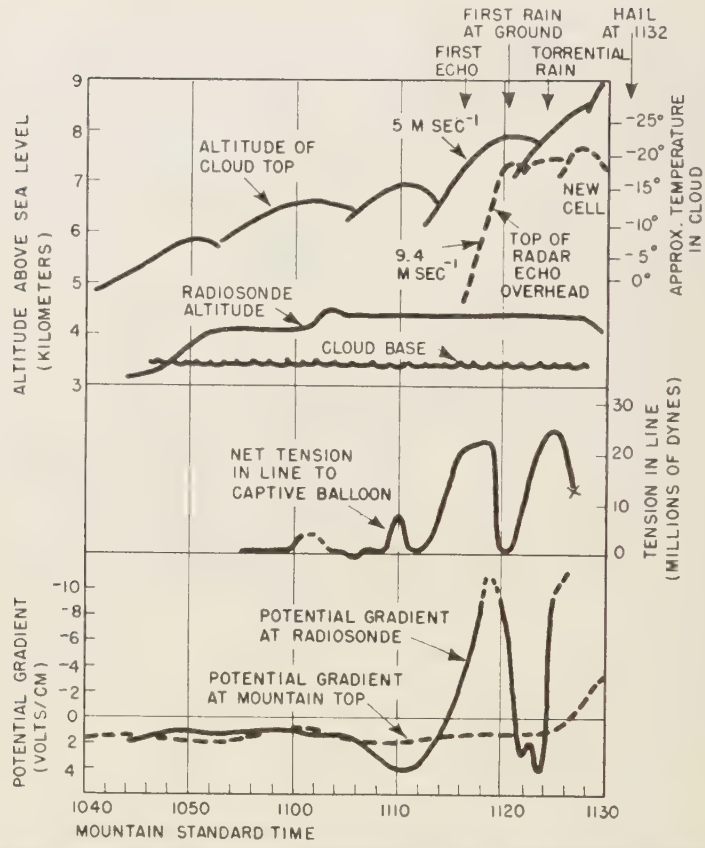

FIG. 3—Sequence of events at initiation of electrification in cumulus; first storm, August 16, 1957, Mt. Withington, New Mexico; this figure illustrates the association between convection and the accumulation of negative charge at the base of the cloud; this storm produced its first lightning stroke at 1148 MST and only seven strokes in the remaining 42 minutes of its life; a rainfall of 2 cm occurred in the 70 minutes between 1120 MST and 1230 MST

2. *Space-charge distribution*—Measurements made with a 3.7-m cubical Faraday cage show that before and during the initial development of the clouds the air on the mountain summit contains a fairly high but variable positive space charge of several hundred elementary charges cm^{-3}.

On the mountain summit the potential gradient frequently exhibits the so-called mountain effect, increasing in the fair-weather direction by a factor of two or more with the onset of convective activity.

Measurements of the electric potential gradient at 4 to 5 km above sea level within the cloud near its base (measurements made with radiosondes supported on tethered balloons) frequently show enhanced fair-weather potential gradients as high as 10 v cm^{-1} as much as 30 minutes before precipitation can be detected.

Measurements from an airplane above the top of the growing cloud show that usually the potential gradient there decreases or has reversed many minutes before the appearance of the radar echo. This result seems to indicate that positive charge is being accumulated within the cloud under the airplane.

3. *Initiation of thunderstorm electrification*—The growth of a large negative-charge concentration in the lower part of the cloud was observed to be closely correlated with rapid in-

creases (2 m sec^{-1} or more) in the height of the cloud top and in the tension of the line holding the tethered balloon. On occasion, large turrets were observed to rise rapidly, then to sink back, to rise higher, to level off for a period, then finally to rise higher yet. Each rise of the cloud top was associated with large reversals of the potential gradient at the cloud base, but upon a decrease in the rate of rise the internal electric field was observed to relax back to the fair-weather values. One example of this sequence is shown in Figure 3. The close association between the increase in electrification and convection was quite noticeable and appears to extend earlier findings of *Reynolds* and others [1955], who reported that "apparently strong vertical air velocities are also required for significant cloud electrification."

Observations with the radiosonde supported on the tethered balloon usually showed that the potential gradient was much larger in the cloud than in the clear air around it. Large increases in the gradient were frequently observed when the balloon entered the cloud base. Similarly, when (because of cloud movement) the radiosonde came out of the cloud into clear air, it was often observed that the potential gradient dropped to a much lower value; conversely, when it re-entered the cloud, the gradient increased. Our observations indicate that within the cloud there is much electrical activity that is not detectable outside the cloud by the normal instrumentation that we and other observers have used. The electric field even from growing thunderstorms as close as 4 or 5 km away was frequently not noticeable until the first lightning stroke occurred, certainly long after the commencement of electrification. Cook, who flew his P-38 closely above the cloud top, found that the reversal of the fair-weather field above the cloud disappeared whenever the cloud top did not rise at an average rate greater than about 1 m sec^{-1} between passes. A possible explanation of these results is the presence of an electrical screening layer around the cloud. This layer, caused by the discontinuity in conductivity at the cloud surface, traps the ions that move to the cloud under the influence of the field produced by charge already in the cloud.

4. *Potential-gradient reversal*—In many cases it was observed that the potential gradient within the cloud, as measured with the radiosonde, reversed and reached values in excess of -10 v cm^{-1} before any radar echo could be detected. The reversal usually came three or four minutes before the first radar return, but on occasion preceded the first echo by half an hour or more. To observe this sequence, however, it was necessary that the radiosonde be in the active cell.

5. *Initiation of precipitation*—An interesting feature of the RHI radar observations made during the summer was that frequently the vertical cross section of the initial echo was hollow and had the form of an inverted cup. Typical examples are shown in Figure 4. On the sev-

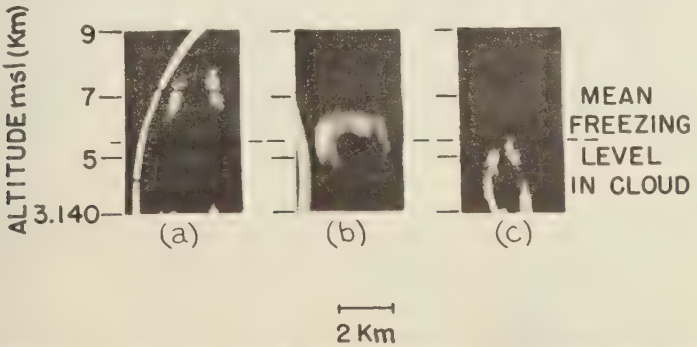

FIG. 4—Photographs of some initial echoes observed near Mt. Withington, New Mexico; (a) 9055 MST, August 9, 1957, distance 7 km, altitude of echo top 7.9 km, estimated temperature $-17°C$; the top of this cup echo has partially disappeared in reproduction; (b) 1017 MST, August 13, 1957, distance 10 km, altitude of echo top 6.4 km, estimated temperature $-8°C$; (c) 1019 MST, August 13, 1957, distance 4 km, altitude of echo top 5.4 km, estimated temperature $-1°C$; the horizontal dark band is due to a graduation on oscilloscope face; the arcs are segments of the range mark at 8 km

eral occasions that the radar echo of the airplane flying over the top of the cloud was simultaneously observed, it was determined that the upper limit of the hollow precipitation echo was 300 to 600 m below the top of the visible cloud. The hollow appearance of the initial radar echo was quite transitory, and the center usually filled in and became reflective in a few minutes.

The visual appearance of the initial virga and rain descending beneath the New Mexico clouds frequently suggests a downward extension of the hollow radar echo. The first precipitation briefly appears to be in the form of a hollow circular cylinder that in a matter of a few minutes becomes a 'solid' rain shaft.

Though these hollow echoes are superficially very similar to the mantle echoes observed by *Harper* and others, [1957] with a 10-cm radar, they are probably basically different. From the fact that the mantle echoes could be seen only with the long-wavelength radar, and from the meteorological conditions at the time, these investigators appear quite certain that the mantle echoes were caused not by precipitation but by a contrast in refractive indices in the atmosphere. Our hollow echoes, on the other hand, proved undeniably to be rain when they formed or moved over us. The fact that we also saw these hollow echoes with a 1.25-cm radar, which we operated on the mountain for a short time, strengthens our belief that they were essentially different from those observed by Ludlam.

The air temperature at the top of the initial radar echoes has been estimated for 24 storms. Of these, six were found to be above 0°C, six were between 0°C and −5°C, six were between −5°C and −10°C, and the remainder were below −10°C. It is of interest that four of the latter six in the highest altitude group were inverted cup echoes and occurred in clouds that grew very rapidly. For example, on August 14, only 18 minutes after the appearance of the cloud, a cup echo with the top at an altitude of 7300 m was observed; in another three minutes, the first lightning stroke occurred! When a radiosonde was in these active clouds, potential-gradient reversals were observed to precede the appearance of the high echoes.

On several occasions with direction by radio from the radar trailer, Cook flew through the regions of the initial cup echoes at higher altitudes. He reported that while the extreme outer portion of the cloud top was covered with a thin cap of small ice crystals,* within the cloud he encountered very heavy rain with no ice present, surrounded by a region without precipitation. Despite several attempts, we did not succeed in directing the airplane into the hollow core of these initial echoes. The identification of the state of the hydrometeors causing the initial echo even in these higher clouds as liquid seems to be a consistent extension to New Mexico of the previous Midwestern work by *Battan* [1953].

It is interesting to speculate on the mechanisms that produce this characteristic echo shape observed so frequently in these thunderclouds. From the observations, it seems that the precipitation giving the initial echo must be produced by a coalescence mechanism. Conceivably the shape of the initial reflecting zone may result from shear that causes a greater frequency of collisions between cloud droplets. Alternatively, the shape may be a result of an accelerated coalescence process caused by the electric field, wherein the shape indicates a region of higher field intensity between the space charge within the cloud and a screening layer near the cloud surface, as suggested by our other observations. Both the mantles and these hollow echoes are interesting phenomena worthy of further study.

6. *Observations of cloud circulation*—When the captive balloon was flying at an altitude of about 7 km in clear air, a static tension of about 4.5×10^6 dynes was produced in the nylon re-

* This sheath of ice crystals on the outer surface of these cold clouds was noticed repeatedly by Cook and on two occasions by the balloon pilots in the flights discussed in Section 10. As the first balloon went through the edge of a young growing cloud, the crystals were seen at an altitude of 6.4 km where the temperature was about −12°C. Here the crystals were estimated to be less than 50 microns across and were in a layer at the outer surface of a cauliflower top of a cumulus tower. On the second balloon flight, through the side of an 'old' cloud, ice crystals were seen as the balloon emerged from the cloud. These were estimated to be 400 microns in size.

From the low radar reflectivity of small ice crystals and from the great separation in the height of the echoes from the cloud and from the airplane when Cook reported that he was just over the cloud, it is believed that the 'initial' radar echoes do not arise from this surface layer of ice crystals. The origin of these crystals and their interaction with the cloud are unknown.

taining line at the winch. As the convective activity proceeded and the balloon became caught in an updraft within a cloud, tensions of as much as 9×10^7 dynes were measured. Estimation of the updraft velocities from the tension on the line yielded values as high as 10 m sec^{-1} with values of about 5 m sec^{-1} commonly occurring in a burst of convection. The increase in tension was usually noted just prior to the reversal of the potential gradient in the base of the cloud where a negative imbalance of charge appeared over the lower radiosonde.

When the captive balloon came near the edge of a convective cloud, the flying line became quite slack; it was frequently necessary to take in 600 to 1000 m rapidly, for the balloon could no longer support this length. Estimates from the loss of effective lift indicate that downdrafts of as much as 4 m sec^{-1} occur at the outside edges of these convective clouds 30 minutes or so before any radar echo is detectable. *Malkus* [1955] has found downdrafts of similar magnitude around nonprecipitating tradewind cumulus.

7. *Negative space-charge accumulation in lower portion of cloud*—On a number of days two radiosondes separated vertically by about 800 m were carried by the same captive balloon. Since the balloon could not rise so high as when it carried a single instrument, the upper radiosonde was frequently at an altitude of about 5 km MSL, just below the freezing level, and the lower instrument was about 400 m above the cloud base.

When the instruments, so arranged, were in the active cell of the cloud, the lower radiosonde invariably reported a reversed potential gradient first, usually soon after increased tension in the balloon line. If the convection continued, the electric field at the ground next reversed from the fair-weather polarity. The upper radiosonde usually reported an enhanced fair-weather potential gradient until the first lightning stroke occurred.

The polarity of the space charge in the air at the mountain top frequently reversed from positive to negative just after the potential-gradient reversal there indicated negative charge overhead at the onset of the cloud electrification. Negative space-charge concentrations as great as 750 elementary charges cm^{-3} were noted under these conditions. When the reversed potential gradient increased to values of 10 v cm^{-1}, corona discharge began from points on the mountain and positive space-charge densities of several thousand elementary charges cm^{-3} were then observed.

For example (see Fig. 5), early in the morning of August 20 the cumulus base was very low, just above the mountain top, and finally descended to the mountain at about 1114 MST. About 1050 MST, a large cloud turret rose rapidly above the mountain ridge just to the south of the station. The first reversal of the potential gradient (reported by a radiosonde 1 km up in the cloud) occurred at 1055 MST. This reversed potential gradient increased somewhat exponentially, reaching -3.5 v cm^{-1} at 1100 MST and going off scale at -10 v cm^{-1} at 1101 MST. The potential gradient at the summit began to decrease slowly at 1050 MST until it reversed at 1059 MST, whereupon it increased slowly in the 'anti-fair-weather' direction, reaching 10 v cm^{-1} at 1107 MST.

The space-charge concentration measured on the summit during the earlier portion of the morning averaged between 100 and 300 positive elementary charges cm^{-3}. At 1052 MST it dropped to essentially zero, where it remained until about 1100 MST, when it became definitely negative. The concentration of this negative charge increased to 250 charges cm^{-3} at 1102.5 MST and to 1000 charges at 1105 MST. At 1106 MST, the polarity of the space charge changed abruptly to positive, apparently coincidentally with the onset of point discharge under the influence of the high potential gradient. Concentrations of positive charge of as much as 1600 elementary charges cm^{-3} were observed at the summit in the next seven minutes.

The negative conductivity of the air under a tree began a sudden increase at 1100 MST, going off scale at 1114 MST with a value of more than 10 times the mean conductivity observed earlier during the morning. The first radar echo above us was detected 2 km south of the summit at 1102 MST, and the first raindrops were detected at the ground shortly after 1105 MST. Only a trace of rain had fallen by 1140 MST.

These observations suggest that with the onset of convection in these clouds, negative charge is accumulated in some manner in the extreme lower portions of the cloud. When the convec-

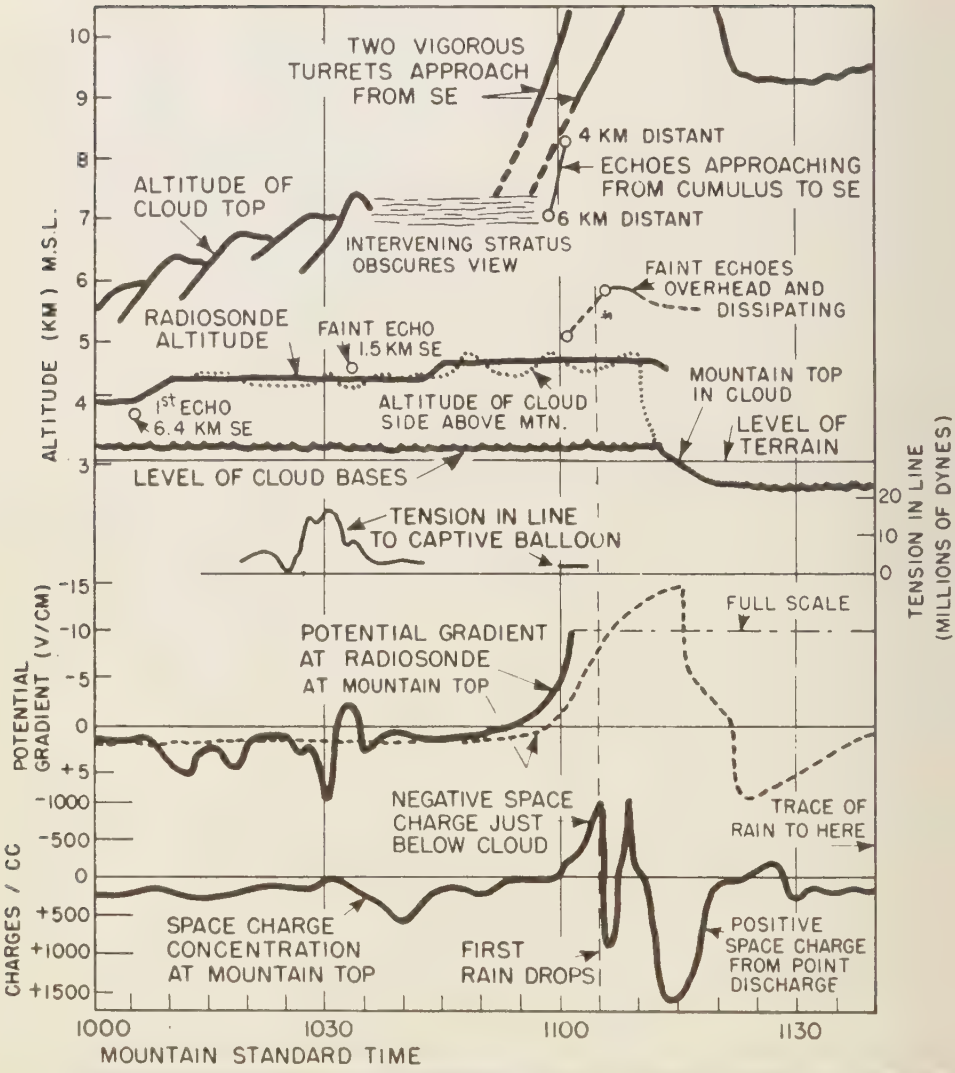

FIG. 5—Development of convection and electrification, August 20, 1957, Mt. Withington, New Mexico (note electrical activity reported by radiosonde at 1030 MST, simultaneous increase in tension on line holding captive balloon, and subsequent formation of a transient, faint radar echo; also note appearance of negative space charge at mountain top shortly after radiosonde in lower part of cloud shows field reversal)

tion continues, the negative charge increases to such an extent that the atmospheric potential gradient beneath the cloud is reversed and rises to high negative values. The presence of negative space charge at the ground so soon after the reversal aloft suggests that downdrafts from the cloud carry some of this negative charge accumulation from the cloud all the way down to the mountain summit. This phenomenon was observed not only on days when the cloud base was down to the mountain top but also when the base was as high as 800 m above the summit.

8. *Charge carried by rain*—Usually the cloud

bases were several hundred meters above the mountain. However, on a few days the summit of the mountain projected well into the cloud. On these occasions, when measurements were made of the charge carried by falling rain, the currents did not differ much from those observed in clear air and seldom exceeded about 2×10^{-14} amp cm^{-2} except following the periods when the potential gradient was sufficient to cause point discharge. During these periods the rain currents attained values of as great as 3×10^{-13} amp cm^{-2}, and the sign of the charge being carried to the earth by the rain was the same as the sign of the charge leaving the earth by point discharge. These observations suggest that the principal mechanism operating to charge the rain was the collection by the falling drops of fast ions produced by corona discharge from points on the mountain.

9. *Cloud polarity*—In observations from the ground, it was difficult to determine the polarity of cloud tops without ambiguity. However, when the aircraft made passes over the clouds there was little question concerning the sign of the uppermost charge. In a score of flights the cloud 'dipole' was found to be of the conventional polarity, with the potential gradient being reversed from the fair-weather sense when the plane was over the electrified cloud turret. In one case of a growing cloud, however, the potential gradient over it was strongly intensified in the fair-weather direction as our aircraft made repeated passes. This indicated that the cloud had an accumulation of negative charge at its top. We have noted similar negative-topped cumulus elsewhere in the United States in studies with other aircraft.

10. *Free-balloon flights into thunderstorms*—Three manned free-balloon flights have been made into clouds by one of the authors in an effort to study directly the nature and growth of the hydrometeors associated with the initial appearance of electrification in cumulo-nimbus clouds. M. D. Ross, Lcdr. USNR, participated in one flight, Paul MacCready in the second. The third flight was made at a prior time with T. O. Haig, Major USAF. Unfortunately, it was impossible with our equipment to be at the proper level and location within the cloud when electrification commenced. However, interesting subsidiary observations were made. Much structure in the updrafts and downdrafts was observed in these flights, particularly beneath the clouds, where vertical velocities as great as ± 5 m sec^{-1} were encountered in and beneath non-precipitating clouds. Contrary to the expectations of some students of cloud circulation, no small-scale turbulence was noticeable within or beneath the clouds, even in vertical currents moving at ± 5 m. sec^{-1}. This finding supports the calculations made by *East* [1957], who concluded that accelerations due to turbulence would be low even within convective clouds.

The ice-crystal sheaths observed around the upper portions of the colder clouds have already been discussed in Section 5.

Horizontal wind shear of possibly 1 or 2 m sec^{-1} between the gondola and the balloon was observed on the second flight when the balloon was just below an extended cloud base from which rain was falling in several isolated sheets.

D. Conclusion

Though our experimental results strongly suggest that falling precipitation may not be the primary cause of electrification, they do not entirely preclude this possibility. For example, it is possible, but scarcely probable, that sufficient precipitation to cause electrification may have been present in the cloud without its having been detectable with radar. Using the data on precipitation reflectivities and rainfall intensities computed by *Atlas* [1957] and by *Wexler* and *Swingle* [1947], we have found that the initial rain in the clouds over Mt. Withington may have been detected as it attained a 'rate'* of about 5×10^{-3} mm hr^{-1}.

Although precipitation may not have caused the initial electrification, it may yet be the primary cause of later electrification. This too appears doubtful, for our records and those of *Reynolds* and his associates [1955, 1956] usually show a rapid, continuous increase in field with no discontinuities to suggest the onset of a second mechanism. The fact that the form and polarity of the early electric field perturbations persist unchanged to the time of the first lightning stroke appears to indicate the continued

* This 'rate' is computed only for further calculation of the possible charge being separated by the initial precipitation elements. Actually, within the cloud these raindrops are moving upward in an updraft of several meters per second, since their fall velocity is probably no greater than ½ m sec^{-1}.

action of the initial charge generating mechanism.

Our understanding of thunderstorms is so limited that it is certainly risky to assume that what we have observed in New Mexico is true of all thunderstorms. Measurements reported by *Fitzgerald* [1956] on storms in the Central West suggest that he too has observed that electrification precedes the initial radar echo. However, this conclusion is somewhat in doubt because the receiver sensitivity of the similar radar he used was stated to be only −76 dbm, giving a possible detection of drops with a median diameter perhaps no smaller than 0.7 mm.

We feel that our findings raise many doubts concerning the validity of the assumption that falling precipitation is the primary cause of charge generation in thunderstorms. We urge that other investigators examine this basic assumption critically and carry out investigations of their own.

Acknowledgments—Adequate thanks to all of the individuals and organizations whose generous cooperation made this work possible would require far more space than is required by this report. We are particularly grateful to our sponsors, the Office of Naval Research and the Bureau of Aeronautics, United States Navy; and to the New Mexico Institute of Mining and Technology, which aided us in countless different ways.

Special thanks are due David Atlas and Marx Brook, without whose help we could not have made the radar observations. We are indebted to coworkers in cloud physics from other organizations who carried out research of their own and made invaluable contributions. These include Seville Chapman, Roland Pilie, and Roy Hendrick of the Cornell Aeronautical Laboratory; Richard Schotland of New York University; James Kraakevik and G. P. Serbu of the Naval Research Laboratory; Paul MacCready, and associates of Meteorological Research, Inc.; and W. L. Webb and others from the White Sands Signal Agency.

References

Atlas, D., Physical synoptic variations of raindrop size parameters, *Proc. 6th Wea. Radar Conf.*, Am. Meteorol. Soc., Cambridge, Mass., 21–30, 1957.

Battan, L. J., Observations of the formation and spread of precipitation in convective clouds, *J. Meteorol.*, 10, 311–324, 1953.

East, T. W. R., The intensity of turbulence in convective clouds, *Quart. J. Roy. Meteorol. Soc.*, 83, 121–126, 1957.

Fitzgerald, D. R., Theoretical and experimental studies of convective cloud electrification, Final Report, Contract AF19(604)1552, University of Chicago, 88–92, 1956.

Gish, O. H., Universal aspects of atmospheric electricity, *Compendium Meteorol.*, p. 117, 1951.

Gunn, R., The electrical charge on precipitation at various altitudes and its relation to thunderstorms, *Phys. Rev.*, 71, 186, 1947.

Gunn, R., Comments in proceedings on the conference on atmospheric electricity, *Air Force Cambridge Research Center, Geophysical Research Paper 42*, p. 242, 1955.

Harper, W. D., F. H. Ludlam and P. M. Saunders, Radar echoes from cumulus clouds, *Proc. 6th Wea. Radar Conf.*, Am. Meteorol. Soc., Cambridge, Mass., 267–272, 1957.

Malkus, J. S., On the formation and structure of downdrafts in cumulus clouds, *J. Meteorol.*, 12, p. 350, 1955.

Lord Rayleigh, The influence of electricity on colliding water drops, *Proc. Roy. Soc.*, 28, 406–409, 1879.

Reynolds, S. E., and M. Brook, Correlation of the initial electric field and the radar echo in thunderstorms, *J. Meteorol.*, 13, 376–380, 1956.

Reynolds, S. E., M. Brook, and M. F. Gourley, Thunderstorm electricity, Report 9, New Mexico Institute of Mining and Technology, Socorro, p. 5, 1955.

Reynolds, S. E., and H. W. Neill, The distribution and discharge of thunderstorm charge-centers, *J. Meteorol.*, 12, 1–12, 1955.

Wexler, R., and D. M. Swingle, Radar storm detection, *Bull. Am. Meteorol. Soc.*, 28, p. 164, 1947.

Workman, E. J., and S. E. Reynolds, Structure and electrification, *Thunderstorm Electricity*, University of Chicago Press, Chicago, pp. 139–149, 1953.

(Manuscript received March 31, 1958.)

Addendum

Excerpts Pertinent to Cloud Physics from a Paper Written by Lord Rayleigh in 1879

(The influence of electricity on colliding water drops, *Proceedings Royal Society*, vol. 28, pp. 406–409)

It has been known for many years that electricity has an extraordinary influence upon the behaviour of fine jets of water ascending in a nearly vertical direction. In its normal state a jet resolves itself into drops, which even before passing the summit, and still more after passing it, are scattered through a considerable width. When a feebly electrified body is brought into its neighbourhood, the jet undergoes a remarkable transformation, and appears to become coherent; but under more powerful electrical ac-

on the scattering becomes even greater than
t first. The second effect is readily attributed
o the mutual repulsion of the electrified drops,
ut the action of feeble electricity in producing
pparent coherence has been a mystery hitherto.
. .
I have lately succeeded in proving that the
ormal scattering of a nearly vertical jet is due
o the rebound of the drops when they come
nto collision with one another. . . .
Under moderate electrical influence there is
o material change in the resolution into drops,
or in the subsequent motion of the drops up
o the moment of collision. The difference be-
ns here. Instead of rebounding after collision,
s the unelectrified drops of clean water gen-
rally or always do, the electrified* drops coa-

* Rayleigh's words, "electrified drops," here can
roperly be interpreted as "neutral drops under
he influence of an external electric field," for sen-
bly neutral drops produced in a field-free space
ill coalesce on collision under the influence of
eak or strong electric fields of either polarity.

lesce, and thus the jet is no longer scattered about. . . .

Some further details on this subject, and other investigations respecting the phenomena of jets, are reserved for another communication, which I hope soon to be able to present to the Royal Society; but I cannot close without indicating the probable application to meteorology of the facts already mentioned. It is obvious that the formation of rain must depend very materially upon the consequences of encounters between cloud particles. If encounters do not lead to contacts, or if contacts result in rebounds, the particles remain of the same size as before; but, if the issue be coalescence, the bigger drops must rapidly increase in size and be precipitated as rain. Now, from what has appeared above we have every reason to suppose that the results of an encounter will be different according to the electrical condition of the particles, and we may thus anticipate an explanation of the remarkable but hitherto mysterious connection between rain and electrical manifestations.

Velocity of Sound in Two-Component Systems*

LEON KNOPOFF

Institute of Geophysics
University of California

Abstract—The velocity of sound has been measured between the liquidus and solidus temperatures in two-component systems. For high frequencies, the results show the transitions to be second order transitions. On this basis, the decrease in velocity in region *F* of the earth's core, reported by Jeffreys, is shown to be inconsistent with the assumption of a simple iron-nickel composition for both the solid inner and liquid outer cores.

A two-component solid-liquid transition may ccur in nature. The earth is usually described s having a liquid iron-nickel outer core extend- ng from 2900 km to 5300 km in depth. Beneath iis is found a solid inner core extending from 300 km depth to the center of the earth. This nner core is most likely a solid iron-nickel alloy *Birch,* 1952; *Knopoff* and *MacDonald,* 1958]. n intermediate region between the liquid and olid portions (called *F* in *Bullen's* [1953] nota- ion) is usually assigned a radius interval of bout 140 km. *Jeffreys* [1939] indicates that the F layer has an anomalous low seismic wave ve- ocity, lower than that in the liquid and solid egions on either side. *Gutenberg* and *Richter* 1938], on the other hand, ascribe to this region velocity variation increasing monotonically rom the lower velocity in the liquid region to he higher velocity in the solid region.

The behavior of the velocity of sound in a ne-component system undergoing a transition nder temperature from the solid to the liquid tate shows the transition to be of the first or- er [*Pochapsky,* 1951; *Shimozuru,* 1956; *Naka- mura,* 1958]. The above experiments on the nelting of pure sodium and pure tin and others n which materials have been taken close to the nelting point [*Siegel* and *Cummerow,* 1940; *Kornfeld* and *Shestikin,* 1942; *Bordoni* and *Nuovo,* 1953] show that significant changes in he elastic moduli take place near the melting oint. It is perhaps hazardous to use the elastic ata to determine the melting point because of he several possible definitions of melting.

In this note the results are reported of the neasurement of the velocity of sound in a two- omponent system taken through the intermedi- ate region between the liquidus and solidus temperatures. For acoustic periods which are short compared with the diffusion rate for the change in composition with pressure within the intermediate region a second order transition for the velocity dependence upon temperature is anticipated.

A simple laboratory experiment will indicate whether an anomalous low velocity exists in the melting interval of a two-component system. Since it is not known whether the earth's inner core is a two-component eutectic or a solid solution, although the latter is more likely for an iron-nickel composition, measurements have been made of the variation of velocity with temperature for both kinds of solids.

The eutectic studied was an indium-tin alloy of composition $In_{67\%}$-$Sn_{43\%}$ (weight percentages). This material has a liquidus at 121°C and a solidus at 116°C [*Smithells,* 1955].

The solid solution studied was a solution of $anthracene_{25\%}$-$phenanthrene_{75\%}$. This material has a liquidus at 138°C and a solidus at 113°C [*Timmermans,* 1936; *Kofler,* 1955].

Each sample was housed in a cylindrical steel cup, 3 cm dia. × 6 cm long. The cup was placed in a solid aluminum bomb, and the bomb and crystal assembly were mounted in a large furnace so that the axis of the cylinder was vertical. Two quartz crystals, housed in small steel cups, were glued onto the machined end of the sample and onto the bottom of the sample cup. The upper transducer cup had a pressure assembly constructed so as to maintain contact with the sample at all temperatures. A stop was associated with this pressure assembly to prevent the crystal from dropping into the melt. Three thermocouples along the sample showed the temperature to be within 0.2°C over the

* Publication No. 126, Institute of Geophysics, University of California

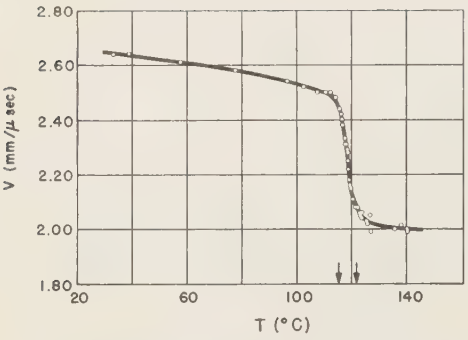

FIG. 1—Variation of compression wave velocity with temperature in $In_{57\%}$-$Sn_{43\%}$; the nominal melting region is indicated by the arrows

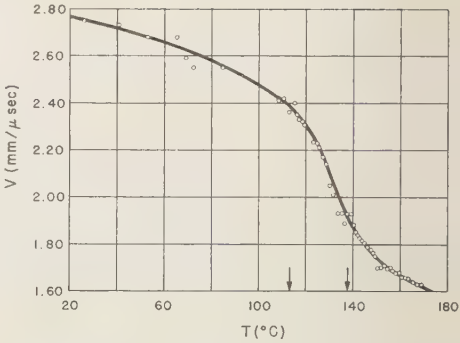

FIG. 2—Variation of compression wave velocity with temperature in anthracene$_{25\%}$-phenanthrene$_{75\%}$; the nominal melting region is indicated by the arrows

entire sample even at the highest temperatures.

The velocity of sound was computed from the time delay of the sound pulse received at one crystal measured with respect to the time of excitation of the other crystal. The excitation of the latter are obtained from an ordinary pulse generator. The time delay was obtained from oscilloscopic observation. Delay times were corrected for the thickness of the steel cups and for the expansion of the system.

The velocity results for the two materials are presented in Figures 1 and 2. The nominal liquidus and solidus temperatures are indicated in these figures. No anomalous low velocity is found in the transition region. The transition is seen to be, at the lowest, a second order transition in both cases. The decrease of the elastic modulus in the vicinity of the solidus can be easily identified.

In order to apply these results to the description of region *F*, we must first compare the frequencies of core waves with the laboratory frequencies used. We shall assume that core wave periods, of the order of seconds, are, as in the laboratory case, small compared with the times for diffusion processes to be important under the influence of the change of pressure in the sound wave. We further assume that acoustic behavior at extreme pressure and temperature is similar to that at one atmosphere and low temperature. Under these assumptions, we conclude that the anomalous low velocity reported by Jeffreys for region *F* in the earth suggests a compositional feature more complex than the simple molten iron-nickel to solid iron-nickel transition usually given. On the other hand, the Gutenberg velocity data are completely consistent with the composition suggested above.

The author wishes to express his appreciation to J. D. Fett for carrying out some of the details of the measurements.

REFERENCES

BIRCH, F., Elasticity and constitution of the earth's interior, *J. Geophys. Research,* **57**, 227–286, 1952.

BORDONI, P. G., AND M. NUOVO, Misure di velocità delle onde elastiche nei solidi a temperatura elevata, *Ricerca Sci.,* **23**, 593–599, 1953.

BULLEN, K. E., *An introduction to the theory of seismology,* University Press, Cambridge, 2nd ed., p. 209, 1953.

GUTENBERG, B., AND C. F. RICHTER, P′ and the earth's core, *Monthly Notices Roy. Astron. Soc. Geophys. Suppl.,* **4**, 363–372, 1938.

JEFFREYS, H., The times of the core waves II, *Monthly Notices Roy. Astron. Soc. Geophys. Suppl.,* **4**, 594–615, 1939.

KNOPOFF, L., AND G. J. F. MACDONALD, The magnetic field and the central core of the earth, *Geophys. J. Roy. Astron. Soc.,* **1**, 216–223, 1958.

KOFLER, A., Schmelzen und Kristallisieren von Mischkristallen: Phenanthen-Anthracen, *Monatsch. Chem.,* **86**, 301–311, 1955.

KORNFELD, M., AND P. SHESTIKIN, Elasticity of a crystal as dependent on temperature, *Doklady Akad. Nauk S.S.S.R.,* **36**, 52–56, 1942.

NAKAMURA, Y., Measurement of elastic wave velocity in polycrystalline tin, especially in the vicinity of its melting point, *Sci. Repts. Tôhoku Univ., Fifth Ser.,* **10**, 28–35, 1958.

POCHAPSKY, T. E., Temperature variation of the compressibility of molten sodium, *Phys. Rev.* **84**, 553–558, 1951.

HIMOZURU, D., Study on the elasticity near the melting point, II, *Bull. Earthquake Research Inst. Tokyo Univ.*, 34, 87–96, 1956.
IEGEL, S., AND R. CUMMEROW, On the elasticity of crystals, *J. Chem. Phys.*, 8, 847, 1940.
MITHELLS, C. J., *Metals reference book*, Interscience Publishers, Inc., New York, 2nd ed., vol. 1, p. 403, 1955.
TIMMERMANS, J., *Les solutions concentrées*, Masson et Cié., Paris, p. 63, 1936.

(Manuscript received October 31, 1958.)

Climatic Stability of Eighteen Degree Water at Bermuda*

ELIZABETH SCHROEDER AND HENRY STOMMEL

Woods Hole Oceanographic Institution
Woods Hole, Massachusetts

DAVID MENZEL AND WILLIAM SUTCLIFFE, JR.

Bermuda Biological Station
St. George's West, Bermuda

Abstract—Temperature soundings in the ocean off Bermuda are available for 85 years. All records show the water mass just beneath the surface to be remarkably constant in temperature and salinity. Oxygen measurements indicate that this water is in convective contact with the atmosphere each winter. More detailed and frequent measurements made by the ship *Panulirus* are here presented for the first time, substantiating this remarkable and puzzling climatic stability of near-surface water in the northwestern Sargasso Sea.

Introduction—Recently there has been an increasing interest in all phenomena which are suggestive of climatic change in the oceans. For example, in June 1958, at a conference held at Rancho Santa Fe under the auspices of the Scripps Institution of Oceanography, various forms of evidence were presented which suggest that there have been significant changes of surface temperature (amounting to several degrees) over vast areas of the North Pacific.

Since little subsurface data from midocean is available to determine how much these temperature fluctuations are limited in depth, it is of interest to present some evidence based on mid-Atlantic hydrographic stations near Bermuda, which exhibits a remarkable climatic stability of waters just below the surface. We have for this purpose several *Challenger* stations (no salinity) made near Bermuda in 1873; two stations from the 1920's; and during the 1930's a fair number of *Atlantis* and *Culver* stations (1932, 10; 1933, 1; 1937, 7; 1938, 13; 1939, 9). During the war years there are none, but afterwards various ships passing Bermuda occasionally made acceptable stations near Bermuda (1949, 4; 1950, 1; 1951, 1), and in 1954 the Bermuda Biological Station vessel Panulirus began a systematic series of hydrographic stations within sight of the island, so that we now can construct a reasonably accurate picture of the seasonal variations of properties over several years in succession.

The feature upon which we wish to focus attention is the body of water between the depths of 150 meters and 450 meters with a range in temperature of from 17°C to 19°C and a salinity of about 36.50 ± .10 ppm with an inflection point in the temperature sounding at about 18°C; for convenience we shall call it *18° Water* although actually its temperature is spread over a finite interval. Immediately below the 18° Water lies the main thermocline; above it lies a shallow surface thermocline subject to wide seasonal variation. The 18° Water is not strictly homogeneous; it has a gravitational stability, and this stability varies from time to time. It is not confined to the vicinity of Bermuda but occurs over most of the Sargasso Sea, an area of about 4 times 10^6 km^2. Toward its southern (about 20°N) and eastern (about 40°W) limits the 18° Water becomes much thinner than at Bermuda, but its characteristic inflection point in the vertical temperature distribution and its temperature-salinity (T-S) relation remain constant. To the north and west, the 18° Water is bounded by the Gulf Stream. Everywhere it looks like a more or less 'homogeneous' layer sandwiched between the shallow surface thermocline and the deeper main thermocline.

At the latitude of Bermuda, and to the north, winter cooling actually wipes away the shallow surface thermocline so that this layer of 18° Water is exposed to the action of surface-cooling and salinity-changing mechanisms associated with each winter's storms, and to renewal of dissolved oxygen by gas exchange across the sea surface. In southern latitudes of the Sargasso

* Contribution No. 992 from the Woods Hole Oceanographic Institution. Contribution No. 242 from the Bermuda Biological Station.

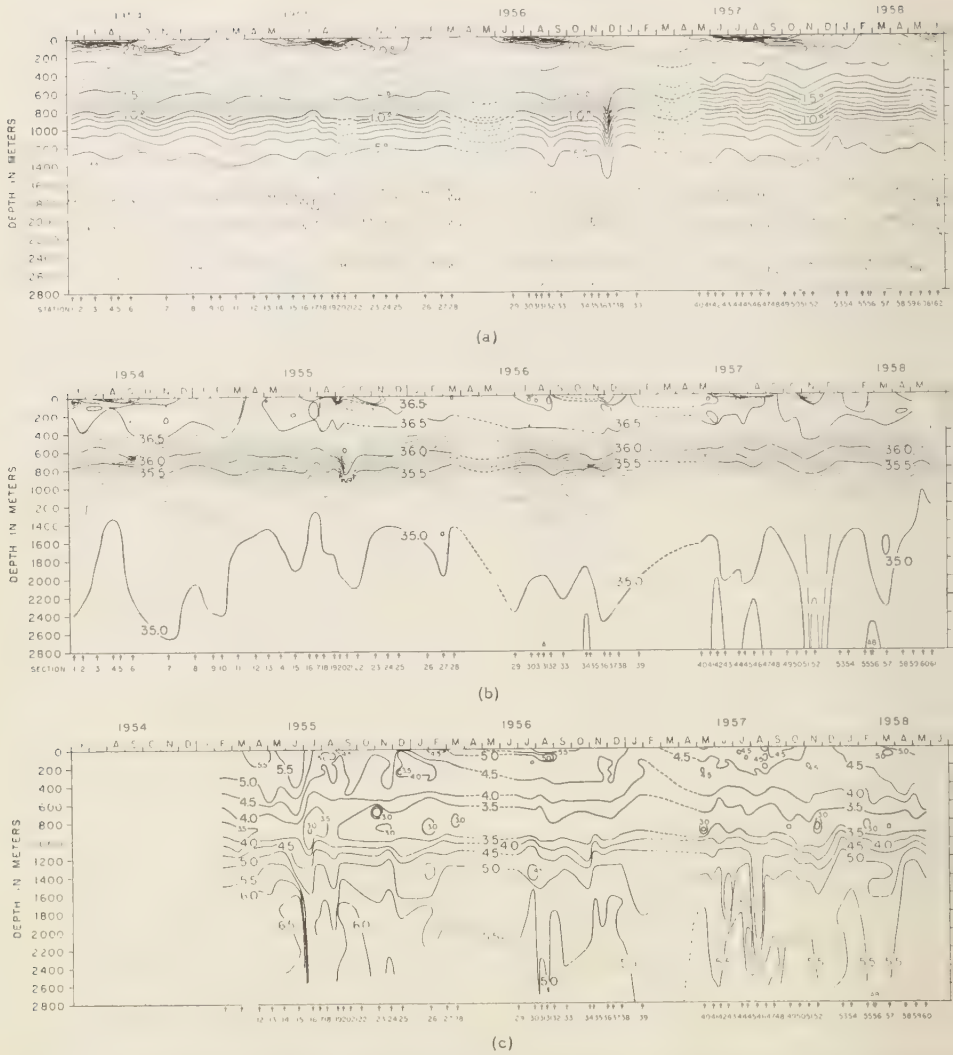

FIG. 1—The vertical distribution of various properties of the deep ocean at Bermuda, as a functio of time; (a) temperature in degrees Centigrade; (b) salinity, in parts per mille; (c) dissolved oxyge in milliliters per liter

Sea the shallow surface does not vary so much seasonally, and never disappears even in winter. Thus in these latitudes the 18° Water never is in direct contact with the atmosphere, and we must envisage it as coming from the north as a slow southward current beneath the surface thermocline. However, in this study no attempt is made to describe the geographic distribution of the 18° Water; discussion will be confined t the 18° Water at Bermuda.

The Panulirus data, 1954–1958—The mos complete and homogeneous series of hydro graphic data for the vicinity of Bermuda is th *Panulirus* series made from 1954 to 1958 b various members of the Bermuda Biological Sta tion. The depths of various contours of equa

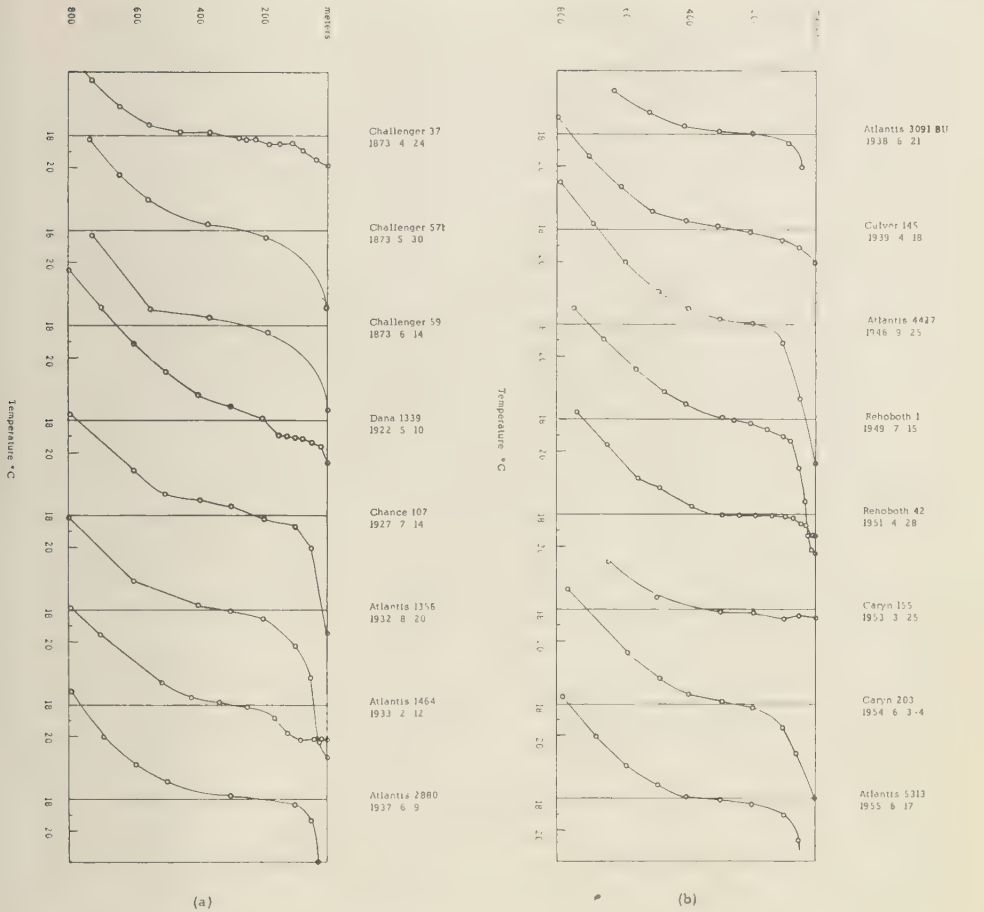

FIG. 2 (a) and (b)—Detail of the temperature structure of the upper 800 meters of water at Bermuda as shown by selected stations made in the late spring of a number of years

temperature, salinity, and dissolved oxygen, plotted as a function of time, are shown in Figure 1. In the upper 150 meters there is a marked development of a seasonal thermocline. Below it there is a mass of more homogeneous water where the isotherms are less crowded vertically; this is the 18° Water. Beneath 450 meters the main thermocline begins. From station to station these isotherms move up and down as much as 100 meters. Evidence from the thermometric cable at Bermuda [*Haurwitz* and others, 1959] suggests that these vertical displacements are mostly the result of sampling errors introduced by short-period internal wave motions.

During each winter the top 150 meters is cooled off and approaches convective equilibrium with the 18° Water down to a depth of about 400 meters; therefore something like one third of the 18° Water is reformed each year. In view of the fact that each winter is variable and different from others, and that a large geographical area (32°–36°N; 40°–73°W) is involved in the cooling, it is truly remarkable that following each year's overturn the water between 150 and 450 meters (the 18° Water) remains so constant in its properties.

Long-term stability of the 18° Water—The *Panulirus* data extend over only four years. How

variable is this 18° Water over longer periods? In the past the sampling has not been frequent enough to allow construction of seasonal profiles such as those in Figure 1. We can compare individual soundings made over an 85-year period, starting with the *Challenger* station in 1873. Samples (made in late spring) are shown in Figure 2. The interesting point here is that the inflection point in the temperature-depth curve for the period of observation is always at 18°C (within a few tenths of a degree).

Salinity of the 18° Water—It is interesting to enquire whether the 18° Water, which from year to year is in intimate contact with the surface, can possibly maintain a constant T-S relationship. The temperature and salinity data for every available (114) hydrographic station in the Bermuda area were plotted on graph paper and smooth curves drawn through points. The salinity was read off the curve at the depth where the temperature curve was exactly 18°C, and it was found that for a period of 36 years the salinity of the 18° Water has been 36.50 ± .02 ppm probable error; that is, it has remained constant within *titration error*. This is really quite surprising in view of the fact that in the fall and early winter, the surface waters near Bermuda have inhomogeneities of salinity of as much as 0.80 ppm over a span of a few miles. Yet a month or so later, when cooling and convection with the 18° Water begins, the salinity somehow returns to 36.50 ± .02 ppm. How is it possible that it does not vary more from year to year?

Renewal and overturn at Bermuda—In view of the fact that the data during the overturn period is rather scanty, one wonders whether there really is convective mixing of the 18° Water right to the surface at Bermuda. The temperature soundings seem marginal; thus even the near homogeneity of *Panulirus* station 57 is not complete homogeneity; and one may ask does vertical mixing of surface water into the 18° Water really occur or does it only seem to occur? The oxygen data from *Panulirus* stations show an unambiguous renewal of oxygen in 18° Water extending to considerable depths, varying from year to year, but always present.

Summary—In summary the following features at Bermuda are revealed: The inflection point in the temperature sounding between the surface thermocline and the deeper main thermocline has always been at 18°C within a few tenths of a degree during the past 85 years, according to all available data; and the salinity at 18° is remarkably uniform—within the titration error. On the other hand, the oxygen renewal each year is quite variable in the 18° Water. Since wintertime surface temperatures, salinities, and oxygen contents are all quite variable, it is puzzling to account for the fact that the 18° Water is so stable climatically.

To what extent some of the phenomena observed are produced by advection from higher latitudes we have no way of knowing; there is no systematic set of hydrographic data comparable to the *Panulirus* data from any other area near Bermuda.

Acknowledgment—In undertaking this study we have had the advantage of many discussions with F. C. Fuglister and L. V. Worthington, to both of whom the 18° Water has been a subject of interest for years. In studying the new *Panulirus* data it occurred to us that finally we had enough material to present a definite case for the amazing climatic stability of the 18° Water at Bermuda, and that this was the time to bring it to the attention of oceanographers interested in climatic change. Part of this work was supported by an AEC contract AT (30-1) -2078 with the Bermuda Biological Station, and part by an ONR contract Nonr 2196 (00) with the Woods Hole Oceanographic Institution.

References

Haurwitz, B., H. Stommel, W. H. Munk, The thermal unrest in the sea, Rossby Memorial Volume, in press, 1959.

(Manuscript received September 8, 1958; revised January 8, 1959.)

Sediment Thickness and Physical Properties: Pigeon Point Shelf, California

David G. Moore and George Shumway

U. S. Navy Electronics Laboratory
San Diego 52, California

Abstract—A 200 sq mi area of the continental shelf off Pigeon Point, California (about 40 mi south of San Francisco), was studied in regard to the thickness and physical properties of unconsolidated sediments. Sediment thicknesses and water depths were determined by a high-power low-frequency echo sounder which acoustically penetrates unconsolidated sediments to record bedrock and other sub-bottom reflectors. Seventeen sediment sampling stations were made in the survey area. Determinations were made of wet density, porosity, compressional sound speed and absorption (at 20 to 30 kc/s), static shear strength, sensitivity, and grain size distribution.

The Pigeon Point shelf is a gently sloping, featureless plain whose surface sediments are mainly unlithified sands and silts. Over much of the area these sediments are several tens of meters thick, but between the 40 and 50 fathom contours the sediments thin, and in the southern part of the area bedrock is locally exposed on the sea floor. Bedrock surfaces beneath the sediment blanket form two prominent terraces believed to have been cut by wave action during lowered Pleistocene sea levels.

Introduction

Between San Francisco and Santa Cruz, off Pigeon Point, the continental shelf is relatively broad compared with many other parts of the California shelf. It is a smooth sedimentary plain, with the 50 fm and 100 fm depth contours parallel and about eight nautical miles apart (Fig. 1) (all references to miles are hereafter understood to mean nautical miles). In July, 1957 the Pigeon Point shelf was surveyed to determine the thickness and areal extent of the unconsolidated sediments overlying bedrock and to measure some of their physical properties.

Sediment thicknesses were determined by means of a short-pulse high-power echo sounder which is capable of obtaining sub-bottom acoustic reflections through several tens of feet of unconsolidated sediments [*McClure* and others, 1958].

This instrument produces a continuous record of bottom and sub-bottom relief which can be studied in detail in the laboratory.

A reconnaissance sediment sampling program was combined with the acoustic reflection traverses, and seventeen samples were obtained by Navy Electronics Laboratory snapper, gravity corer, and box dredge. The samples were analyzed for particle size distribution, porosity, wet density, and mechanical shear strength. In selected samples compressional sound velocity and attenuation were measured.

Navigation was by dead reckoning, the shoreward end of traverses being tied to shore points by sextant-angle fixes where possible. During much of the survey period a swell from six to 18 feet high somewhat decreased the efficiency of the sounding equipment.

The writers wish to thank C. J. Shipek for assistance on the survey cruise.

Bathymetry

In contrast to the generally narrow and relatively shallow continental shelves off most of Southern California, the region of this survey was specifically chosen as a broad, smooth shelf area with its flattest portion in the 50–60 fm range and lying several miles offshore. Depth contours in the study area, prepared from Coast and Geodedic Survey boat sheets, together with soundings taken on the present survey show this to be the case (Fig. 1). For more than 20 miles in the northwest-southeast direction the 50 and 100 fm contours are roughly parallel to each other. From the 50 fm contour (5 to 8 mi offshore) seaward to the poorly defined shelf-break at about 64 fm, the shelf is a smooth-surfaced, sediment-covered plain with a gentle seaward slope of about 0.15 degree/mile. Shore-

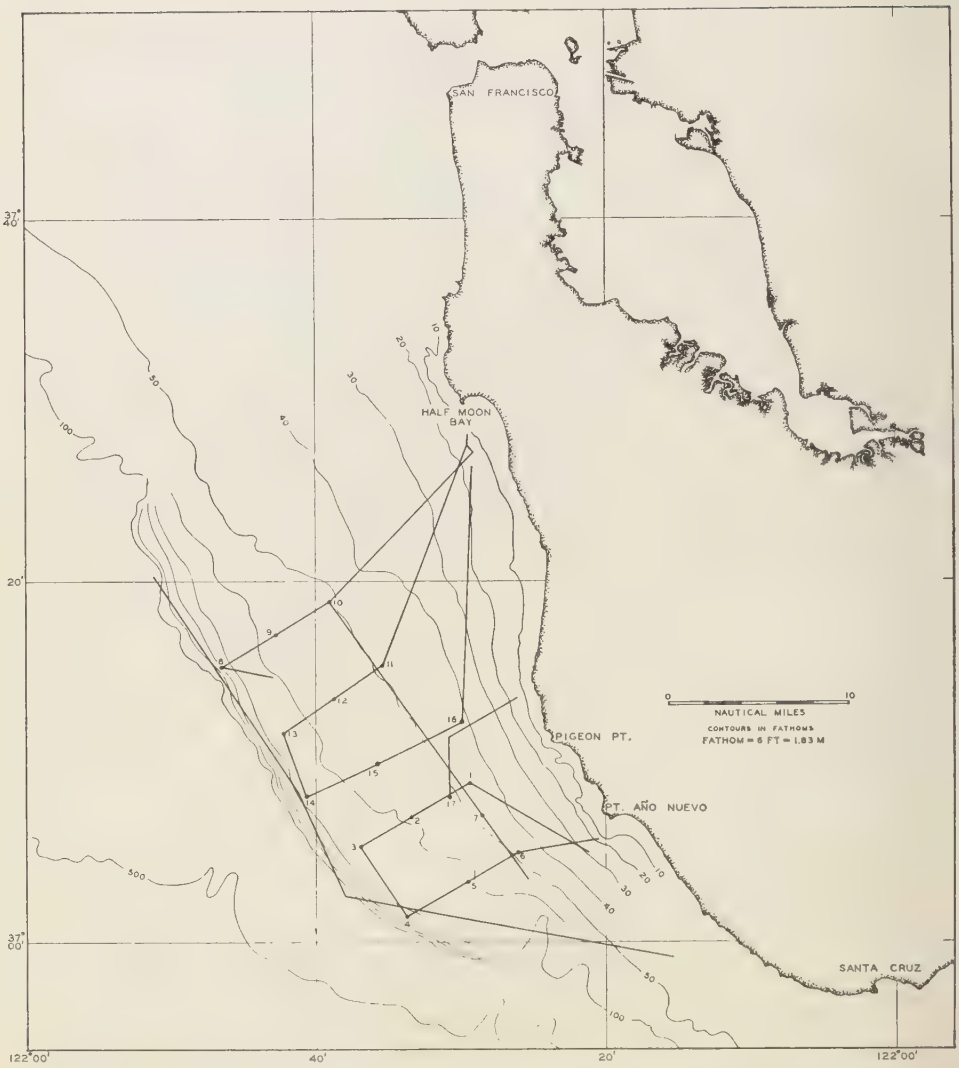

FIG. 1. Location of Pigeon Point shelf showing sounding traverses, sample stations, and bathymetry in survey area

ward from the 50 fm contour the bottom slope becomes somewhat steeper and the surface more irregular.

BOTTOM MATERIALS

Particle size distributions for 17 sediment samples were determined by the pipette and settling tube method, using the Wentworth size classification. The sediments are represented on a triangular sand-silt-clay diagram (Fig. 2) which serves to name them [*Shepard,* 1954] and gives a rough measure of their sorting and size distribution. All samples except No. 17 contain less than 20 pct clay and therefore are classed as sands, silty sands, sandy silts, and silts. Sample 17 is a marginal clayey silt, but,

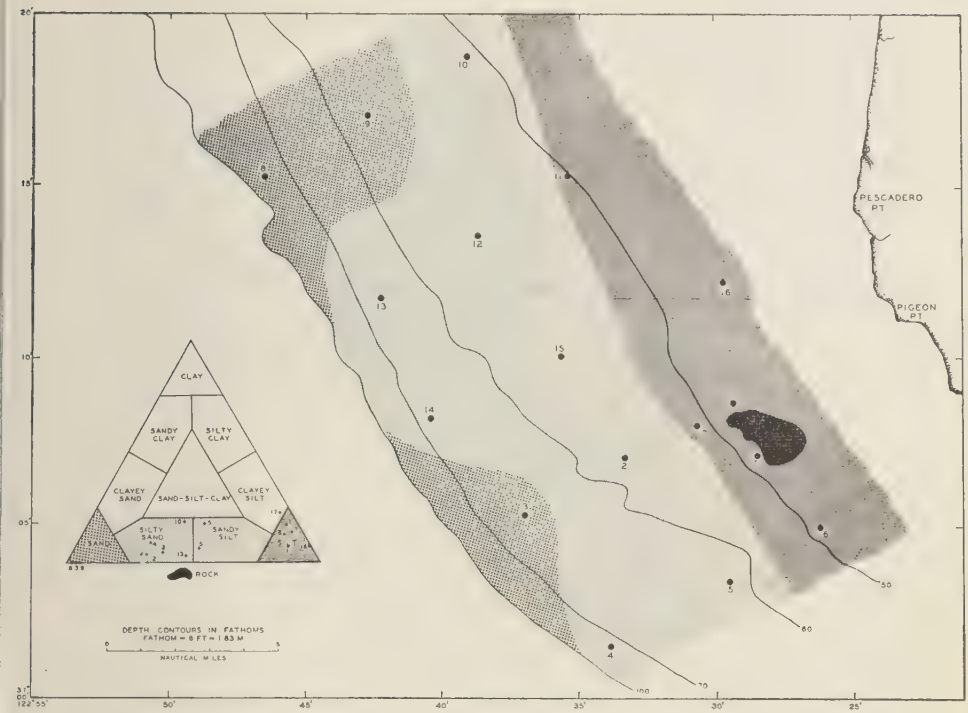

FIG. 2—Types of surface sediments and their distribution on Pigeon Point shelf

for simplicity, is included with the silts on the chart showing the areal distribution of sediment types (Fig. 2).

The areal distribution of sediments forms a simple but anomolous pattern, with sands on the outer shelf grading shoreward into silty sand, sandy silt, and finally the silt lying roughly along the 50 fm contour. This pattern probably would be reversed as the coarser deposits nearer shore are approached.

The sands on the outer part of the Pigeon Point shelf are believed to be relict (following the classification of *Emery,* 1952) from some ancient depositional cycle. They were probably deposited or reworked during a lowered Pleistocene sea level and their present exposure indicates conditions of non-deposition on the outer shelf in subsequent time. The silt deposits along the inner part of the survey area are believed to mark the outer limit of deposition of modern land-derived detritus. Between these modern silty deposits and the relict sands of the outer shelf are the mixed silty sands and sandy silts. The significance of this distribution is further discussed in the section on the sediment thickness survey.

Near the 50 fm contour in the southern part of the survey region an area of exposed bedrock was located (Figs. 2 and 4A). A small dredge towed over this area (Station 7) collected a boulder of fine-grained sandstone, thinly color-banded and well indurated with calcareous cement. It contained no fossils and is of unknown age. Apparently this rock outcrop has no pronounced effect on the surrounding sediments which are among the finest textured in the area.

PHYSICAL PROPERTIES OF SEDIMENTS

Data on sediment median diameter, grain size, sorting, porosity, wet density, static shear strength, sensitivity, sound speed, and absorption are given in Table 1.

Particle size distribution—Median diameters ranged from 0.031 mm (5.0 ϕ, medium silt) to 0.088 mm (3.51 ϕ, very fine sand). The phi unit for designating grain diameters is related to the

TABLE 1—*Physical properties of Pigeon Point sediments*

Station	Porosity	Wet density g/cm³	Median dia.		Sorting σ_ϕ	Shear strength kg/cm²	Sensitivity	Sound speed km/s	Absorption db/m
			ϕ	mm					
7	0.646	1.63	4.92	.033	1.35	.007	7.7	1.676 at 26.2°C	5.7 at 21.1 kc/s
6	0.604	1.68	4.92	0.33	1.06	.015	4.7	1.559 at 27.4°C	9.1 at 27.3 kc/s
1	—	—	4.79	.036	1.93	—	—	—	—
5	0.618	1.72	4.41	.047	2.70	.009	4.0	1.536 at 25.8°C	—
17	0.583	1.74	4.51	.044	1.36	.009	2.9	—	—
16	0.550	1.73	5.01	.031	0.61	.011	6.5	1.526 at 24.3°C	20.5 at 31.1 kc/s
11	0.518	1.77	4.41	.047	0.50	.015	8.8	—	—
15	—	—	4.11	.058	0.64	.010	7.5	—	—
13	0.507	1.88	4.01	.062	0.43	.011	2.7	—	—
2	0.464	1.88	3.90	.067	0.59	.009	—	1.755 at 27.8°C	13.7 at 30.8 kc/s
14	0.469	1.89	3.70	.077	0.50	.018	6.2	—	—
10	0.462	1.90	4.01	.062	0.19	.018	7.2	—	—
12	—	—	3.80	.072	0.38	—	—	—	—
4	0.420	1.93	3.80	.072	1.08	.009	3.8	—	—
8	—	—	3.51	.088	0.21	—	—	—	—
9	—	—	3.51	.088	0.16	—	—	—	—
3	—	—	3.51	.088	0.10	—	—	—	—

diameter, d, in mm by the expression $\phi = -\log_2 d$. The degree of dispersion or sorting of grain sizes in each sample can be expressed by the phi deviation measure, σ_ϕ, which is determined from the 84th and 16th percentile diameters by the relation $\sigma_\phi = \frac{1}{2}(\phi_{84}-\phi_{16})$ [*Inman*, 1952]. The sediment values ranged from 0.10 for the best sorted sand on the outer shelf, to 2.70 for a sandy silt on the central shelf in the zone of mixed modern and relict deposits.

Porosity and density—At the time of collection, sediment samples were stored in airtight containers to allow later measurements of natural wet bulk densities and porosities. Porosity, the ratio of pore volume to total bulk volume, was determined from the volume of water lost through oven drying at 105°C to 110°C. Porosities ranged from 0.420 to 0.646 (Table 1). Bulk densities, determined in the laboratory by weighing known volumes of wet sediment ranged from 1.63 g/cm³ to 1.93 g/cm³ (Table 1).

Vane shear strength—Sufficient material was available from 12 of the 17 samples to perform vane shear strength tests. The apparatus used for these tests was similar to one developed by *Evans* and *Sherratt* [1948]. It had a rotatable vane which was inserted into the sediment. A controlled, increasing torque was applied to the vane until failure occurred along the resulting cylindrical surface of shear. Details of the instrument are described by *Moore* (in press). To minimize disturbance of the sediment, the shear strength was measured in the jars in which the samples were placed after sampling; for the five samples in which sound speed was measured, the shear strength measurements were made immediately following the acoustic measurements, and on the same material. Shear strengths ranged from 0.007 kg/cm² to 0.018 kg/cm² (Table 1).

After each sample was measured for undisturbed shear strength, the vane was rotated completely around in the sample several times and the test then rerun to measure the disturbed, or remoulded, strength [*Skempton*, 1948]. The ratio of the undisturbed to the remoulded strength is called the 'sensitivity' of the sediment. It is indicative of the development of the skeletal structure and intergrain bonding in the undisturbed material [*Terzaghi* and *Peck*, 1948]. Most fine sediments have a sensitivity between two and four; sensitive sediments range from

four to eight, and more sensitive materials may be much greater. *Skempton* and *Northey* [1952] proposed a sensitivity scale ranging from insensitivity (= 1) to quick (> 16). *Rosenquist* [1952] later suggested an even greater extension of this scale to > 64 in order to classify certain extra-quick Norwegian clays. The Pigeon Point samples ranged in sensitivity from 2.7 to 8.8 (Table 1).

Sound speed and absorption—Using the resonant chamber method [*Shumway*, 1956], compressional sound speed was measured in five samples and absorption was measured in four samples. These samples were specially collected for this purpose in order to minimize disturbance. The four samples were measured in the laboratory a few days after collection. Sound speeds at room temperature ranged from 1.526 km/s to 1.676 km/s (Table 1). Absorptions ranged from 5.7 db/m at 21.1 kc/s to 20.5 db/m at 31.1 kc/s.

Interrelationships of Physical Properties

In a suite of natural, unconsolidated sediments, varying degrees of correlation are expected between measured physical properties. These interrelationships are investigated not only because they shed light on the sedimentation processes involved in the deposition of the materials, but also because it is desirable to know the degree to which certain properties are predictable from other measures. In conventional sedimentological work, median diameter and sorting are generally studied, and frequently porosity and wet density are investigated. In the present study the additional measures of shear strength, sensitivity, sound speed, and absorption are available and may be compared with the more conventional measures and among themselves.

Table 1 has been arranged somewhat arbitrarily to show to good advantage variations of the measured parameters from sample to sample. Porosity and wet density for a suite of sediments of nearly the same mineralogical composition are inversely related. The sample sequence is arranged to show decreasing porosity and increasing wet density, but because the correlation between the two is not perfect, three instances are shown where the trend of increasing (or decreasing) values is not perfect.

Median diameter is seen to increase in a fairly uniform manner as porosity decreases; that is, the finer sediments, with their higher contents of silt and clay, are more porous. As the porosity decreases and the median diameter increases, the sediments become better sorted. These relationships are the usual ones for shallow-water marine sediments.

Shear strength and sensitivity are apparently independent of porosity, wet density, and median diameter for this suite of samples. A weak positive correlation between shear strength and sorting is indicated, for well sorted sediments generally are stronger than those of poor sorting.

Absorption values are lowest in the two sediments of highest porosity. All four absorption values are typical for the porosities and median diameters involved (*Shumway*, 1958b).

Sediment Thickness Survey

The sediment thickness survey provides a generalized three-dimensional picture of the unconsolidated Quaternary sediments that have accumulated in the area and defines the morphology of the underlying bedrock surface. Sediment thickness along the traverses was read directly from the acoustic reflection records using a mean sound velocity in the sediments of 1.462 km/sec. The five sound speeds measured in the sediment samples had a mean of 1.57 km/sec when measured at room temperature (26.3°C mean). Bottom water on the Pigeon Point shelf in July has a temperature of approximately 8.5°C. A temperature correction of approximately 0.035 km/sec would apply for these shelf sediments [*Shumway*, 1958a], giving a mean *in situ* surface sediment velocity of 1.53 km/sec. Because this is close to the nominal 1.46 km/sec calibration velocity of the Sonoprobe, the calibrated value was retained for direct reading of sediment thickness. Inasmuch as sound speed in the sediments probably increases somewhat with depth of burial, the sediment thicknesses given here are minimal.

The effectiveness of the acoustic reflection equipment in penetrating sediment is in part dependent on the state of the sea, ship noise, and, of course, on electronic and mechanical adjustments. During this survey the buried bedrock surface could not be detected when covered by more than about 10 to 12 meters of sediment. Elsewhere, under more favorable conditions, bedrock reflections under as much as 25 meters of

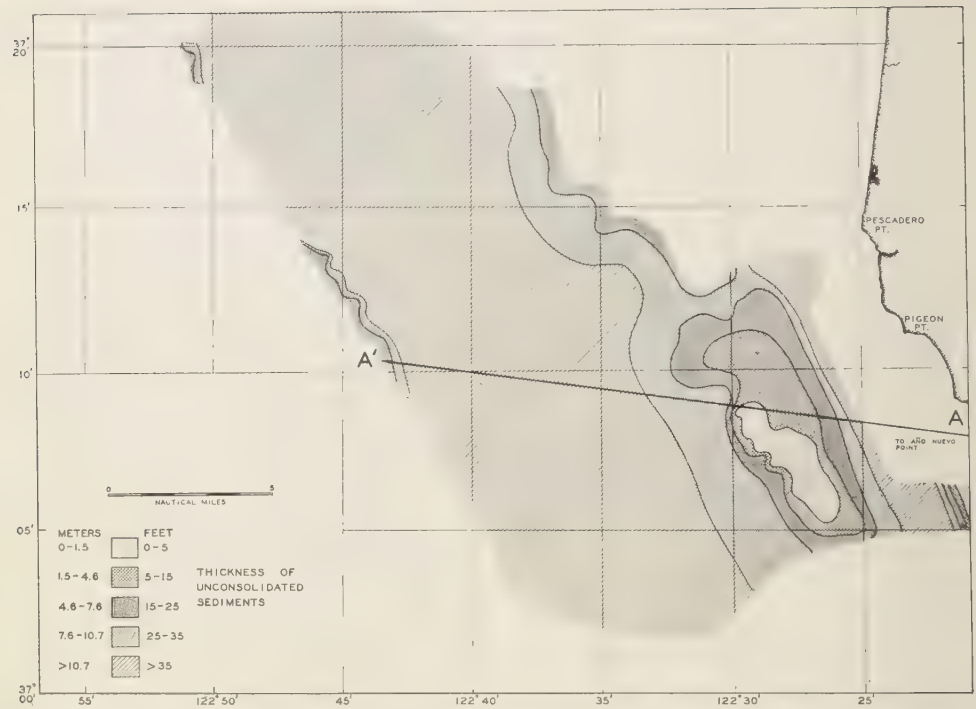

FIG. 3—Isopach map showing thickness of unlithified sediments on Pigeon Point shelf; Section A-A′ is given in Fig. 5

sediment have been recorded. In constructing the sediment isopach map (Fig. 3), it was necessary to class much of the overburden thickness as more than 10 meters.

Along the shoreward edge of the area surveyed, roughly straddling the 50 fm depth contour, a low discontinuous rise of the bedrock surface causes an elongate region of relatively thin sediment cover. Locally, in the southeastern part of the area, bedrock is exposed on the sea floor (Figs. 3 and 5). This rock locality had not been charted previously. Traverses seaward and landward from this exposure show continuously increasing sediment thickness. On two of the seaward traverses bedrock was traced to a burial depth of 12 to 14 meters before the record was lost in background noise (Fig. 4a and b). In a narrow zone along the outer deep edge of the shelf, reflections from the surface of the buried rock were detected from 4.5 to 11 meters below the bottom and locally peaked to within three meters (Fig. 4c).

The geological significance of the varying thickness of unconsolidated sediments is best shown on the section A-A′ across the shelf in a westerly direction from the vicinity of Año Nuevo Point (Fig. 5). Section A-A′ was selected to show the exposed rock both near the 50 fm depth and near the outer edge of the study area. Data for the inner part of the profile, 25 fm and less, was extrapolated from the traverse one half mile south of Año Nuevo Point. This same information is shown in plan in Figure 3.

The profile of the sea floor shown in Figure 5 is a smooth surface with an outer break in slope at 115 meters below sea level. Between 115 and 92 meters there is a very gently sloping flat surface. From 92 to about 20 meters the slope is steeper and concave upward. Nearest the shore there is a more gentle slope to present sea level.

Beneath this relatively simple shelf surface lies a more complicated and terraced bedrock surface. This irregular profile might be structural in origin, but an explanation of the origin

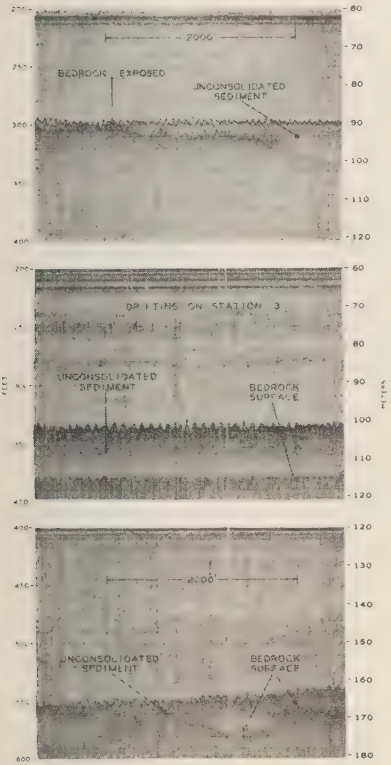

FIG. 4a—Acoustic reflection record of traverse seaward from exposed rock on southeastern shelf; note bedrock surface dipping beneath unlithified sediment

FIG. 4b—Bedrock surface 45 ft. below sea floor, recorded while drifting on station; saw-toothed appearance of bottom and sub-bottom surfaces results from ship's motion in riding sea-surface waves

FIG. 4c—Recording of bedrock near sediment surface on outer edge of shelf; traverse is parallel to the shelf edge; note irregular surface of buried rock

of these terraced rock surfaces must also account for the anomalous size distribution of the exposed shelf sediments discussed earlier. A sequence of geological events explaining the present rock sediment relationships shown in Figures 2 and 5 is suggested as follows: The bedrock was emplaced in the body of the present shelf probably by structural processes at some time after its initial deposition and lithification. One or more periods of marine abrasion followed, probably during early or middle Pleistocene glacial ages, which formed the outer, deepest terrace. (Fig. 5, mile 9-½ to mile 20, 104 to 160 meters below sea level). This period of planation was probably terminated by a glacially controlled, relatively rapid rise in sea level. Sand and later silty-sand sized detritus was deposited in the wake of this slow transgression and during the interglacial period. The sediments reached a considerable thickness on the central part of the ancient shelf, which corresponds roughly with the outer part of the present shelf. Subsequently, glaciers again expanded over the continents, sea level was lowered, and another period of marine erosion and abrasion followed. The amount of lowering of sea level in this later period was about 16 meters less than the earlier low which cut the outer terrace, possibly as a result of subsidence of the land. The soft sediments previously deposited over the earlier terrace were truncated and later the rock platform of the middle bedrock terrace was formed. Thus an erosional platform extending from the outer break-in-slope of the present shelf to a point about 45 meters below present sea level was formed; the outer, flattest part was cut in soft sediments and the inner, steeper part cut in bedrock (Fig. 5, mile 17 to mile 4, 115 to 46 meters below sea level).

This later period of marine erosion probably occurred in Wisconsin time and the depth of the present break-in-slope at the edge of the shelf, therefore, was regulated by the level of the eustatically lowered Wisconsin sea (*Dietz* and *Menard*, 1951). This relatively wide Wisconsin erosional platform probably was cut during a slow submergence [*Bradley*, 1958]. A later, more rapid submergence could explain the steep slope from 46 to about 21 meters below sea level. After the last relative rise of the sea to approximately its present level, late Pleistocene to recent shelf sediments have almost entirely covered the inner part of the Wisconsin erosional terrace, and the outer part cut in unlithified sediments still is largely exposed. The lens of sediment on the inner shelf (Fig. 5, mile 3-½ to mile 9) therefore is essentially Recent, and the bulk of the outer, more extensive, unlithified materials are pre-Recent and probably pre-Wisconsin in age.

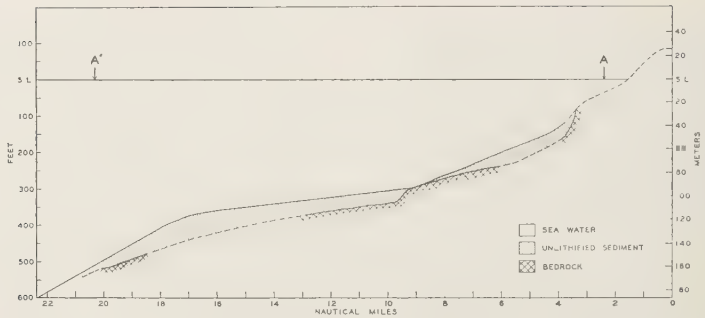

FIG. 5—Section across Pigeon Point shelf WNW from Año Nuevo Point (see Fig. 3); sea floor profile from present sounding records and U. S. Coast and Geodetic Survey soundings; bedrock profile from acoustic reflection records; dashed lines indicate no sub-bottom recorded

REFERENCES

BRADLEY, W. C., Submarine abrasion and wave cut platforms, *Bull. Geol. Soc. Am.*, 69, 967–974, 1958.

DIETZ, R. S., AND MENARD, H. W., Origin of abrupt change in slope in continental shelf margin, *Bull. Am. Assoc. Petrol. Geologists*, 35, 1994–2016, 1951.

EMERY, K. O., Continental shelf sediments of Southern California, *Bull. Geol. Soc. Am.*, 63, 1105–1108, 1952.

EVANS, I., AND G. G. SHERRATT, A simple and convenient instrument for measuring the shear resistance of clay soils, *J. Sci. Instr. and Phys. in Ind.*, 25, 411–414, 1948.

INMAN, D. L., Measures for describing the size distribution of sediments, *J. Sediment Petrol.*, 22, 125–145, 1952.

MCCLURE, C. D., H. F. NELSON, AND W. B. HUCKABAY, Marine sonoprobe system, new tool for geologic mapping, *Bull. Am. Assoc. Petrol. Geologists*, 42, 701–716, 1958.

MOORE, DAVID G., Vane shear strength, porosity and permeability relationships of some sieved cohesionless sands, *Proc. XX Intern. Geol. Congr.*, in press.

ROSENQUIST, I. TH., Considerations on the sensitivity of Norwegian quick-clays, *Geotechnique*, 3, 195–200, 1952.

SHEPARD, F. P., Nomenclature based on sand-silt-clay ratios, *J. Sediment Petrol.*, 24, 151–158, 1954.

SHUMWAY, GEORGE, A resonant chamber method for sound velocity and attenuation measurements in sediments, *Geophysics*, 21, 305–319, 1956.

SHUMWAY, GEORGE, Sound velocity vs. temperature in water-saturated sediments, *Geophysics*, 23, 494–505, 1958a.

SHUMWAY, GEORGE, Sound speed and absorption studies of marine sediments by a resonance method, unpublished Ph.D. thesis, Univ. of California (Scripps Inst. Oceanog.), 1958b.

SKEMPTON, A. W., Vane tests in the alluvial plain of the River Forth near Grangemouth, *Geotechnique*, 1, 111–124, 1948.

SKEMPTON, A. W., AND R. D. NORTHEY, The Sensitivity of Clays, *Geotechnique*, 3, 30–53, 1952.

TERZAGHI, K., AND R. B. PECK, *Soil Mechanics in Engineering Practice*, Wiley and Sons, N. Y., 566 pp., 1948.

(Manuscript received April 18, 1958; revised November 25, 1958.)

An Improved Radio Snow Gage for Practical Use

K. Itagaki

Hokkaido University
Sapporo, Japan

Abstract—A new type of radio snow gage has been developed. Its main features are: (1) A Geiger-Müller counter is buried under the snow layer so that the effect of temperature on the counter can be neglected. (2) The information obtained by this snow gage is sent by Morse code. (3) The relation between the water equivalent of snow and the number of Morse code is made to be linear. (4) The information of temperature and humidity are sent at the same time. The mechanism and the results obtained by this snow gage are described.

Preface—In the northern part of Japan the greater portion of precipitation occurs as snow, and the snow survey is important in hydrological study in Japan. First, the distribution of snow pack in a basin must be studied. For this purpose it is necessary to make a considerable number of samplings. When enough data are collected so that it is possible to choose the representative points, measurements at those points are preferably made as the function of time.

For this latter purpose a pre-established gage is advantageous in saving time and effort, and if possible a telemetering snow gage would be the most useful instrument. A radioactive snow gage, measuring the absorption of gamma radiation by snow [*Gerdel* and others, 1950; *Doremus*, 1951; *Onuma*, 1955], would be the most suitable method for telemetering. By this method the measurement of the water equivalent of snow does not disturb the accumulated snow layer at all, and continuous measurement at a certain point can be made. Moreover, the radioactive method is suitable for telemetering because the measurement of radiation is made by the use of electricity.

It is excellent to carry out the snow survey by the use of radioactivity, but the construction of equipment which is stable in operation, compact, and easy to install in a mountainous area at low cost is not so easy. The author designed a simple and stable system which has several distinctive features in the method of measurement and transmission and in the way of using G-M counter. The equipment is set in the basin of Lake Shikaribetsu, where we have conducted the snow surveys for several years [*Higashi* and others, 1956]. The snow survey was started in December, 1955, to obtain the data for the programming operation of Shikaribetsu hydroelectric plants.

General arrangement of the system—The general arrangement of the system is shown schematically in Figure 1. A radiation source is suspended above the snow layer, and just below this source a G-M counter is placed below ground level. The counting rate of the G-M counter is converted into current by the counting-rate meter. The output current of the counting-rate meter is translated into Morse code by the code translator and is sent to the receiving base station by the use of a 414 Mc/s UHF transmitter.

There are two main features in this system. The first is that the G-M counter is buried under the snow layer. Thus the temperature of the G-M counter is kept at about 0°C throughout the snow season; therefore, the effect of temperature on the G-M counter can be neglected. Moreover, most radiation from the radioactive fallout ejected by possible atomic and hydrogen bomb experiments is absorbed in the snow layer. The second feature is seen in the communicating system. The output pulses of the G-M counter are not sent directly, but its counting rate is translated into Morse code. This not only results in a reduction in the noise disturbance but reduces the effect of fading which was experienced in earlier field tests. Sometimes the signals faded out almost entirely, even when the signals were received at a point from which the transmitting station could be seen. Noise and fading cause the miscount of pulses, when the pulses are sent directly. But if these pulses are translated into Morse code and sent repeatedly, the problem of miscount will disappear. There are other advan-

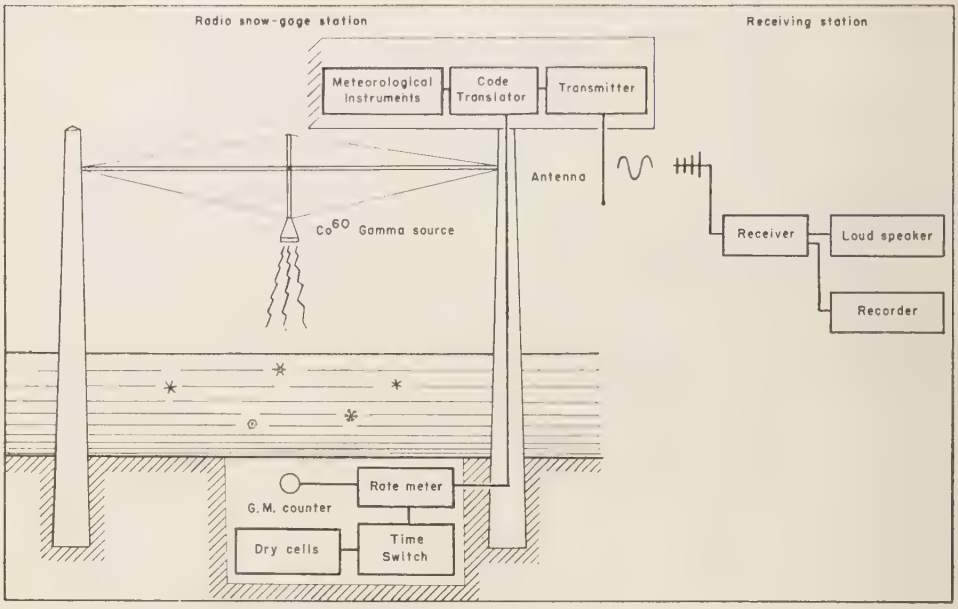

FIG. 1—General arrangement

tages in this mode of communication. Several other elements such as temperature and humidity can be sent by Morse code at the same time. If modulated waves are used, and the modulation frequencies are different from each other, several stations can be handled by one receiver.

Both the transmitter and the receiver are put into operation twice a day by time switch, in order to reduce the current consumption and wear. The transmitter side is usually in the remote mountain district, where transportation sometimes has to be done on foot. Therefore, the weight and the size of one unit must not exceed that which one person can carry on his back. The largest unit in the system is 30 kg in weight and 50 × 40 × 25 cm in dimension.

Principle of measurement—The most suitable radiation for the present purpose is the hard gamma ray which penetrates through a deep layer of snow. The absorption of gamma rays is expressed by

$$I = I_0 e^{-\mu d} \tag{1}$$

where I_0 is the intensity of the original radiation and I is the intensity after absorption by the material of thickness d. The mass absorption coefficient defined by $k = \mu/\rho$, where ρ is density, depends only on the material but not on its phase.

In the case of snow, ρd is the water equivalent of snow H_w. Thus (1) is

$$I = I_0 e^{-kH_w} \tag{2}$$

This shows that the absorption of gamma rays depends only on the water equivalent of snow but not on other elements such as depth of snow, density, and liquid water content. The mass absorption coefficient k depends on the energy of radiation and is known when the radioactive isotope is specified. *Gerdel* and others [1950] measured the absorption curve of gamma rays emitted from Co^{60} by water and obtained the value of k. *Onuma* [1955] obtained a slightly different result, but his measurement was made without a collimator and is not applicable to the present study. The author adopted the value of k obtained by Gerdel. If the number of Morse code R is proportional to I

$$\alpha R = I_0 e^{-kH_w} \tag{3}$$

α is a constant. Therefore, the difference of the water equivalent of snow per unit step of the Morse code is

$$dH_w/dR = -(\alpha/kI_0)e^{kH_w} \tag{4}$$

FIG. 2—The container of Co^{60} suspended freely in the outer case; (a) beam; (b) outer case; (c) lead collimator suspended freely

Thus, in the higher region of H_w, the difference of the water equivalent of snow per unit step of the Morse code increases too rapidly to be used practically. This situation can be avoided by inserting the logarithmic circuit. If the characteristics of the counting-rate meter are changed to be

$$\ln I = \beta R \tag{5}$$

by adding the logarithmic circuit. Then

$$\beta R = \ln I_0 - kH_w \tag{6}$$

Thus the number of Morse code varies linearly with the water equivalent of snow. For the logarithmic circuit a well-aged vacuum tube (Type 1T4) was used as a vacuum-tube voltmeter.

The e_g-i_p characteristic of a remote cutoff vacuum tube is similar to the logarithmic curve in a certain range; that is

$$\ln (e_g) = \gamma - \delta i_p \tag{7}$$

When the output voltage of the counting-rate meter is connected to the grid of this vacuum tube, the output current is proportional to the logarithm of I and has in linear relation to H_w.

Details of the system—For the radiation source the radioisotope Co^{60} is the most suitable source for the present purpose, as chosen by earlier researchers. Co^{60} emits 1.17 Mev and 1.33 Mev gamma rays and 0.32 Mev beta rays. The half life is 5.3 years [*Whitehouse* and *Putman*, 1953, p. 384]. As the difference of gamma ray energy is small it can be regarded as monochromatic for the present purpose, and the beta ray can be shielded with a thin metal sheet. In this system three ten-millicurie tubes of Co^{60} sealed in the lead container together with a collimator were suspended freely from a fixed beam, as shown in Figure 2. The gamma ray was collimated to the G-M counter placed just below this source.

The scintillation counter has a better efficiency as a gamma ray detector than the G-M counter, but it requires high stability of power supply and the current consumption is large. In the present situation, such condition cannot be expected for long-period operation without manual adjustment. Therefore the G-M counter was used in our system.

The ordinary G-M counter of alcohol quench does not work at temperatures below 0°C because of condensation of alcohol vapor in the G-M counter. It fails to operate because of the change of ratio of the component. To avoid this difficulty a quenching agent must be used which

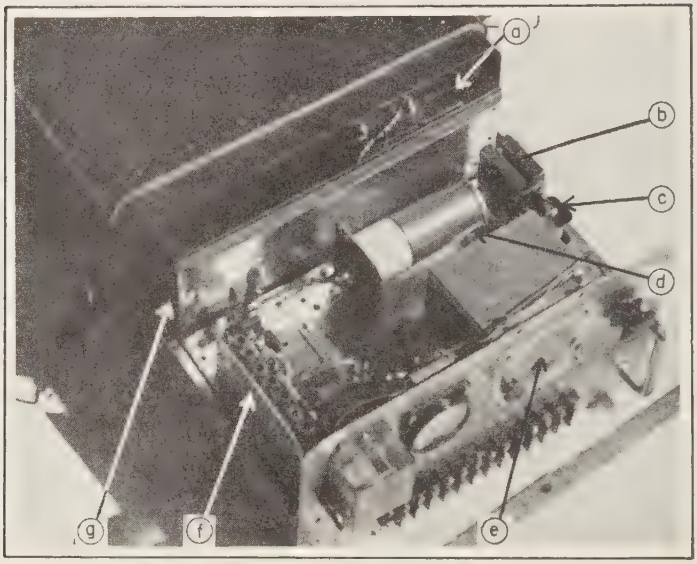

Fig. 3—The assembly set underground; in the box behind the chassis are kept the high-tension supply and the time switch; (a) dry cell for the time switch; (b) lead shield; (c) beta check relay; (d) G-M counter; (e) time switch; (f) counting-rate meter; (g) the case of G-M counter supply

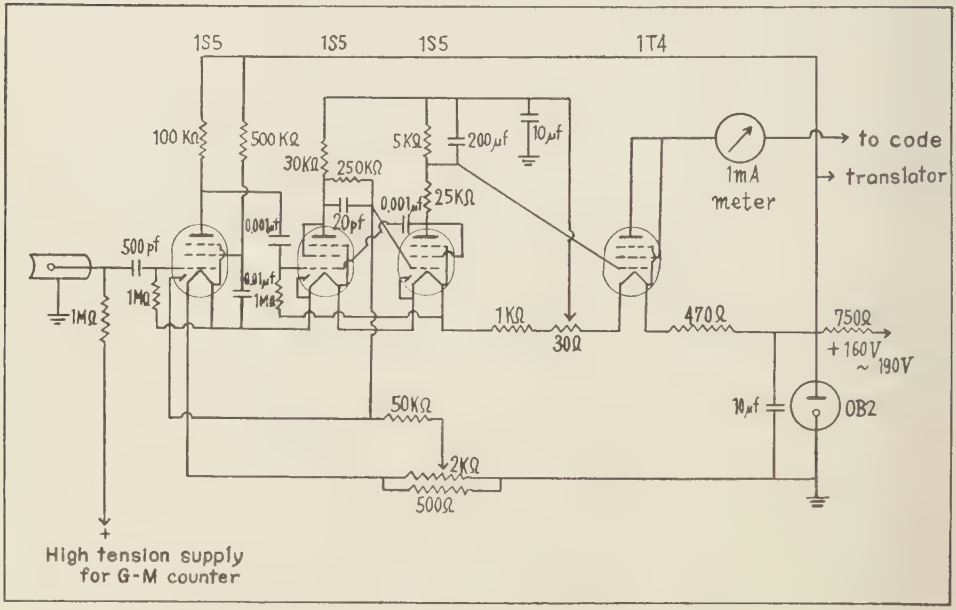

Fig. 4—Circuit diagram of counting-rate meter and logarithmic circuit

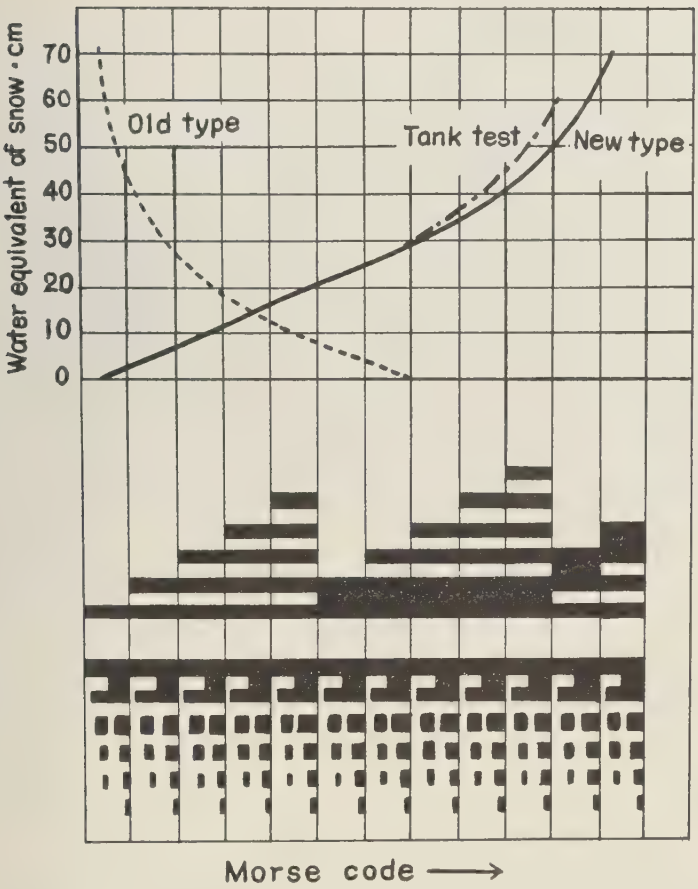

FIG. 5—Relation between Morse code and water equivalent of snow

has high vapor pressure at low temperature. Ethylformate is one of the quenching agents having this property. Two types of G-M counter with ethylformate as quenching gas were made, and their temperature dependency was investigated [*Higashi* and *Itagaki*, 1956]. (These counters operate at temperatures even below −40°C or −50°C, but since they are kept under the snow layer where the temperature is always at nearly 0°C, the variation of the counter characteristic with temperature need not be considered.) The counting efficiency may be changed by some other cause such as the change in voltage of power supply, or the life of G-M counter may come to an end when the measurement covers a long period. Therefore, the checking device using Sr^{90} as a standard beta ray source was adopted. During the observation period this Sr^{90} source is shielded, and it is brought to the window of the lead shield by an electromagnet during the checking period. As the gamma ray cannot be shielded, the calibration is made by the increase of counting rate produced by the standard beta ray source. The G-M counter, standard beta ray source, and counting-rate meter are shown in Figure 3.

The circuit diagram of the counting-rate meter combined with logarithmic circuit is shown in Figure 4. Output pulses of the G-M counter, amplified by a 1S5, drive the counting-rate meter, which is constructed of a univibrator of two 1S5's and RC filters; the output of the

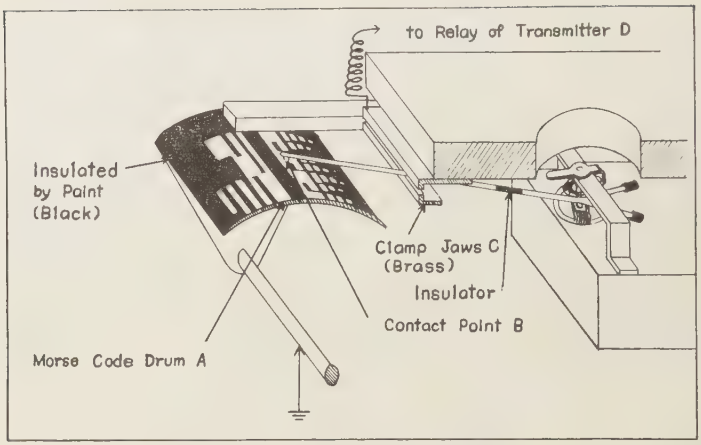

FIG. 6—The code translator of snow gage; the current passes through the order A,B,C,D

counting-rate meter drives the logarithmic amplifier. This counting-rate meter is sensitive to the change in the A supply so that its voltage is stabilized by an OB2 together with the B supply. When the condition of operation is stabilized by this method, it does not change at all so long as the OB2 is firing. The relation between the water equivalent of snow and Morse code is shown in Figure 5 by the full line. Two other curves are shown in Figure 5. The one is the result of the measurement made in a water tank $40 \times 40 \times 70$ cm in dimension. This is shown by the dot-dash line. This curve deviates a little from the calculated value shown by the full line, owing to the scattered gamma rays from the side wall of the tank. We used the calculated curve for the analysis of the actual observation and consistent results were obtained. The dotted curve shown is the result of the old-type counting-rate meter circuit without logarithmic circuit. This curve decreases with increasing number of Morse code. The same curve is inverted by the inversion of phase when the logarithmic circuit is inserted. Besides, the linearity is much improved in the latter case as is shown in Figure 5. The curve obtained with the instrument of new type may be considered to show the linear relation between 0 and 50 cm of water equivalent. The steeper slope of the curve in the high water equivalent region is due mainly to the incompleteness of the logarithmic circuit and partly to the background counts.

The intensity of radiation measured by the G-M counter is converted into the electric current by a counting-rate meter; this current is translated into Morse code, and is transmitted to the receiving station. The code translator, shown in Figure 6, is composed of two parts; a milliammeter with a contact on its pointer and a drum with the Morse code engraved on the surface. When in action, the drum rotates on its axis and through a relay keys a transmitter with the code letter which corresponds to the meter reading. An important feature of the present system is that information on other items can be sent at the same time. In addition to the knowledge about the snow pack, this gage sends a message on temperature and humidity by Morse code. A bimetallic thermometer and a hair hygrometer are used. Indicators of the thermometer and the hygrometer, which have contact points as the pointer of the milliammeter has, slide on another Morse code drum to translate these meteorological elements into the Morse code. Thus with one rotation of the axis of the drums, the codes of snow pack, temperature, and humidity can be transmitted with the identifying code respectively in this order.

A 414 Mc/s 0.3 watt audio-frequency modulated transmitter is employed in sending the information. The transmitter and the code translator, together with the meteorological instruments, are mounted on the top of one of the two pillars, to which the beam suspending source Co^{60} is attached. The lead wire between the instrument on the top of the pillar and that set

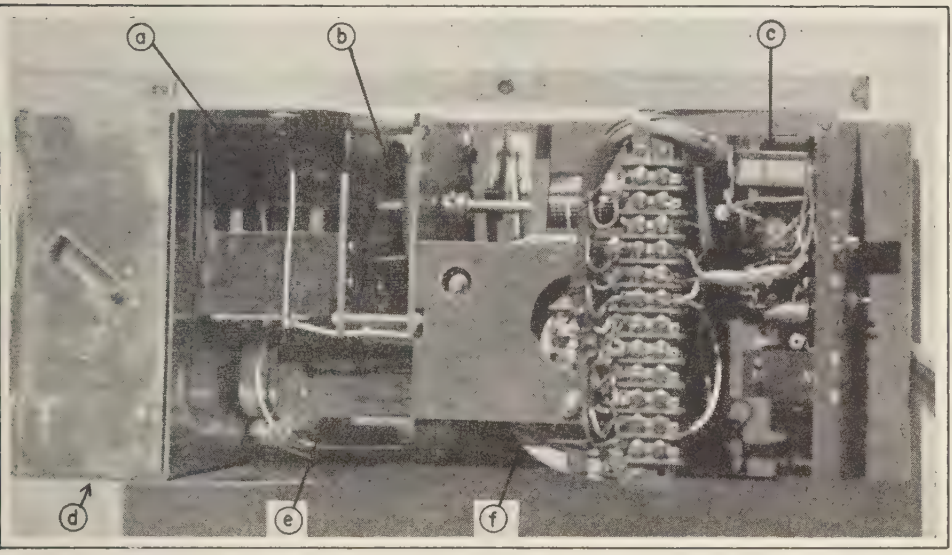

FIG. 7—Interior of the pole top assembly; (a) code translator for meterological instruments; (b) reduction gear; (c) transmitter; (d) meteorological instruments covered by the aluminum shield; (e) motor; (f) code translator for snow gage

underground is covered with a polyvinylchloride tubing in order to prevent water leakage. The terminals of the lead wire for the test are set on the top of the pole so that the test operation can be carried out after the underground parts are covered by snow. Figure 7 shows this assembly.

In the first year of field test, the time switch was operated by a pendulum clock driven by a dry cell. This failed because of the tilting of the clocks caused by frost heaving. We replaced the pendulum clock with a clock of balance-wheel type driven by a motor. This clock worked satisfactorily. The circuit operating the observation works for a few minutes, and immediately after this the circuits for operating the standard beta ray source follow for several minutes. This cycle is repeated every 12 hours. Such mechanism is difficult to design by using simply the axis of the hour hand of the clock. Therefore, a mechanical circuit is used which utilizes both the axes of the hour hand and of the minute hand. By this method the time switch can easily operate the circuits with about 2.5-minute intervals every 12 hours.

The necessary power for the G-M counter, the counting-rate meter, and the transmitter is supplied by dry cells. The high tension source of the G-M counter is supplied by eighteen BL-045S cells connected in series, which gives 1215 volts. These cells are encased in a bakelite box in order to prevent leakage.

As the working current of the counting-rate meter is about 100 ma at 180 volts, the counting-rate meter supply needs a capacity of more than three ampere hours extending over six months of operation. One hundred and twenty pairs of AM-1G cells connected in series serve this purpose. One pair is two cells connected in parallel.

The supply of the motor and the relay and the A supply of the transmitter need one ampere or 30 ampere hours capacity at 12 volts. This is supplied by eight sets of AM-1G cells connected in series. One set is seven cells connected in parallel. The clock of the time switch is operated by a flat No. 3 cell.

The G-M counter, the counting-rate meter, and the time switch are encased, together with the G-M counter supply and the time switch supply, in a waterproof steel case $30 \times 30 \times 18$ cm in dimension. This case is placed so that its upper face is level with the ground surface. The other batteries are enclosed in a steel case $50 \times 40 \times 30$ cm in dimension and buried separately.

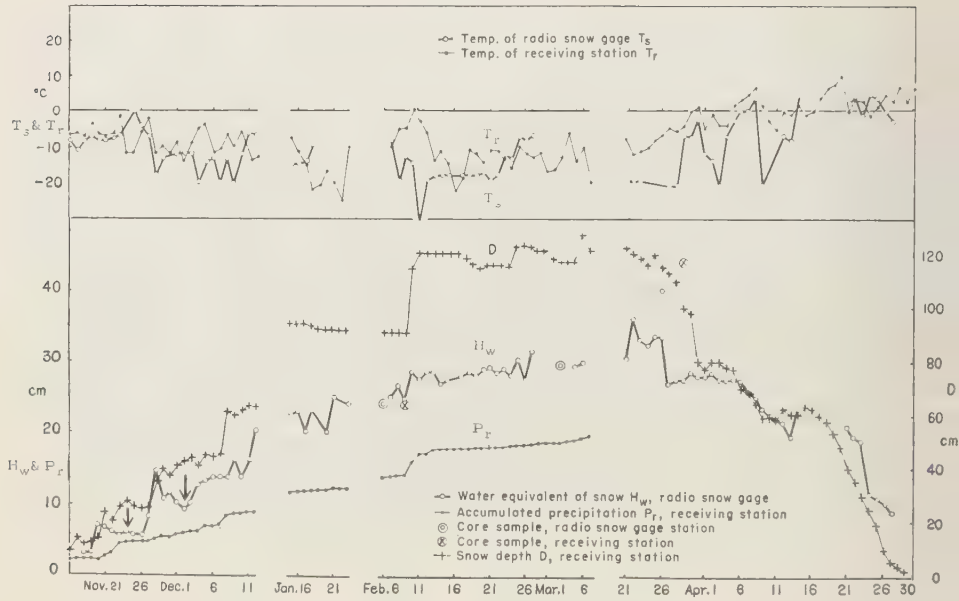

FIG. 8—Results obtained by this snow gage at the basin of Lake Shikaribetsu

The output of the receiver is connected to circuits which drive the recorder and the loudspeaker. The Yagi antenna of four elements is used for the receiver. The distance between the transmitter and the receiver is about 10 km. Although there is no obstacle between these stations and the receiver has sufficient gain, a considerable fading was experienced. Any failure in receiving the pulses would become a serious problem, but this difficulty is eliminated by sending the signal in Morse code.

The recorder, the time switch, and the receiver are connected to synchronize the time switches of transmitter and receiver. Besides, the connection is designed so that the recorder of the receiving set is not started by any sudden noise, but only by the Morse code.

Result of the observation—After finishing the test of individual parts, the first outdoor test was carried out in the courtyard of the Faculty of Science of Hokkaido University, where it recorded the melting of snow in the spring of 1955. The results showed good agreement with the direct measurements of water equivalent of snow by using a snow sampler. A slight modification was made to this set and it was brought to the basin of Lake Shikaribetsu in the fall of 1955 for the field test. This first field test was continued throughout the whole snow season of 1955–1956. There were several interruptions caused by stopping of the clock of the time switch by frost heaving. Satisfactory results were not obtained in this field test.

The apparatus, therefore, was developed as described above and a second field test was made in the winter of 1956–1957. The data obtained in this second field test are shown in Figure 8. The water equivalent of snow H_w measured by the new radio snow gage is shown by a heavy full line. This gage worked for the whole winter season, November 1956 to April 1957, with several short interruptions which were caused by the defects of the recorder of the receiving set. The curve shown with small black circles represents the accumulated precipitation P_r observed at the receiving station. The difference in altitude between the location of the snow gage and that of the receiving station is about 200 m, and the amount of the deposited snow is much less at the receiving station than at the snow gage. The increases, however, are more or less the same, because the distance between two stations is only 10 km. Two curves H_w and P_r show a satisfactory parallelism. The

curve marked with small crosses shows the snow depth D observed at the receiving station. The parallelism of D and H_w is also satisfactory. In the course of the second field test, core tests were made three times at the snow gage station in order to check the values obtained by the radio snow gage. These values are indicated by double circles in Figure 8. The water equivalent of snow shows a considerable fluctuation in a small area, and ten per cent difference is often observed when measurements are made at two spots a few meters apart. Considering this fluctuation, the values obtained by cores coincide quite well with the values of the radio snow gage. The decrease in H_w in the initial stage, marked by arrows, is considered not due to the error of this snow gage but due to some factor such as the melting or blowing away of snow.

Thus the apparatus here described is considered to have reliability for practical operation but it is not quite fully satisfactory. The major shortcoming is that the range of measurements is not wide enough, being limited between 0 and 60 cm of H_w. The other difficulty is the large amount of current consumed by the stabilizer and the register. A set of dry cells weighing 60 kg is needed for a half year's operation. Work is in progress to eliminate these disadvantages.

Acknowledgments—The writer expresses his best thanks to U. Nakaya of the Faculty of Science of Hokkaido University for his instruction and advice. Appreciation is also expressed for the helpful assistance of S. Koenuma of Hokkaido University. Thanks are given to A. Higashi of Hokkaido University, who motivated this research and gave many suggestions for this work. This research was sponsored by the Hokkaido Electric Power Company.

References

Doremus, John A., Telemetering system for radioactive snow gage, *Electronics,* 24, 88–91, 1951.

Gerdel, R. W., B. Lyle Hansen, and W. C. Cassidy, The use of radioisotopes for the measurement of the water equivalent of a snow pack, *Trans. Am. Geophys. Union,* 31, 449–453, 1950.

Higashi, A., K. Higuchi, and K. Itagaki, Snow survey in the Lake Shikaribetsu basin, *Geophys. Bull. Hokkaido Univ.,* 4, 65–81, 1956.

Higashi, A., and K. Itagaki, A radioactive snow gage for practical use (1), *J. Appl. Phys. Japan,* 25, 93–98, 1956.

Onuma, M., On the radioactive snow gage, *Researches on Snow and Ice,* 2, 139–147, Japanese Society of Snow and Ice, Tokyo, 1955.

Whitehouse, W. J., and J. L. Putman, *Radioactive Isotopes,* App. 4, pp. 379–413, Oxford University Press, London, 1953.

(Manuscript received April 15, 1958; revised November 22, 1958.)

Letters to the Editor

ON THE SEAT OF THE L CURRENTS CAUSING GEOMAGNETIC TIDES

K. S. RAJA RAO
Meteorological Office
Poona 5, India

Martyn [1947] has shown that the lunar tidal variations in the $F2$ layer critical frequencies at Huancayo exhibit a pronounced semi-diurnal oscillation. The harmonic coefficients of the $foF2$ are

P_1	P_2	P_3	P_4	t_1	t_2	t_3	t_4
0.018	0.10	0.013	0.02	9.78	4.33	6.55	5.94

where the P's are expressed in Mc/s and the t's are in lunar hours. The present author [*Raja Rao* and *Sivaraman*, 1958] has investigated the geomagnetic tidal variations at Kodaikanal for the period 1950–1954 and found that the amplitude of the lunar semi-diurnal oscillation of the horizontal intensity of the geomagnetic field is given by

$$\Delta H = 3.32 \sin (2t - 39°)\gamma$$

It is the purpose of the present note to compare these results, as both of the stations, Huancayo and Kodaikanal, are in the geomagnetic equatorial region:

Geomagnetic latitude of Kodaikanal	+36′
Geomagnetic latitude of Huancayo	−36′

The semi-diurnal lunar oscillations in the $foF2$ at Huancayo and the lunar oscillations in the geomagnetic field at Kodaikanal are plotted against lunar time (expressed in solar hours). These curves are shown in Figure 1.

The close agreement between these two curves shows that lunar $foF2$ variations are nearly in phase with the geomagnetic variations in the geomagnetic equatorial region. On the other hand, the L variations in the E layer as shown by *Appleton* and *Weekes* [1939] are given by the expression

$$0.93 \sin(2t + 112°)\text{km}$$

which shows that the semi-diurnal lunar oscillations in the E layer show a phase difference of

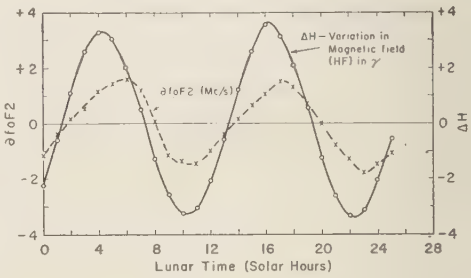

FIG. 1—The semi-diurnal lunar oscillations in the $foF2$ at Huancayo and the lunar oscillations in the geomagnetic field at Kodaikanal

151° with the L variations in the geomagnetic field. As the latitudes are different, the results may not be directly comparable.

As the maximum electron density N_{max} is proportional to $(fo)^2$, the relation being given by the equation

$$N_{max} = \frac{\pi m}{e^2} (fo)^2$$

the maximum amplitude of the $foF2$ variations should correspond to the maximum electron density and hence to the maximum ionospheric current. It is possible that these L currents in the $F2$ layer, caused by the gravitational action of the moon, produce the (lunar) semi-diurnal oscillations in the geomagnetic field.

Chapman and *Bartels* [1940] have constructed the diagrams for equivalent external current systems for S and L, assuming a height of 100 km above the surface of the earth for the current layer. The diagram would be very little altered if the height is assumed to be 200 or 300 km instead of 100 km.

Further, it is known that there is an increase in the Sq and L currents from the sunspot minimum to sunspot maximum. The increase is of the order of 50 pct in Sq while in L it is of

the order of 20 pct. It is, therefore, likely that the S and L current systems are not situated in the same ionospheric layer. As the seat of the S current system is known to be in the E layer, the seat of the L system can be located in the $F2$ layer.

The large amplitude (56 km) detected in the lunar oscillations in the height of the $F2$ layer as compared with the amplitude of 1 km in the E layer height will probably explain the large lunar variations better than E-layer variations.

The geomagnetic control of the $F2$ layer as represented by the dip in the graph of the noon values of $foF2$ plotted against the geomagnetic latitudes [*Liang* and *Appleton*, 1947] may be in some way related to the lunar tidal action on the $F2$ layer and the geomagnetic field.

The above facts lend support to the view that the long-sought seat of the L current system causing geomagnetic tides may be situated in the $F2$ layer.

References

Appleton, E. V., and K. Weekes, Lunar tides in the upper atmosphere, *Proc. Roy. Soc. London, A*, **171**, 171–187, 1939.

Chapman, S., and J. Bartels, *Geomagnetism*, vol. II, p. 695, Oxford University Press, 1940.

Liang, P. H., and E. V. Appleton, F_2 ionization and geomagnetic latitudes, *Nature*, **160**, 642–643, 1947.

Martyn, D. F., Atmospheric tides in the ionosphere, *Proc. Roy. Soc. London, A*, **190**, 273–288, 1947.

Raja Rao, K. S., and K. R. Sivaraman, Lunar geomagnetic tides at Kodaikanal, *J. Geophys. Res.*, **63**, 727–730, 1958.

(Manuscript received November 17, 1958.)

TEMPERATURE DISTRIBUTION AND MOISTURE TRANSFER IN POROUS MATERIALS

D. A. DE VRIES

Physics Department, Technological University
Eindhoven, Netherlands

J. R. PHILIP

California Institute of Technology, Pasadena
and C.S.I.R.O., Australia

In the present communication we wish to comment on a recent paper by *Woodside* and *Kuzmak* [1958]. Experimental work of the National Research Council Division of Building Research [*Kuzmak* and *Sereda*, 1957] has been entirely consonant with our theory of moisture movement in porous materials under temperature gradients. This further publication of the Ottawa group involves ideas connected with our theory, as they recognize.

We are surprised to read Woodside and Kuzmak's suggestion that the average temperature gradient across the air-filled space is six times the over-all gradient in the dry case. The magnitude of this quantity depends of course on the choice of the averaging method. In computing an average one must take account of the basic problem, which, here, is vapor transport.

Vapor transport—The fine structure of the temperature field may differ in important particulars from the fine structure of the vapor field, since the boundary conditions governing transfer across the pore are quite different in the two cases. The vapor boundary conditions are difficult to predict precisely without more knowledge of the absorbed phase than we have at present. It was recognition of this point which led us to emphasize the fact that our treatment of the temperature-gradient effect was a first approximation only [*Philip* and *de Vries*, 1957]. We believe that the distinction between the thermal and the vapor fields warrants much clearer recognition than we find in the Woodside-Kuzmak paper.

In the case of heat transfer, the soil-air interface represents a surface of refraction of the stream surfaces. However, in the vapor field, this same interface is itself a stream surface, across which there can be no transport. It is easily seen that, in cases similar to the model of Figure 5(a) of the paper we discuss (a soil-air 'dry' system) the heat and vapor flow patterns in the air space will differ radically. The heat flux densities will be greatest in the region near the point of horizontal (in the figure) contact between spheres and least in the vertical (in the figure) plane of contact. On the other hand, vapor flux densities will be greatest near this plane and almost zero near the points of horizontal contact.

The Woodside-Kuzmak averaging method is, apparently, an attempt to obtain a weighted average temperature gradient which bears some significant relationship to the heat fluxes across the air space. Even as such, it has some notable shortcomings, such as the neglect of the 45 per cent or so of the total air space which lies outside the vertical (in the figure) cylinders enclosing the spheres. But the more fundamental objection is that any such average is irrelevant, in view of the different flow patterns of the two fields. It seems entirely incorrect to choose a method of averaging temperature gradients which (in this extreme case) is weighted in favor of small regions which carry large heat flows, but which, in view of the vapor boundary conditions, carry little or none of the vapor flow.

The most rational average to take is a simple volume average in the air space (and it can be argued that even this may exaggerate the temperature-gradient effect). This is the average used in our work, and yields $\bar{F} = 2.04$ for the case where Woodside and Kuzmak estimate $\bar{F} = 6.02$.

As we indicated in presenting our theory, the fine structure effect alone does not account for the failure of the classical theory by a factor of 5 to 10. It must be recognized also that islands of liquid water present in the medium provide means of accelerated transport and are not the inert obstacles to diffusion which the classical theory has implied.

We have discussed the Woodside-Kuzmak 'dry' case in some detail, since it is for this case

that their $\bar{F}$ differs so markedly from ours. (Their $\bar{F}$ for the 'wet' model would not differ significantly from ours.) It must not be overlooked, however, that the 'dry' case is an artificial one, because vapor transport becomes zero as the moisture content becomes zero [see equation (14) of *Philip* and *de Vries*, 1957].

The whole matter of the volume-averaged temperature gradient receives further attention in the following section.

Heat transfer—In the final paragraph of their discussion Woodside and Kuzmak make a number of statements which are erroneous or irrelevant, or both. Most of these are connected with heat transfer through the unit cell, and tend to be somewhat divorced from the aspects of vapor transport we have discussed above. We examine these statements below.

(a) "If the Philip and de Vries method [*de Vries*, 1952] for calculating $\bar{F}$ is used, a value of 2.04 is obtained for the air-dry condition of the model, compared with the above measured value of 6.02."

Our comments: 1. In making this comparison Woodside and Kuzmak apparently overlook either (i) that our $\bar{F}$ (or ζ) is based on the volume-average, or (ii) that their own $\bar{F}$ is not based on the volume-average.

2. Whatever their value of 6.02 is, it is certainly not "measured." It is a value derived by a very special averaging process, which is quite definitely irrelevant in this heat transfer context (and which has not been justified in the vapor transport context, for that matter). [Note that the Woodside-Kuzmak observed temperatures are not in dispute. In fact the temperature differences they report are as we should expect, approximating to the results obtained if the spherical surface was isothermal.]

(b) "The Maxwell-Burger-Eucken theory, on which the Philip and De Vries method is based, assumes that the distances between particles are large compared with the particle size."

Our comments: 1. Firstly, we shall show that the value of $\bar{F}$ computed by our method does not depend in any critical sense on the validity of the Maxwell-Burger-Eucken theory. We introduce the symbols E, E_a, E_s to denote the volume-averaged temperature gradients in the whole cell, the air-space, and the soil, respectively, and the symbols x_a, x_s to denote the volume fractions of air and soil. Then, by definition,

$$\bar{F} = \frac{E_a}{E} = \frac{E_a}{x_a E_a + x_s E_s} = \frac{1}{x_a + x_s E_s/E_a}$$

Evidently $\bar{F}$ will be maximum when $E_s/E_a \to 0$, that is, when $k_s/k_a \to \infty$, so that we have the result that the maximum value of $\bar{F}$ which is physically possible, $\bar{F}_{max}$, is given by $\bar{F}_{max} = 1/x_a = 2.12$ in the model under discussion.

We have the following, stronger result, useful when k_s/k_a is known, as it is in the present case. It is easily shown that E_s/E_a assumes its minimum value when the soil and air volumes form a 'sandwich' in which the flux is through slabs of soil and air in series, and that this minimum value is k_a/k_s. It follows that the maximum value of $\bar{F}$ which is physically possible for a given k_s/k_a, $\bar{F}_{max}' = (x_a + x_s k_a/k_s)^{-1} = 2.09$ in the model under discussion.

The various results of computations of $\bar{F}$ for this model are collected in Table 1. The close

TABLE 1—*$\bar{F}$ values for the Woodside-Kuzmak 'dry' cell*

Basis of computing $\bar{F}$	Computed value
Woodside-Kuzmak	6.02
Maximum possible for any configuration (values larger than this physically impossible whatever the value of k_s/k_a)	2.12
Maximum possible for any configuration and actual value of k_s/k_a (values larger than this physically impossible in this case)	2.09
Philip-de Vries (Maxwell-Burger-Eucken)	2.04

agreement between our value 2.04 and the values of $\bar{F}_{max}$ and $\bar{F}_{max}'$ is most decidedly not evidence that the Maxwell-Burger-Eucken theory is wrong. It merely points to the fact that in these circumstances, where k_s/k_a is large, the value of $\bar{F}$ is insensitive to the particular model used. In consequence, our value of 2.04 does not depend on the Maxwell-Burger-Eucken theory in any critical sense. What small error exists is certainly negligible in the present context.

2. The limitations of the Maxwell-Burger-Eucken theory, arising from the particle spacing assumption, are well known, the theory having

been examined at length in a paper cited by Woodside and Kuzmak [*de Vries*, 1952.]

We can assert quite definitely that, for the model under discussion, use of the Maxwell-Burger-Eucken theory will yield a good, though slightly high estimate of $\bar{F}$. The error is about +2 per cent, in sharp contrast to Woodside and Kuzmak's belief that the Maxwell-Burger-Eucken theory yields about one-third the correct value.

(c) Finally, they conclude, as a result of comparing our 2.04, their 'observed' value, 6.02, and $\bar{F}_{max}'$, 2.09, that "the Maxwell-Burger-Eucken theory, because of the assumption concerning the distances between particles, is not applicable to most granular materials." Our comments: 1. They compute $\bar{F}_{max}'$, but recognize neither that it represents the maximum value of $\bar{F}$ which is physically possible, nor the significance of the closeness of our value to $\bar{F}_{max}'$ [see (b) 1. above].

2. We need only add that it has been shown by extensive investigations reported in the cited paper [*de Vries*, 1952] that this theory, although approximate, can be used to predict the thermal conductivity of a wide variety of soils.

References

De Vries, D. A., Het warmtegeleidingsvermogen van grond, *Mededel. Landbouwhogeschool Wageningen*, **52**, 1–73, 1952.

Kuzmak, J. M., and P. J. Sereda, The mechanism by which water moves through a porous material subjected to a temperature gradient, Part I, The introduction of a vapor gap into a saturated system, *Soil Sci.*, **84**, 291–300, 1957; Part II, Salt tracer and streaming potential to detect flow in the liquid phase, *Soil Sci.*, **84**, 419–422, 1957.

Philip, J. R., and D. A. de Vries, Moisture movement in porous materials under temperature gradients, *Trans. Am. Geophys. Union*, **38**, 222–232, 1957.

Woodside, W., and J. M. Kuzmak, Effect of temperature distribution on moisture flow in porous materials, *Trans. Am. Geophys. Union*, **39**, 676–680, 1958.

(Received October 7, 1958; revised December 31, 1958.)

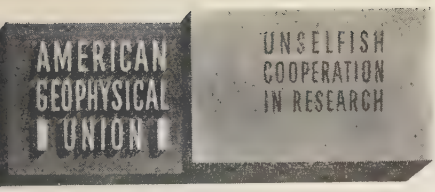

AMERICAN GEOPHYSICAL UNION

1515 Massachusetts Avenue, N.W., Washington 5, D. C.

Established by the National Research Council in 1919 for the development of the science of geophysics through scientific publication and the advancement of professional ideals.

APPLICATION FOR MEMBERSHIP

Please refer to qualifications on reverse side and designate below type of membership desired:

Member ($10) ☐ Associate ($10) ☐ Student ($3) ☐

Application forms for Corporation Membership are available upon request.

1. _____ _____ _____
Surname *First Name* *Middle Name*

2. _____
Preferred mailing address for publications

_____
Permanent address

3. _____ 4. _____
Place *Month* *Day* *Year of Birth* *Country of citizenship/naturalization*

5. _____
Nature of work and title and/or military rank; name and address of organization with which you are associated.

6. Check section or sections with which affiliation is desired.

☐ Geodesy
☐ Seismology
☐ Meteorology
☐ Geomagnetism and Aeronomy
☐ Oceanography
☐ Volcanology, Geochemistry, and Petrology
☐ Hydrology
☐ Tectonophysics

7. EXPERIENCE (List below)

Dates: From To Name and address of organization Title, duties, nature of work

8. EDUCATION (List below)

Dates: From To School Address Major Subject Degree, if any

*9. References: Please list below names and addresses of two or three references; include members of the AGU or others who know you well.

*10. Titles of technical contributions or publications, particularly those in the geophysical sciences, and where published.

*11. Brief statement of any special interests or qualifications in the geophysical sciences.

Date_____ _____
Written Signature

* Applicants for student membership may omit Questions 9, 10, and 11, but must fill in Question 12. Please return form with check or money order payable to American Geophysical Union, 1515 Massachusetts Ave., N.W., Washington 5, D. C.

(over)

12. (STUDENT MEMBERS ONLY) The person whose signature appears on the reverse side is known to me and is a student majoring in_____(subject) at_____ (Name of college or university) expected to graduate in_____(year) with the degree of_____

☐ He is a full-time student, or ☐ a teaching or research assistant enrolled in more than half of a full-time academic program.

_____
(Signature of faculty sponsor)

☐ Check here if faculty sponsor is a member of AGU and willing to act as a regular sponsor for associate membership as well.

_____
(Typed or printed name of sponsor)

_____
(Title)

QUALIFICATIONS FOR MEMBERSHIP IN THE AMERICAN GEOPHYSICAL UNION

The membership of the AGU shall consist of Members, Associate Members, Student Members, and Corporation Members.

Those eligible as candidates for election to the grade of MEMBER shall be:

MEMBER (a) Persons who have made an active contribution to geophysical research through observation, publication, teaching, or administration. Definite evidence should be presented to the Membership Committee. "Publications" may include books, articles, unpublished manuscripts, inventions, or development of geophysical instruments.

(b) Persons who have made active practical application of geophysical research. It should be shown that the nominee's work has not been purely routine, but that it has tended to create new knowledge of, or to broaden or strengthen the application of, geophysical research. In general, the minimum qualifications for membership will be not less than three years of professional experience in some phase of geophysics.

Those eligible as candidates for election to the grade of ASSOCIATE MEMBER shall be:

ASSOCIATE MEMBER Persons who have an active interest in physical processes of the Earth or technical assistance in the application of geophysics. In general, the minimum qualification for associate membership will be acceptable training or experience in some field of geophysics or allied science.

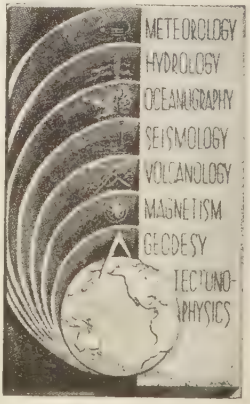

CORPORATION MEMBER Corporations and other interested organizations shall be eligible as candidates for election to CORPORATION MEMBERSHIP. They shall have the privilege of designating a representative who has the rights and privileges of Members (use special form).

STUDENT MEMBER Those eligible as candidates for election to the grade of STUDENT MEMBER shall be persons who are graduate or undergraduate students in residence at least half-time and who are specializing in the geophysical sciences. Teaching or research assistants enrolled in more than half of a full-time academic program may also be eligible for Student Membership. Student Members shall have all the privileges of Members except that they shall not vote or hold office.

American Geophysical Union

PROPOSAL FOR CORPORATION MEMBERSHIP

To the Executive Committee, American Geophysical Union
1515 Massachusetts Ave., N.W., Washington 5, D. C.

Gentlemen:

As an indication of our interest in the aims and activities of the American Geophysical Union, and to assist in maintaining and extending its program of publication and other work in the development of the geophysical sciences, the undersigned applies for Corporation Membership in the AGU and, until further notice, agrees to pay annual dues, currently at the rate of $100 per unit of corporation membership, in accordance with the information set forth on the back of this sheet.

Company or Organization_____

By _____ Title _____
(Signature)

Address_____

City _____ State _____

General fields of activity _____

_____

_____

_____

The following person is designated as our representative in this membership_____

_____ Title _____

Number of units of membership desired (this will be taken as one unless otherwise indicated)_____

Place_____

Date _____

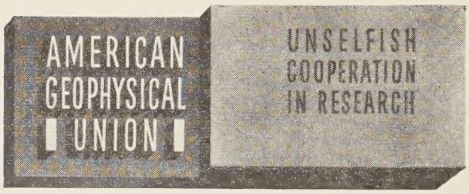

INFORMATION CONCERNING CORPORATION MEMBERSHIP

The American Geophysical Union is a non-profit scientific organization established by the National Research Council. It is the American National Committee of the International Union of Geodesy and Geophysics, and its Executive Committee is the Committee on Geophysics of the National Research Council.

Extracts from the Statutes:

Article 3. Membership—The membership of the American Geophysical Union shall be as follows:

(e) *Corporation Members*—Corporations and other organizations interested in geophysics elected by the Executive Committee of the Union. The designated representative of each such organization shall enjoy the privileges of a Member.

Extracts from the By-Laws:

(2) . . . Members of class (e) shall pay dues of $100 for each calendar year; . . .

(21) One copy of each issue of (a) the *Transactions*, (b) *Journal of Geophysical Research*, (c) any published *List of Members and Officers*, and (d) any other publication which may be approved for *free distribution* to the membership by the Executive Committee of the Union, shall be sent to each . . . Corporation Member. . . . Each . . . organization in good standing may purchase any available publication of the Union at a discount from printed price list to non-members. The General Secretary is authorized to establish discounts for sales of publications.

Action of the Executive Committee, November 29, 1946:

(1) A list of corporation members shall be published on one or more pages immediately after the final page of text in each issue of the *Transactions*.

(2) A list of corporation members shall be included in the Membership Directory as a distinct unit.

AMERICAN GEOPHYSICAL UNION
1515 Massachusetts Ave., N.W.
Washington 5, D. C.

Information for Contributors
to the *Journal of Geophysical Research*

Manuscripts—Send manuscripts to J. A. Peoples, Jr., Department of Geology, University of Kansas, Lawrence, Kansas. Manuscripts, including proof copies of figures, should be submitted in triplicate to expedite review and publication. Manuscripts should be in English, typewritten on heavy paper on one side of page only, double spaced (including abstracts and references), with generous margins.

Ample space should be allowed for mathematical expressions, which should be typed or very plainly written by hand. Particular attention should be given to legibility of subscripts and superscripts and to differentiation between capital and lower case letters. Unusual symbols and cumbersome notation should be avoided. Fractional exponents should be used in preference to root signs, and the solidus (/) should be used for fractions wherever its use will save vertical space.

Authors are urged to have their papers critically reviewed by their associates for scientific validity, manner of presentation, and use of English before submitting them for publication.

Abstracts—An abstract must accompany each manuscript. It should be a concise but comprehensive condensation of the essential parts of the paper, suitable for separate publication, and adequate for the preparation of general indexes to geophysical literature.

References and footnotes—References should be indicated in the text by the insertion in brackets of the author's name and the year of publication, thus: [*Trelease*, 1951]. If the author's name is part of the text, only the year is bracketed. If there are two or more references citing different papers published in the same year by the same author, distinguish them by the letters a, b, c after the year. At the end of the paper, list all references alphabetically by the authors' names. Include in each entry the following: name of senior author, followed by his initials; names of junior authors, each preceded by his initials; title of paper (or book); title of publication or journal; volume number; inclusive page numbers; year of publication. Abbreviations of journals follow the style used in *Chemical Abstracts*. If in doubt, give the full title of the publication or journal. When a book is cited, add the publisher's name, the city of publication, and the total number of pages. Reference to specific pages may be made in the text if appropriate. Acknowledge unpublished reports and private communications in the text, not as references. Avoid footnotes to the text; use parenthetic sentences instead of footnotes if possible.

Tables and figures—Material suitable to tabular form should be arranged as a table and may be typewritten on a separate page. Tables must be numbered according to their sequence in the text, and each table should have a title. Column headings should be short and self-explanatory; more complete explanation may be given in footnotes to the table. Authors should avoid repeating in the text material which is given in tables or figures.

Figures should be prepared with the column width of this Journal in mind (a scale of two to four times that of the published figure is usually adequate). Lettering and symbols should be large enough to stand reduction and remain legible. Captions should be typed on a separate page, not lettered in the figures. Necessary legends or lettering in the figures should be executed to meet competent drafting standards, not typewritten. If the author cannot arrange for suitable lettering, he may send the drawings with the lettering lightly penciled in or shown on a proof copy, and the lettering will be done at the editorial office.

Line drawings should be in India ink on white paper or tracing cloth. Coordinate paper should be avoided, but, if used, it must be blue-lined and the coordinate lines which are to show must be inked.

Photographs are acceptable only if they have good intensity and contrast. They should be unmounted, glossy prints.

Figures should be identified by numbering lightly in pencil, and 'top' of each figure should be indicated.

Acknowledgments—Acknowledgments should be made only for significant contributions by the author's professional associates. A brief closing statement will usually suffice.

References

American Chemical Society, *List of periodicals abstracted by Chemical Abstracts*, Chemical Abstracts Service, Ohio State Univ., Columbus, 314 pp., 1956.

American Institute of Physics, *Style manual*, American Institute of Physics, New York, 28 pp., 1951.

American Mathematical Society, A manual for authors of mathematical papers, *Bull. Am. Math. Soc.*, 49, no. 3, pt. 2, 1–16, 1943.

Emberger, M. R., and M. R. Hall, *Scientific writing*, Hareourt, Brace and Co., New York, 468 pp., 1955

Taft, K. B., J. F. McDermott, and D. O. Jensen, *The technique of composition*, 3rd ed., Farrar and Rinehart, New York, 628 pp,. 1941.

Trelease, S. F., *The scientific paper—how to prepare it, how to write it*, Williams and Wilkins Co., Baltimore, 175 pp., 1951.

U. S. Geological Survey, *Suggestions to authors of the reports of the United States Geological Survey*, 5th ed., U. S. Govt. Printing Office, Washington, 255 pp., 1958.

William Byrd Press, *Mathematics in type*, Richmond, 58 pp., 1954.

(Journal of Geophysical Research, Vol. 64, No. 3, March 1959)

Contents